A NOVEL ROLE OF CORTACTIN IN EXOSOME SECRETION AND TUMOR PROGRESSION

By

Seema Sinha

Dissertation
Submitted to the Faculty of the
Graduate School of Vanderbilt University
in partial fulfillment of the requirements
for the degree of

DOCTOR OF PHILOSOPHY
in

Cancer Biology
August, 2016
Nashville, Tennessee

Approved

Alissa M. Weaver, M.D., Ph.D.

Robert J. Coffey, M.D.

Rebecca S. Cook, Ph.D.

Matthew J. Tyska, Ph.D.

Rebecca A. Ihrie, Ph.D.

DEDICATION

To my loving, selfless, and brave parents.

In loving memory of Jhaiji, my loving aunt!

ACKNOWLEDGEMENTS

I would like to thank my mentor Dr. Alissa Weaver for making me a tough, and a critical scientific thinker. She has taught me that no matter what, one has to keep moving forward and follow science. I will value those lessons in all of my future endeavors. I want to give special thanks to members of the Weaver lab “WEAVER FEVER” both past (Kevin Branch, Tyne Miller, Kaitlin Costello, Eric Wirtz, Nan Hyung Hong, Kellye Kirkbride, Christi French, Selma Maacha, and Andrew McKenzie) and present (Mallory de Araujo Miles, Bong Hwan Sung, and Lizandra Jimenez) for their continued support throughout my graduate school career. Also, many many thanks to Aron Parekh and Rachel Jerell for their constant encouragement throughout this journey. This journey would not have been as enjoyable or fun without all of them. Special thanks to Nan Hyung Hong, Kellye Kirkbride, Christi French, and Nathan Grega-Larson for their help with various experiments that were important for the success of this project. I also want to give a special shout out to my committee members, Dr. Matthew J. Tyska, Dr. Robert Coffey, Dr. Rebecca Ihrie, and Dr. Rebecca Cook for their selfless support throughout my graduate school journey. I am really honored and humbled to have received guidance from such eminent scientists. I would also like to acknowledge Vanderbilt University Microscopy Core for training with confocal microscopy along with electron microscopy. I also want to thank Dr. Hayes McDonald for his help with the proteomics analysis. Special thanks to Dr. Robert Coffey and his team for use of NanoSight.

This work was graciously made possible through the financial support of the American Heart Association pre-doctoral fellowship award (10PRE4030003). Additionally, this project was supported by National Institutes of Health grants R01 CA163592 (AMW), R01-DK075555 and R01-DK095811 (MJT), CTSA grants UL1 RR024975 and TR000445-06, grants supporting the VUMC CISR: CA68485, DK20593, DK58404, HD15052, DK59637 and EY08126, American Cancer Society RSG-09-170-01-CSM (AMW), and AHA (NGL).

Most importantly, I would like to thank my parents who have been my pillars throughout my life. They have taught me everything that I know today and have given me the confidence to follow my dreams. I am truly honored to be their daughter. Their word of wisdom and encouragement at every step that I had fallen has kept me going, for which, I am forever thankful! I would also like to thank my brother Vivek, Tina, and Tanay for their unconditional love and support. My best friend, Tilottama Roy for lending me her ears for my complaints and eyes for me to see the successful completion of this dissertation work. And to my extended family and lovely friends that I have had the privilege of meeting across the globe, thank you, thank you, thank you, thank you!

TABLE OF CONTENTS

Page

DEDICATION iii

ACKNOWLEDGEMENTS iv

LIST OF TABLES viii

LIST OF FIGURES ix

LIST OF ABBREVIATIONS xi

Chapter

I. INTRODUCTION 1

Overview 1
Exosome discovery 2
Exosome biogenesis: ESCRT- dependent and –independent mechanisms 2
Exosome secretion 7
Exosomes contribute towards cancer progression 10
Actin cytoskeleton machinery and its role in membrane trafficking 11
Cortactin and its cellular functions 14

II. MATERIALS AND METHODS 20

Cultured cells 20
Cellular growth conditions 20
Retroviral and lentiviral generation of shRNA and overexpression vectors 21
Protein harvest 22
Immunoblot analysis 24
Antibodies 24

Exosome isolation and characterization 25
Differential centrifugation 25
Density gradient 25
Nanosight Particle Tracking Analysis (NTA) 26

Ultra-structural analysis of cells and exosomes by electron microscopy 26
Transmission Electron Microscopy of cultured cells 26
Negative staining of exosome samples 27
Multivesicular endosome biogenesis assay by TEM 28
Scanning electron microscopy of cultured cells 29

Immunofluorescence imaging 29

Constructs used for fixed and live imaging 29
Confocal microscopy 30
Total Internal Reflection Fluorescence Microscopy (TIRFM) 30
Invadopodia assay 31

Mass Spectrometry and LC MS/MS analysis 31
Shotgun Proteomics Analysis 31

Rescue of cortactin knockdown (KD) phenotypes by exosomes 32
Serum independent growth 32
Transwell invasion 33
Orthotopic mouse model for head and neck cancer (HNSCC) 33

Data Analysis and Statistics 34
Fixed imaging conditions 34
Live imaging conditions 35
Statistics 36

III. CORTACTIN PROMOTES EXOSOME SECRETION BY CONTROLING BRANCHED ACTIN DYNAMICS 38

Introduction 38
Results 41
Cortactin regulates exosome secretion 41
Cortactin does not control exosome cargo composition 45
Cortactin regulates MVE trafficking 51
Interaction of cortactin with Arp2/3 and F-actin is critical for exosome secretion 66
Cortactin, Rab27a, and Coronin 1b coordinately control cortical branched actin dynamics and exosome secretion 69
Discussion 76

IV. CORTACTIN REGULATES TUMOR GROWTH VIA EXOSOME SECRETION 81

Introduction 81
Results 84
Cortactin expression correlates with patient survival in HNSCC cancer 84
Exosomes promote serum independent growth and transwell invasion 87
Autocrine secretion of exosomes is critical for HNSCC tumor progression *in vivo* 93
Discussion 96

V. DISCUSSION AND FUTURE DIRECTIONS 98

REFERENCES 103

LIST OF TABLES

Table Page

1. List of cell lines and vectors used 23

2. Coefficient of variation for proteomics dataset 47

3. Genes found in HNSCC 11q13 amplicon 83

LIST OF FIGURES

Figure Page

1. Extracellular vesicles released from the cells 3

2. Membrane trafficking pathways in a cell 9

3. Structure of cortactin 16

4. Characterization of cell lines for exosome secretion 42

5. Cortactin levels control exosome secretion 48

6. Cortactin does not control exosome cargo selection 50

7. Cortactin affects MVE trafficking downstream of biogenesis 54

8. Cortactin expression does not affect morphology of CD63-positive structures 57

9. Cortactin affects number but not speed of MVE 60

10. Cortactin controls MVE docking at the PM 62

11. Cortactin and Rab27a affect MVE docking 64

12. Binding of cortactin to Arp2/3 complex and F-actin is critical for exosome secretion 68

13. Cortactin, Rab27a, and Coronin coordinately control invadopodia dynamics 72

14. Cortactin affects coronin 1b localization to invadopodia 74

15. Model for regulation of exosome secretion by Cortactin, Rab27a, and Coronin 79

16. High cortactin mRNA expression levels in HNSCC tumors is associated with decreased patient survival 85

17. Cortactin mRNA expression in patients 86

18. Cortactin dependent oncogenic phenotypes are controlled by exosomes *in vitro* 90

19. Cortactin dependent oncogenic phenotypes are controlled by exosomes *in*

vivo 94

LIST OF ABBREVIATIONS

MVE	Multivesicular endosomes
ILV	Interluminal vesicles
RNA	Ribonucleic acid
miRNA	microRNA
ESCRT	Endosomal Sorting Complex Required for Transport
VPS	Vacuolar protein sorting
ESCRT-0	Endosomal Sorting Complex Required for Transport-0
ESCRT-I	Endosomal Sorting Complex Required for Transport- I
ESCRT-II	Endosomal Sorting Complex Required for Transport- II
ESCRT-III	Endosomal Sorting Complex Required for Transport- III
HRS	Hepatocyte growth factor regulated tyrosine kinase substrate
TSG101	Tumor susceptibility gene 101
STAM	Signal transduction adaptor molecule
AAA+	ATPase associated with diverse cellular activity
VPS4	Vacuolar protein sorting 4-A
E6	Embryonic development day 6
E8	Embryonic development day 8
E11	Embryonic development day 11
PLP	Proteolipid protein
NPC1	Niemann-Pick type C1
LE/Lys	Late endosomal/lysosomal structures

PLD2	Phospholipase D2
PC	Phosphatidylcholine
PA	Phosphatidic acid
SNARE	Soluble NSF-attachment protein receptor complex
MET	Hepatocyte growth factor receptor
G-actin	Globular actin
F-actin	Filamentous- actin
ATP	Adenosine triphosphate
ADP	Adenosine diphosphate
Arp2/3	Actin related protein 2/3
NPF	Nucleation promoting factor
WASP	Wiskott-Aldrich syndrome protein
N-WASP	Neural Wiskott-Aldrich syndrome protein
WAVE	WASP family verprolin homologue
WHAMM	WASP homologues associated with actin, membrane, and microtubules
WASH	WASH and SCAR homologue
VCA	Verprolin homology, cofilin homology, and acidic domain
B2AR	β2 adrenergic receptor
SH3	SRC homology 3 domain
DAG	Diacylglycerol
PKCβ	Protein kinase Cβ
Cdc42	Cell division control protein 42 homolog

N-WASP	The Wiskott-Aldrich Syndrom protein
AMAP1	A Multiple-domain Arf-GAP Protein 1
ASAP1	Ankyrin repeat PH domain 1
HDAC6	Histone deacetylase 6
WIP	WASP interacting protein
MMP2	Matrix metalloproteinase- 2
MMP9	Matrix metallopeptidase- 9
MT1-MMP	Matrix metalloproteinase- 14
CTTN	Cortactin
FGF	Fibroblast growth factor
FADD	Fas-ligand associated protein with death domain
KD	Knockdown
OE	Overexpression
FDR	False discovery rate
TCGA	The cancer genome atlas
CCND1	Cyclin D1
ROS	Reaction oxygen species
UC	Ultracentrifuge
DG	Density gradient
MV	Microvesicle
PI	Phosphoinositide
$PI(3,5)P_2$	PI (3,5) bisphosphate
V-ATPase	Vacuolar ATPase

PLP	Myelin proteolipid protein or lipophilin

CHAPTER I

INTRODUCTION

Overview

The cellular cytoskeletal machinery plays a key role in regulating several organelle functions including membrane trafficking. Several cargo proteins including transmembrane proteins and soluble proteins are trafficked to the plasma membrane. The soluble protein may undergo secretion into the extracellular environment, while the transmembrane protein may recycle back from the plasma membrane and undergo endocytosis. These transmembrane proteins upon reaching the endosomes are trafficked to either sorting endosomes or recycling endosomes. Cargoes that undergo sorting including transmembrane and cytosolic bioactive molecules are further processed and transported to the late endosomes (also known as multivesicular endosomes) where they can either be degraded by fusing with the lysosomes or trafficked back to the plasma membrane where the multivesicular endosomes can fuse, dock and release their contents into the extracellular milieu. Actin polymerization and depolymerization is important during these events involving endocytosis, endocytic maturation, as well as exocytosis. This dissertation work discusses a novel role of an actin binding protein, cortactin and its function in the endocytic pathway where it regulates exosome secretion by promoting docking of the late endosomes, specifically multivesicular endosomes (MVE), at the plasma membrane. This

work has implications for many disease pathologies including tumor progression as exosomes have been shown to play a key role in cancer aggressiveness.

Exosome discovery

Exosomes are 40nm-100nm secretory vesicles that are derived from the late endosomal compartments called multivesicular endosomes (MVE). Exosomes were originally discovered in both normal and neoplastic cell lines as a part of microvesicle population containing 5'-nucleotidase activity [2]. Following this initial finding, exosomes were further shown to play an important role in the transferrin receptor fate in sheep reticulocyte maturation *in vitro* [3]. The transferrin receptor is a membrane receptor that undergoes endocytosis and is recycled to the plasma membrane. The sheep transferrin receptor pathway following endocytosis was traced using electron microscopy and was found to be present within the small vesicles (~50nm in size) that are inside the larger MVEs [4]. This pioneering work showed for the first time the entire fusion profile of the transferrin receptor that is present within exosomes, which are being secreted into the extracellular environment upon fusion of MVE with the plasma membrane [4].

Exosome biogenesis: ESCRT- dependent and –independent mechanisms

Exosomes are formed during the endosomal maturation process. During transition from early endosome to late endosomes, the endosomal membrane undergoes inward invagination leading to the formation of interluminal vesicles (ILVs). ILVs are also referred to as exosomes. The endocytic compartments containing ILVs are known as multivesicular endosomes. During the process of inward budding of ILVs, several cargo proteins, mRNA, miRNA, lipids, and

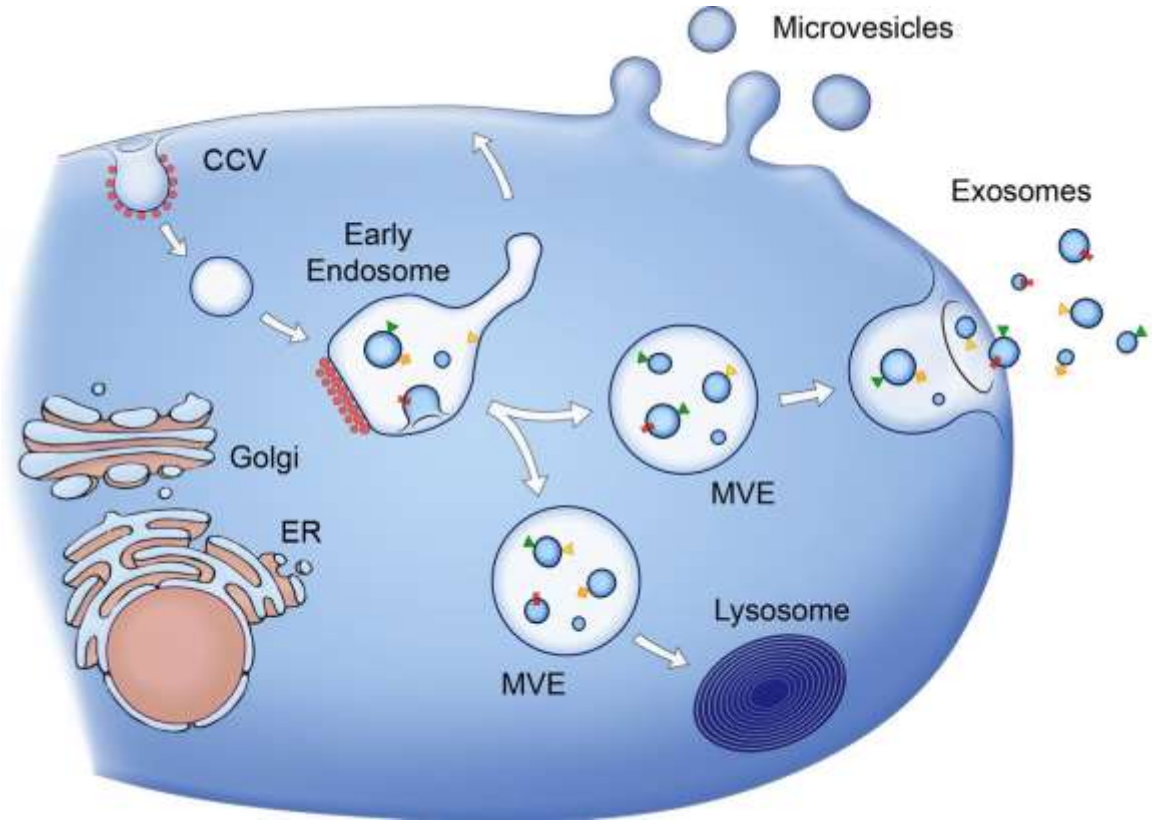

Figure 1. **Extracellular vesicles released from the cell.** The diagram depicts the endocytic pathway where ILVs are formed by inward invagination of the endosomal membrane. This gives rise to MVEs. The MVE then either fuse with lysosomes or are targeted to the plasma membrane where upon fusion with the membrane, exosomes are released into the extra cellular environment. Besides exosomes, cells also release microvesicles that are directly shed from the cell surface. Figure is taken from [1].

cytosol is sorted into these vesicles [5-10]. Multivesicular endosomes can then fuse with lysosome that contains lysosomal hydrolases and ensures degradation of multivesicular endosomes and its contents [11]. Alternatively, MVEs can also be trafficked to the plasma membrane where they fuse with the plasma membrane, releasing their content into the extracellular milieu (Figure 1).

The process of ILV formation by inward invagination of the endosomal membrane is a tightly regulated process. The best described mechanism for ILV formation involves the endososmal sorting complex required for transport (ESCRT) family proteins. This process is highly evolutionarily conserved [12]. Components found in this process were first characterized in yeast. These components were identified as a part of the vacuolar protein sorting (*vps*) mutants that had a defect in protein transport to the vacuole (an equivalent of yeast lysosome) [13]. Amongst the 46 *vps* identified mutants, 13 mutants displayed a characteristic phenotype of an exaggerated prevacuolar organelle similar to an aberrant endosome and hence were given the term 'class E compartment' [14, 15]. All of these 13 class E mutants exhibited deficiency in MVE biogenesis and blocked delivery of the cargo proteins to the vacuole (lysosome). Further biochemical characterization of these yeast mutants led to the identification of the ESCRT-I, ESCRT-II and ESCRT-III complexes.

The ESCRT protein family comprise of approximately 30 proteins that assemble into four complexes namely the ESCRT -0, I, II, III, and Vsp4. The ESCRT-0 complex comprises of HRS (hepatocyte growth factor regulated tyrosine kinase substrate) that recognizes monoubiquitinated cargo proteins and

associates with STAM (signal transduction adaptor molecule, additional ESCRT-0 component), and two non-ESCRT proteins namely Esp15 and clathrin [16, 17]. Depletion of the HRS or STAM leads to a decrease in exosome secretion and defects in the ILV formation [18, 19]. The HRS protein then facilitates recruitment of the tumor susceptibility gene 101 (TSG101) of the ESCRT-I complex [20, 21]. The ESCRT-I further recruits ESCRT-III via ESCRT-II or Alix [22]. Functionally, the ESCRT-0 sequesters and acquires ubiquitinated cargo proteins, the ESCRT-I and –II complex play a role in membrane deformation to form buds, and the ESCRT-III drive vesicle scission [23]. Ultimately, the ESCRT machinery dissociates from the membrane by AAA+ ATPase VPS4 [24]. Overall, the ESCRT machinery plays a critical role in ILV biogenesis, which has implications in higher mammals. Indeed, a knockout of the ESCRT proteins like HRS and TSG101 leads to a morphogenesis defect in mice. They die at an embryonic development day 11 (E11) and E8 and E6 [25, 26].

Exosomes biogenesis can also occur through alternative mechanisms; the ESCRT-independent mechanisms. Several studies have highlighted the importance of lipids, tetraspanins, as well as heat shock proteins in this pathway. This stemmed from the fact that cells depleted of the ESCRT components were still capable of forming a MVE [27]. This was initially demonstrated in oligodendroglial cell lines. The inhibition of an enzyme that hydrolyzes sphingomyelin to ceramide (nSMase) by GW4869 (hydrochloride hydrate), an inhibitor of neutral sphingomyelinases led to a significant decrease in the myelin proteolipid protein or lipophilin (PLP)-bearing exosome release [28]. Hence

suggesting that the PLP bearing exosomes are sorted into MVE independent of ESCRT complex, however, requiring ceramide synthesis. In addition, the MVE are also enriched in exosomes containing cholesterol. Specifically in patients with Niemann-Pick type C1 disease, loss of function of the *npc1* gene leads to an excessive accumulation of the cholesterol and sphingolipids in the late endosomal/ lysosomal (LE/Lys) structures. This accumulation of lipids within the LE/Lys compartments leads to demylelination and neurodegeneration. Under both, the cholesterol accumulation due to *npc1* loss or U18666A treatment, there is an accumulation of cholesterol in the MVE that also resulted in the upregulation of exosome secretion [29]. Besides cholesterol, phospholipase D2 (PLD2) that promotes the hydrolysis of phoshatidylcholine (PC) to phosphotidic acid (PA) has been shown to promote exosome biogenesis. The running model is that the PA induces curvature of the inner endosomal membrane supporting ILV formation [30, 31]. Furthermore, exosomes are also enriched in the four-transmembrane spanning proteins called tetraspanins [32]. CD63 and CD81 tetraspanin proteins have been shown to promote protein sorting independent of the ESCRT's into ILVs [33, 34]. Specifically, in melanoma, CD63 has been shown to promote sorting of the melanosomal protein into ILVs [34].

Additionally, a small integral protein of the LE/Lys origin called SIMPLE has been shown to be secreted in association with the exosomes [22]. The stromal fibroblast cells carrying mutant form in the Charcot Marie-Tooth disease patients, CMT1C, also secrete decreased amounts of CD63 and ALIX containing exosomes. Overall, the potential mechanistic role of SIMPLE along with

additional ESCRT-independent exosome pathway effectors is still poorly understood. Hence, future studies addressing the mechanistic characteristics of each of the above ESCRT-independent pathways of exosome biogenesis and sorting are essential.

Exosome secretion

Over the past few years, mechanisms driving the fusion of MVEs to the plasma membrane are being unraveled. Studies have shown the role of Rab GTPases that regulate the secretion from the late endosomes and/or the recycling endosomes. These Rab GTPases include Rab27a, Rab27b, Rab5, Rab11, and Rab35 [5, 35-39]. Interestingly these Rab GTPases are known to control distinct steps in the membrane trafficking pathway (Figure 2). For instance, Rab27a is important for docking of MVE to the plasma membrane [36]. Furthermore, several Rab proteins are involved in vesicle budding, vesicle and organelle motility along the cytoskeletal machinery along with the docking at the plasma membrane, resulting into a fusion in a well coordinated manner [40].

In addition to the Rab GTPases, at the plasma membrane, fusion process involves the soluble NSF-attachment protein receptor (SNARE) complexes. For example the SNARE proteins SNAP-23 along with VAMP7 and VAMP8 are involved in a Ca^{2+} mediated fusion of secretory lysosomes with the plasma membrane in several different cell types [41-43]. Interestingly, the SNARE protein, VAMP7 inhibition impaired lysosomal secretion but not necessarily exosome secretion [44]. These data would suggest multiple mechanisms via which the fusion and docking events are occurring at the plasma membrane. One model would be

perhaps coordination between the Rab GTPases as well as the SNARE complexes during different stages of exosome secretion.

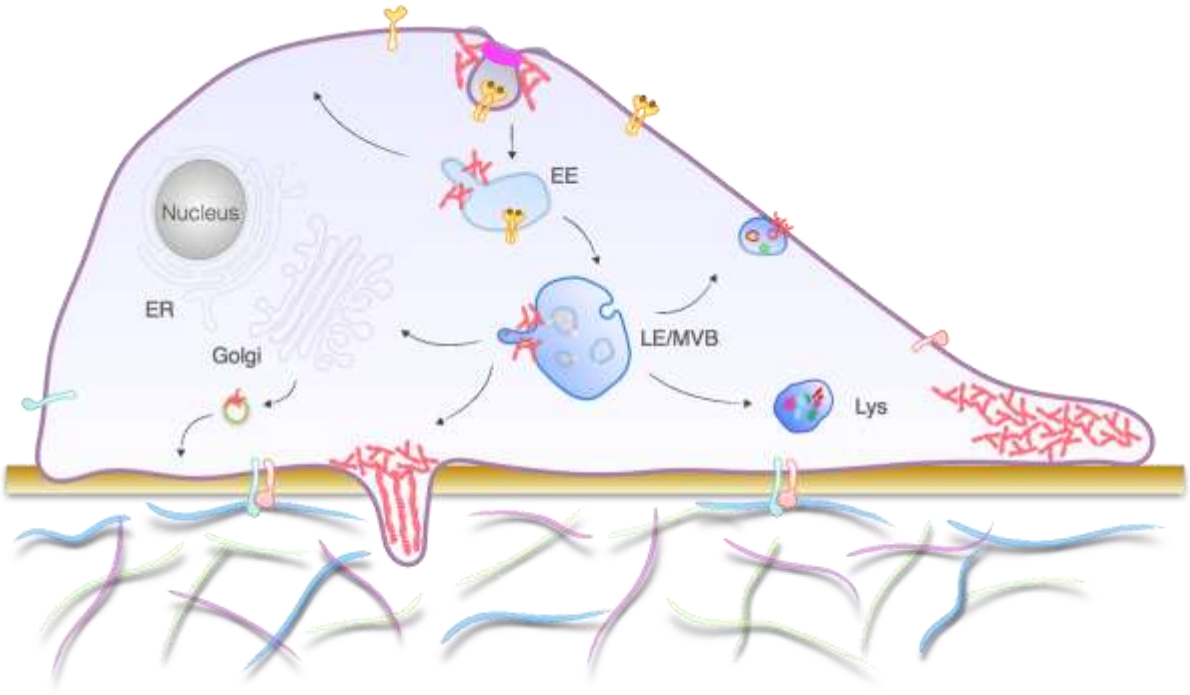

Figure 2 Membrane trafficking pathways in cell. Actin polymerization is important at several steps in the membrane trafficking pathway. From endocytosis, LE/Lys maturation, and exocytosis. In addition, Rab GTPases like Rab5 and Rab27a play a key role in transition from early endosome to late endosome and MVE docking at the plasma membrane. Image courtesy of Nan Hyung Hong.

Exosomes contribute towards cancer progression

Since the discovery of exosomes in 1980s, the exosome secretion has been linked to several pathological diseases including cancer, neurodegenerative diseases, and infectious diseases.

Transformation of the epithelial cells alone does not account for a disease as devastating as cancer. The interaction of the stroma plays an integral role as well. Ultimately this leads to cancer aggressiveness by promoting localized invasion of the primary tumor along with metastasis formation. During each step of tumor formation and progression, exosomes play an important role [45]. The exosomes released at the site of primary tumor can contribute towards localized invasion and increased cell motility [35, 46]. Also, exosomes disseminated from the primary tumor promote vascular leakiness [37, 47]. Exosome can also reach distant organs where they play an important role in the pre-metastatic niche formation that leads to metastasis [37, 48, 49]. Specifically, work done by Peinado et.al. 2012 shows that the exosomes derived from melanoma tumor containing the receptor tyrosine kinase MET increased metastatic behavior of the primary tumors by educating the bone marrow progenitors cells. However, exosomes secreted from a less aggressive tumor did not have the same effect [37]. Furthermore, recent studies have shown how exosomes bearing specific cargo proteins can determine key pre-metastatic niche sites. For example, in a pancreatic cancer, liver instead of any other organ took up exosomes derived from Pan02 cells more efficiently. This observation was seen in other tumor models as well including breast, colorectal, uveal etc. It was determined that different tumors bear different

integrins that target exosomes to specific organs where the integrins interact with a cell associated extracellular matrix (ECM) mediating uptake of exosomes by the organ. In the case of a pancreatic cancer, $\alpha_v\beta_5$ expressing exosomes were found in the liver [49]. Overall, better understanding of the regulation of exosomes is key to unraveling future treatment strategies for cancer patients.

Actin cytoskeleton machinery and its role in membrane trafficking

The remodeling of the actin cytoskeleton machinery provides dynamic forces that are key to numerous biological processes like sensing environmental forces, vesicular trafficking and cytokinesis [50]. Also, the actin cytoskeleton is important during budding, fission and transport of golgi derived vesicles [51]. Additionally, during endocytosis, the actin cytoskeleton provides physical force needed for membrane invagination and for the scission of endocytic vesicles from the plasma membrane [52]. The filamentous-actin (F-actin) dynamics has been shown to be important at various steps during the clathrin-mediated endocytosis including coated pit formation, constriction and vesicle scission [53].

Actin is known to exist in two states within the cell, namely, the monomeric globular (G)-actin and the filamentous (F)-actin. F-actin is formed by spontaneous addition of adenosine triphosphate (ATP)-bound G-actin at the barbed (or plus (+)) end and dissociation of adenosine diphosphate (ADP)-bound monomers at the pointed (or minus (-)) end. This process is spatiotemporally regulated by a number of actin-binding proteins, nucleation factors (e.g., Arp2/3 complex, formins), actin monomer-binding proteins, capping proteins, and stabilizing/destabilizing factors [54-57]. In order to initiate formation of new actin

filaments, nucleation factors like formins and the actin-related protein 2/3 (Arp2/3) complex are needed. Formins that associate at the barbed end mediate actin nucleation, such as those in the stress fibers. Also, the Arp2/3 complex nucleates and organizes branched filament networks in structures like the lamelapodia. On it's own, Arp2/3 has very weak nucleation activity, hence a need for nucleation promoting factors (NPFs). Most mammalian NPFs belong to the Wiskott-Aldrich syndrome protein (WASP) family (Class I), including WASP, neural WASP (N-WASP), WASP family verprolin homologue (WAVE/SCAR), WASP homologues associated with actin, membrane, and microtubules (WHAMM), and WASP and SCAR homologue (WASH). The Class I NPFs have verprolin homology, cofilin homology, and acidic (VCA) domain. They bind to the G-actin via V motif and Arp2/3 via CA motif. The Class II NPFs includes cortactin that interacts with Arp2/3 and F-actin via Arp2/3 interacting acidic region and the 4^{th} repeat region of the protein (Figure 3) [58]. This interaction usually results in weak activation that may not be physiologically relevant in the absence of a Class I NPF. However, the key function of Class II NPFs is likely to support a synergistic activation of the Arp2/3 complex along with the Class I NPFs. Members of the WASp family proteins initiate actin polymerization in different subcellular locations and SCAR/WAVEs are responsible for activating the Arp2/3 complex in lamellipodia [59], while the N-WASP regulates endocytosis at the plasma membrane along with the formation of specialized invasive structures such as the podosomes and invadopodia. Additionally, WHAMM is important for Golgi function, while WASH is important for endosomal sorting [60-62].

For the past several decades, exocytosis has been extensively studied. The process of exocytosis is important in several cellular and biological processes as it is a key to cell-cell communication. Besides playing an important role in the endocytosis, branched actin networks that are at the surface of the endosomes play a role in regulating several steps involving the cargo sorting via regulation of membrane 13tabilizin and fission and eventually leading to the exocytosis. For example, silencing of the Arp2/3 complex or inhibiting actin polymerization using inhibitory drugs have been shown to result in enlarged endosomes [63, 64]. Another study showed that the membrane tubules carrying cargos such as the β2 adrenergic receptor (B2AR) are stabilized by branched actin networks. However, upon perturbation of the actin assembly, it led to a defective accumulation of B2AR in the endosomes [65]. Also, WASH was recently identified as a major Arp2/3 NPF on the endosomes that is important during cargo sorting. Knockdown of WASH resulted in endosomes with exaggerated tubules suggesting a defect in fission [61, 62]. This excessive 13tabilizin in WASH knockdown cells is also associated with the impaired transport of various cargos, including transferrin receptor, integrins, mannose-6-phosphate receptor, and EGFR [61, 62, 66-68].

Local actin dynamics at the site of exocytosis leads to an increase in cell surface along with the secretion of cargos that are being carried within vesicles and MVEs. Studies have shown the assembly of F-actin around secretory vesicles allowing for an efficient fusion [69]. Hence, actin functionally stabilizes secretory vesicles during the docking process at the plasma membrane. Work

done by Yu et.al. 2007 show that the fusion of secretory vesicles with the plasma membrane initiates local actin assembly. Incorporation of diacylglycerol (DAG) from the plasma membrane to the secretory vesicle along with recruitment of the protein kinase Cβ (PCK) occurs. Ultimately, this leads to activation of the GTPase Cdc42 [70]. Cdc42 activation further promotes actin coat polymerization by activating downstream effectors Toca1 and N-WASP [69-71]. In addition, the exocyst complex also plays a key role in promoting tethering of secretory vesicles with the plasma membrane. Specifically, Exo70 binds to the Arp2/3 complex and promote cell migration [72].

One of the key docking sites found at the plasma membrane are called invadopodia. Invadopodia are actin-rich protrusions that are found to be associated with sites of proteolytic degradation [73]. Invadopodia are characteristic of invasive cancer cells. Src kinase signaling and Src kinase substrates are found to be associated with the invadopodia formation. Some of them include cortactin, dynamin, AMAP1/ ASAP1, N-WASH, and Tks5. Also, recently exosome secretion was found to be critical for both invadopodia formation and function [35].

Cortactin and its cellular functions

Cortactin, an actin-nucleation promoting factor is not only critical for regulating actin cytoskeleton, but also serves as a key player in aggressive cancers [74, 75]. Cortactin was originally identified as a substrate for Src non-tyrosine kinase receptor molecule and received its name due to localization at cortical actin structures [76]. Mechanistically, cortactin has been extensively

investigated over the past decade for its role in cell migration and invasion. Structurally, cortactin protein has four main domains (Figure 3). The N-terminal end of the protein is thought of as an actin assembly region where interaction with Arp2/3 complex and F-actin can be found at the acidic and repeat domain. The C-terminal end of the protein is thought of as a signaling end, where phosphorylation by several kinases can take place in the proline rich region followed by an SH3 domain where interaction with several proteins like cytoskeletal, and those involved in membrane trafficking, and signaling takes place. Hence also serving a scaffolding function [77].

Cortactin comprises of three main splice variants, namely A, B, and C. The three major variants comprise of 6.5, 5.5, and 4.5 of the cortactin repeat domains [78, 79]. Loss of repeat regions due to alternative splicing has been shown to affect binding affinity of cortactin with the F-actin, along with decrease in localization at cortical actin and decrease in cell motility [78-80]. In addition, post-translational modification of cortactin has been shown to affect both cell migration, and invadopodia activity. For example, phosphorylation of tyrosine, serine and/or threonine residues of cortactin can occur via numerous upstream factors. Some of these factors are fibroblast growth factor (FGF), epidermal growth factor (EGF), platelet-derived growth factor (PDGF), and integrin activation [81-86]. Most of the phosphorylation is known to occur within the proline rich region of cortactin (Figure 3). For instance, Src kinase phosphorylation of cortactin affects the SH3 domain accessibility, while the tyrosine phosphorylation increases binding affinity of cortactin to the SH3 domain and its binding partner

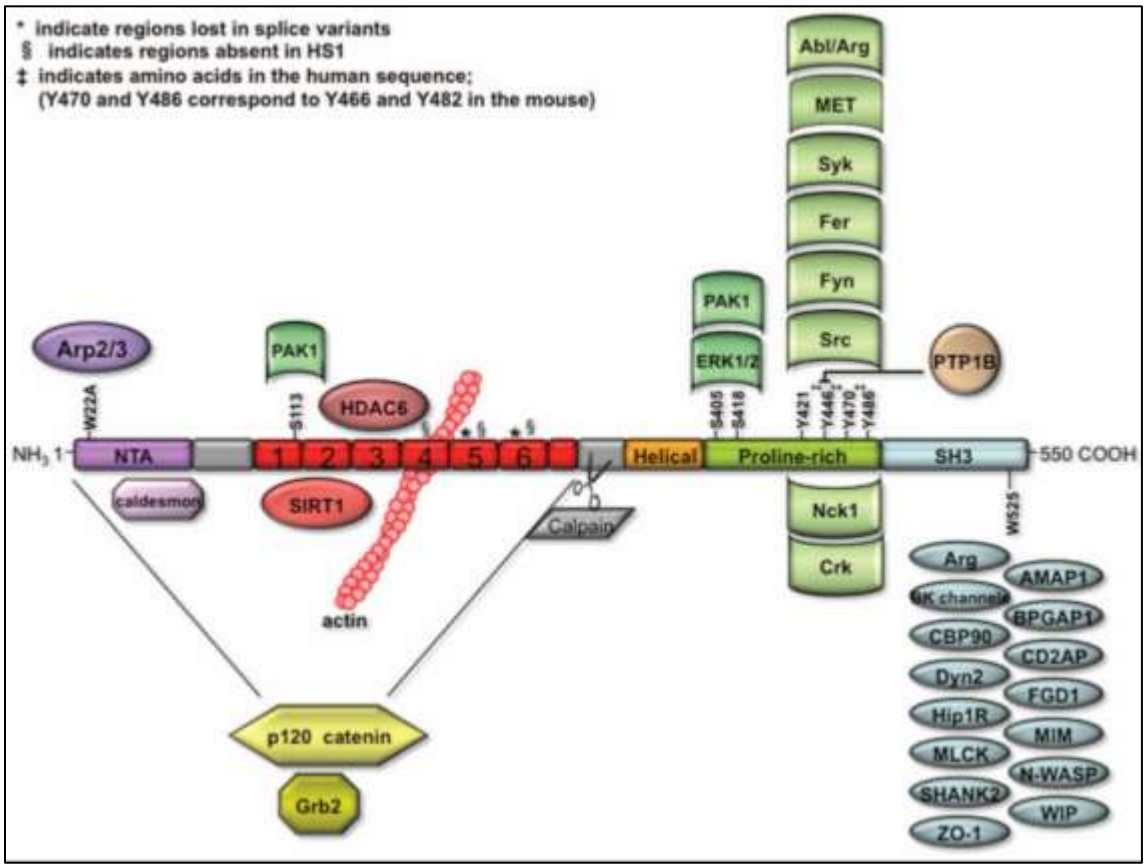

Figure 3. Structure of cortactin. The above schematic of the protein cortactin displays four main regions of the protein. The N-terminal region, an actin assembly region where interaction with Arp2/3 and F-actin takes place. The C-terminal end, a signaling end, consists of proline-rich region followed by SH3 domain. Figure is taken from [58].

Dynamin 2 [87]. Also, Erk phosphorylation increases accessibility to the SH3 domain that results in an increased binding of N-WASp with cortactin [88]. This interaction further supports Erk-regulated cell motility and lamellapodia dynamics. Furthermore, acetylation of cortactin within tandem repeats is also reported. Acetylation of cortactin affects F-actin binding as well as cell motility [89, 90]. On the other hand, cortactin deacetylation by HDAC6 regulates invadopodia activity and cortactin acetylation at invadopodia [91].

Cortactin and its association with the Arp2/3 and F-actin play an important role in various cellular activites including cell migration and invasion. In vitro studies have shown that cortactin regulates branched actin assembly via various mechanisms. For example, activation of Arp2/3 complex, stabilization of branched actin; further enhancing activation of Arp2/3 complex by WASp along with scaffolding of key actin regulators N-WASP and WIP [92-95]. One unique function of cortactin is to stabilize newly polymerized actin networks as it has an affinity towards ATP-bound and ADP-Pi bound actin [93, 96]. Infact, upon knockdown of cortactin, faster turnover of actin occurs [97]. Overall, cortactin plays an important role in 17tabilizing newly polymerized branched actin networks. This stabilization of the actin network is of importance, especially during the exocytosis process where secretory vesicles including MVEs dock at the plasma membrane.

Cortactin mediated regulation of cell motility and invasion could in part be due to its role in regulating membrane trafficking. Indeed, previous work done in our lab has demonstrated that cortactin manipulation affects secretion MMP2,

MMP9, surface expression of MT1-MMP, and apolipoprotein A1 from cancer cells [98]. This could be due to several reasons. Firstly, cortactin mediated regulation of trafficking from the Golgi compartments [99]. Secondly, cortactin mediated regulation of trafficking from LE/Lys compartments [46, 63, 77, 100]. Indeed, both MMP9 and MT1-MMP have been found to be associated with LE/Lys and MVEs compartments and this association has been shown to be important for delivery of MVEs to invadopodia [35, 101-103]. Besides MMPs, cortactin also regulates secretion of extracellular matrix proteins (ECM) like fibronectin (FN) from LE/Lys compartments [100]. One of the questions that still remain unanswered is what determines trafficking of LE/Lys and MVE compartments to the plasma membrane versus fusion with the lysosomes? Does cortactin help in determining these distinct populations? What additional factors does cortactin associate with during the trafficking of sub-populations destined for different locations within a cell? This is of importance because much of the earlier interest in cortactin stemmed from the finding that cortactin gene, CTTN, which is present on 11q13 amplicon is amplified in head and neck cancer as well as breast cancer [104]. Subsequently cortactin overexpression was also observed in several different cancer types such as melanoma, ovarian, gastric, colorectal, hepatic, and esophageal [105-111]. While the 11q13 amplicon comprises of additional genes much work has been done on FGF family members, FADD, Cyclin D1, and cortactin [112, 113]. Amongst these genes, study done by Rodrigo et.al., reported that independent of cyclin D1 amplification, a major oncogene in various cancers, cortactin amplification correlated with a decreased patient survival [114]. In addition

to amplification, overexpression of cortactin has been shown to correlate with poor prognosis independent of the tumor stage and the lymph node status ([114], Figure 16, 17). Studies done in our lab in HNSCC have shown that cortactin overexpression regulates invasiveness of cancer cells. There is a significant increase in invadopodia activity and in a semi-orthotopic mouse model; cortactin expression regulates invasive ability *in vivo* [98, 115]. In my dissertation work I show that cortactin mediated MVE trafficking that leads to exosome secretion can account for cortactin associated aggressive cancer traits both *in vitro* and *in vivo* (Chapter IV).

CHAPTER II

MATERIALS AND METHODS

Cultured Cells

Cellular growth conditions

Head and neck squamous cell carcinoma (SCC61) parent cell lines manipulated for cortactin expression were used (refer Table 1). They were obtained from Dr. Wendell Yarbrough laboratory, currently at Yale University. SCC61 were maintained in Dulbecco's Modified Eagle's Medium (DMEM) (Life Technologies, Carlsbad, CA). DMEM was supplemented with 20% fetal bovine serum (FBS) (Hyclone; GE Healthcare Life Sciences, Marlborough, MA), 0.4μg/ml hydrocortisone to maintain SCC61 parent cell lines. Cortactin knockdown (KD) and cortactin KD/ rescue mutant cell lines were maintained in SCC61 parent cell media with 4μg/ml puromycin (Calbiochem, San Diego, CA) or 4μg/ml puromycin and 10μg/ml blasticidine (Invivogen, San Diego, CA) as a selection antibiotic. Cortactin overexpression (OE), cortactin OE (shLacZ), and cortactin OE (Rab27a knockdown) cell lines were maintained in SCC61 parent cell media with 10μg/ml blasticidine or 10μg/ml blasticidine and 4μg/ml puromycine as a selection antibiotic. SCC61 shLacZ and Rab27a KD cells were maintained in SCC61 parent cell media supplemented with 10μg/ml blasticine. SCC61 Rab27aKD (shLacZ) and Rab27a (Coronin 1b KD1/2) were maintained in SCC61 parent media with 10μg/ml blasticidine and 4μg/ml puromycine selection

antibiotic. HT1080 fibrosarcoma cell lines were obtained from American Type Culture Collection (ATCC, Manassas, VA). HT1080 parent and cortactin manipulated cell lines (refer Table 1) were maintained in DMEM supplemented with 10% bovine growth serum (BGS) (Hyclone, GE Healthcare Life Science, Marlborough, MA) and 4μg/ml puromycin as a selection antibiotic for cortactin KD and control (Sc) cells. MDA-MB-231 cells were obtained from ATCC. MDA-MB-231 cells were maintained in DMEM, 10% FBS and 10μg/ml blasticidine for cortactin control (mock vector) and cortactin OE cells lines (refer Table 1). Phoenix 293 packaging cells (Phoenix cells) were obtained from Dr. Gary Nolan, Stanford University and 293FT cells were obtained from ATCC. They were maintained in DMEM supplemented with 10% FBS (heat inactivated for 30 min at 56^0 C for Phoenix cells and regular for 293FT cells) (refer Table 1).

Retroviral and lentiviral generation of shRNA and overexpression vectors

Retroviral and lentiviral methods of RNAi-mediated knockdown or cDNA overexpression were utilized for this doctoral dissertation work. For generating stable cortactin scramble control (Sc) and cortactin KD1/2 cell lines, retroviral vectors containing the targeted sequence (refer Table 1) were generated by inserting into pRetroSuper as previously described [96]. To generate stable cell lines with lentiviral shRNA vectors (shLacZ, Rab27a-1) (refer Table 1) were cloned into pLenti6/Block iT™ (Invitrogen) as previously described [35]. Also, pKLO.1 lentiviral expression system (Dharmacon) was used for generating Coronin1b stable knockdown and Rab27a KD in cortactin OE cell lines (refer Table 1). Stable cortactin expression constructs were made by inserting full-

length or mutant mouse cortactin molecules from pCDNA or LZRS constructs [100] into pLenti6-v5 (Life Technologies) using gateway cloning system. Empty pLenti6-v5 construct was used as the empty vector control for cortactin overexpression experiments.

Protein harvest

Cells were trypsinized to determine cell number or $1x10^5$ cells were seeded in a 6-well dish (Corning, Corning, NY) overnight and harvested by adding Sodium Dodecyl Sulphate lysis buffer (10mM Tris (pH 7.4), 1% Sodium Dodecyl Solution (SDS), and double distilled water (ddH_2O)) supplemented with protease inhibitor cocktail (P8340, Sigma, St. Louis, MO). Harvested cells were then boiled at 95^0C for 10 min. The sample was then passed few times through 1ml TB syringe 27G x ½ needle (Becton, Dickson and Company, Franklin Lakes, NJ), spin for 15 min at 13,000 RPM at 4^0C. The supernatant was then collected. Protein concentration was then determined using BCA assay (Thermo Scientific, Waltham, MA).

Protein concentration in exosomes was determined by diluting the exosome sample at 1:1 ration with the SDS lysis buffer. The sample was boiled at 95^0C for 10 min. Sample was then cooled for 5 min at 4^0C. Micro BCA assay was used to determine protein concentration (Thermo Scientific, Waltham, MA). Both cell and exosome lysates were then stored at -80^0C.

Table 1: List of cell lines used and vectors used.			
Cell types	Vector expression system	Expressing constructs	Selection marker
SCC61 (scramble)	pRetroSuper	5'-gaccgcacatgagatgaga-3'	Puromycin
SCC61 (cortactin KD1)	pRetroSuper	5'-gcacgagtcacagagagat-3'	Puromycin
SCC61 (cortactin KD2)	pRetroSuper	5'-aagctgagggagaatgtct-3'	Puromycin
SCC61 shLacZ	pLenti/Block iT	Addgene, [35]	Blasticidine
SCC61 Rab27a sh1	pLenti/Block iT	5'-gtgcgatcaaatggtcatgcc-3', [35]	Blasticidine
SCC61 cortactin OE/ control	pLenti6-V5 and pKLO.1	Dharmacon, [100]	Blasticidine and puromycine
SCC61 cortactin OE/ Rab27a sh1	pLenti6-V5 and pKLO.1	Dharmacon, [100]	Blasticidine and puromycine
SCC61 cortactin KD1/ WT cortactin	pRetroSuper and pLenti6-V5	[100]	Puromycin and blasticidine
SCC61 cortactin KD1/ W22A	pRetroSuper and pLenti6-V5	[100]	Puromycin and blasticidine
SCC61 cortactin KD1/ Δ4RP	pRetroSuper and pLenti6-V5	[100]	Puromycin and blasticidine
SCC61 cortactin KD1/ 3Y	pRetroSuper and pLenti6-V5	[100]	Puromycin and blasticidine
SCC61 cortactin KD1/W525K	pRetroSuper and pLenti6-V5	[100]	Puromycin and blasticidine
SCC61 Rab27a sh1/ shLacZ	pKLO.1	Dharmacon	Blasticidine and puromycin
SCC61 Rab27a sh1/ coronin 1b KD1	pKLO.1	Dharmacon (TRCNC0000116423)	Blasticidine and puromycin
SCC61 Rab27a sh1/ coronin 1b KD1	pKLO.1	Dharmacon (TRCNC0000116424)	Blasticidine and puromycin
SCC61 shLacZ	pKLO.1	Dharmacon	Puromycin
SCC61 MT1 MMP sh1	pKLO.1	Dharmacon (TRCN0000050853)	Puromycin
SCC61 MT1 MMP sh3	pKLO.1	Dharmacon (TRCN0000050855)	Puromycin
HT1080 (Sc and cortactin KD)	pRetroSuper	[100]	Puromycin
MDA MB 231 (control and cort OE)	pLenti6-V5	[63]	Blasticidine
293 FT and Phoenix			

Table 1: Cell lines used to study the role of cortactin in exosome secretion. Listed are the cell lines that were engineered to expresses cortactin and it's mutants, cortactin KD, Rab27a KD, Coronin 1b KD, and MT1MMP KD. The table also lists the source of the vectors used along with the selection markers.

Immunoblot Analysis

Protein lysate was boiled in 5x Laemmli sample buffer containing β-mercaptoethanol and DTT for five minutes and then separated using SDS polyacrylamide gel electrophoresis (SDS-PAGE). Proteins were transferred to nitrocellulose membranes 0.2μ (Bio-Rad Laboratories, Inc., Hercules, CA) using the Protein Electrophoresis chamber (Bio-Rad Laboratories, Inc., Hercules, CA) system. Membranes were blocked in 5% nonfat dry milk dissolved in TTBS (100mM Tris-HCL pH 7.5, 150mM NaCl, 0.1% Tween-20) for one hour at room temperature and incubated in primary antibody overnight at 4˚C. All antibodies used in immunoblot analysis and the concentrations at which they were used can be found in Table 2. Following primary antibody incubation, immunoblots were washed three times in TTBS (50 mM Tris, 150 mM NaCl, and 0.05% Tween 20 pH 7.6). Following these washes, immunoblots were incubated for an hour in HRP-conjugated secondary antibodies or alexa-680 or alexa-800 conjugated seconday antibodies. The immunoblots were then washed three times with TTBS for 15 min to remove excess secondary antibodies. Finally, regular or femto chemiluminescence (ECL) regent (Thermo Scientific, Waltham, MA) or Odyssey (LI-COR biosystem, Lincoln, NE) was used for film or immunoblot exposure for visualization of protein expression levels.

Antibodies

The antibodies used are mouse anti-TSG101 (clone 4a10, GeneTex), mouse anti-Flotillin1 (610820, B.D. Bioscience), mouse anti-cortactin (4F11, Millipore), rabbit anti-CD63 for WB (ab68418 or ab134045, Abcam) and mouse anti-CD63

for IF or endocytosis-EM studies (ab8219, Abcam), mouse anti-Coronin 1b for WB (ab119071, Abcam), rabbit anti-Coronin 1b for IF (kind gift from Dr. James E. Bear, UNC Chapel Hill), rabbit anti-EGFR (1005: sc-03, Santa Cruz), rabbit anti-MMP9 (ab38898, Abcam and Calbiochem), rabbit anti-Rab27 for WB (r4655, Sigma), mouse anti-MMP2 (F68, Daiichi Fine Chemical), rabbit collagen Type 1 (600-406-103, Rockland), and mouse anti-MT1-MMP (Clone ID8 [116])

Exosome Isolation And Characterization

Differential centrifugation strategy

Nearly 3 x 10^6 SCC61, HT1080, and MDA-MB 231 cells per T150 flask (Cornin, Corning, NY) were seeded. Once the cells reached 80% confluence, cells were cultured in 15 ml of OptiMEM (Thermo Fisher Scientific, Waltham, MA) per T150 flasks for 48 h. Ultra centrifuged exosomes (UC exosomes) were isolated from conditioned media by serial centrifugation at 300g for 10 min, 2,000g (4,000 r.p.m. in Ti45 rotor) for 30 min, 10,000g for 30 min (9,300 r.p.m. in Ti45) and 100,000g (30,000 r.p.m. in Ti45) for 16 h - 18 h to respectively sediment live cells, dead cells, debris and microvesicles and UC exosomes. UC exosomes were then normalized to the total cell number that is determined after 48 h condition media collection. For example, for every 10 x 10^6 million cells, UC exosomes was resuspended in 50 μl of ice cold 1X PBS.

Density gradient strategy

Further purification of UC-exosomes by density gradient, a discontinuous iodixanol gradient was prepared. Solutions (40% (w/v), 20% (w/v), 10% (w/v) and

5% (w/v)) of iodixanol were made by diluting OptiPrep (60% (w/v) aqueous iodixanol, Axis-Shield PoC, Oslo, Norway) with 0.25 M sucrose/10 mM Tris, pH 7.5 from the bottom to the top of a 14 X 89 mm polyallomer tube. UC exosomes were added on a top of the gradient and continuous gradient was made through UC at 100,000g (24,000 r.p.m. in SW40 Ti rotor) for 18 h. Twelve density gradient (DG) fractions were collected and diluted in PBS before pelleting through another round of ultracentrifugation at 100,000g for 3 h, washing and resuspension in PBS.

Nanosight Particle Tracking Analysis (NTA)

UC exosomes were diluted with ice cold PBS (1:1000 or 1:500) to a final volume of 1ml. DG exosomes were diluted with ice cold PBS (1:100) to a final volume of 1ml. The sample was then passed through the nanosight chamber. Once the laser beam run through the sample, based upon the principle of diffraction and Brownian motion, particle (MV or UC/DG exosome) concentration per ml is determined. Also, with the help of NTA analysis, size of the particles is determined. Graph Pad prism v.6 is used to plot particle traces along with graph plots.

Ultra-Structural Analysis Of Cells And Exosomes By Electron Microscopy

Transmission Electron Microscopy (TEM) of cultured cells

0.5 million cells (SCC61 Sc, and cortactin KD) were seeded on day 1 and cultured overnight. Next day the dishes containing cells were fixed for 1 h at room temperature and then overnight at 4^0C with 2.5% Glutaraldehyde in 0.1M

Cacodylate buffer with 1% CaCl. The dishes were slowly rocked all the time during fixation. Following overnight fixation, samples were washed extensively to remove unbound glutaraldehyde. Samples were then osmicated for 1 h in 1% aqueous Osmium tetroxide. Unbound osmium was removed by washing extensively. Following this, samples were en bloc stained in ethanolic uranyl acetate (UA) for 10 min. Followed by 2 times changes of 25% ethanol (10 min each) to thin our any UA precipitate. Dehydration is continued through increasing concentrations of ethanol and finally embedding in Epoxy resin is carried out. Thin sections were then overlayed on formvar copper grids for visualization. Samples were imaged on FEI/Tecnai 12 electron microscope at various magnifications.

Negative staining of exosomes

Formvar carbon film-coated grids (FCF-200-Cu; Electron Microscopy Sciences, Hatfield, PA) were washed in double distilled water, followed by 100% ethanol. For each step, excess liquid was removed by wicking with filter paper. The sample (10 μl) was added to the grid for 5 min. Grids were immediately stained with 2% phosphotungstic acid, pH 6.1 for 20s and allowed to dry overnight. Grids were imaged using a FEI Tecnai T12 TEM (120 kV LaB6 source), Gatan cryotransfer stage, and AMT XR41-S side mounted 2K X 2K CCD camera, 2102 SC. All exosome images were collected at 50,000X with an Advanced Microscopy Techniques CCD camera.

Multivesicular endosome visualization by TEM

For visualization of CD63 positive MVE, SCC61 control and cortactin-KD1 cells were incubated for 30 min at 37^0C with anti-CD63 antibody (MEM-259 ab8219 Abcam, Cambridge, MA) labeled with HRP (Z 25054, Molecular Probes, Eugene, OR). Cells were then washed with PBS and fixed for 1h in 3% glutaraldehyde in 0.1M sodium cacodylate (NaCaC) buffer. After several washes in 0.1M NaCaC, cells were incubated with DAB (Electron Microscopy Sciences, Hatfield, PA) in 0.05M Tris-HCl, at pH 7.6. The enzymatic reaction was started by adding H2O2 to a final concentration of 0.01% and allowed to proceed for 30 min. The cells were washed 3X with 0.05M Tris-HCl buffer. After a brief wash with water, cells were washed 3X with 0.1M NaCaC buffer. The cells were then post fixed with 1% osmium tetroxide in 0.1M NaCaC buffer, then washed with 0.1M NaCaC buffer and cells are scrapped, re-suspended in pellet in 0.1M NaCaC buffer and then briefly washed with water. The cells were then incubated with 1% UA (en bloc) for 10 min. Next, cells were dehydrated through a graded ethanol series (30%, 50%, 75%, 85%, 95%) for 15 min each. Cells were further dehydrated with 100% ethanol and propylene oxide (PO). Following this, cells were infiltrated with a 3:1 mixture of PO and epoxy resin for 30 min then 1:1 ratio of PO and resin for 1h and subsequently overnight. The next day, samples were infiltrated with 1:3 mixture of PO and resin followed by 6 changes of pure resin for 36h. Then the pellet was embedded for 48h in epoxy resin at 60^0C. Sections (70nm) were collected on copper grids and cells were counterstained with 2%

uranyl acetate and Reynold's lead citrate. Samples were imaged on FEI/Tecnai 12 electron microscope at various magnifications.

Scanning electron microscopy of cultured cells

Samples were fixed in 2.5% Gluteraldehyde in 0.1M Cacodylate buffer, pH7.4 at room temperature (RT) 1 hour then transferred to 4ºC, overnight. The samples were washed in 0.1M Cacodylate buffer, then incubated 1 hour in 1% osmium tetraoxide at RT then washed with 0.1M Cacodylate buffer. Subsequently, the samples were dehydrated through a graded ethanol series and then 3 exchanges of 100% ethanol, followed by critical point drying. Samples were dried in a Tousimis Samdri-PVT-3D critical point dryer, then mounted on aluminum stubs with carbon adhesive tabs. The samples were then sputter coated with gold/palladium target using the Cresssington Sputter Coater. After coating for 90 seconds, the samples were imaged using the Quanta 250ESEM.

Immunofluorescence

Constructs used for fixed and live imaging

EGFP-CD63 was a kind gift from Dr. Gillian Griffiths. mEGFP-F-Tractin was a gift of Dr. Robert Fischer at NHLBI and was created by cloning the 9-52 stretch of the F-actin binding protein ITPKA [117] into pCMV-Tag2A-mGFP. For mCherry-MMP9, pCEP4-MMP9 was used as a template. mCherry was added to the c-terminus of MMP9, which was then subcloned into pENTR vector and recombined into pLenti6-v5 using gateway cloning system (Life technologies,

Carlsbad, CA). EGFP-Rab5 Q79L construct was commercially obtained (Addgene, Cambridge, MA).

Confocal Microscopy

To visualize CD63 in Rab5Q79L-positive endosomes, 5 X 10^5 SCC61 control and cortactin-KD cells were cultured on Fibronectin-coated glass coverslips in 6-well or 35 mm dishes. Cells were transfected with EGFP-Rab5Q79L and 24 h later were fixed using 4% PFA for 10 min, and then permeabilized for 15 min with 0.1% Saponin in 3% BSA in PBS. Primary antibody anti-CD63 (MEM--259 ab8219 Abcam, Cambridge, MA) was incubated in 0.05% Saponin (A18820, Alfa Aesar, Haverhill, MA) and 3% BSA (RPI, Mount Prospect, IL) in PBS for 1 h at room temperature. Secondary antibody anti-mouse Alexa 647, and rhodamine phalloidin in 3% BSA in PBS were incubated for 1 h at room temperature. Similar steps were followed for immunofluorescent staining of CD63 in other experiments. Confocal images were obtained with a Zeiss LSM 510 (63X PlanApo objectives) using Argon2, HeNe, and HeNe2 lasers (fixed imaging) or Zeiss LSM 710 (63X PlanApo objectives) (live imaging). All the secondary probes were commercially obtained from Invitrogen/ ThermoFisher scientific, Waltham, MA.

Total Internal Reflection Fluorescence Microscopy (TIRFM)

TIRF microscopy was performed on a Nikon TiE inverted light microscope equipped with a perfect focus, Nikon TIRF illuminator, a ×100/1.49 numerical aperture TIRF objective (used in combination with a ×1.5 optivar), and Neo 5.5 cMOS camera (Andro).

Invadopodia Assay

An equal number of SCC61 shLacZ, Rab27a-KD, cortactin-OE (control), cortactin-OE Rab27aKD, SCC61-scramble, cortactin-KD1,2 cells were seeded on 10 μM FITC-labeled FN coated on top of 2% crosslinked gelatin on MatTek dishes, prepared as previously described [118] . Cells were cultured in invadopodia media (1:1 ratio of DMEM & RPMI media containing 10% Fetal Bovine Serum (HyClone; GE Healthcare Life Sciences, Marlborough, MA) and 5% Nuserum (Gibco; Thermo Fisher Scientific, Waltham, MA). 20 ng/ ml EGF (Invitrogen; Thermo Fisher Scientific, Waltham, MA) is added fresh each time for 18h before fixing and immunostaining. Cells were fixed with 4% PFA for 10 min, permeabilized using 0.1% Triton X in 3% BSA for 10 min, blocked with 3%BSA for 20 min. Cells were then incubated overnight with anti-coronin 1b (1:250) at 4^0C. The next day, cells were incubated with Rhodamine-Phalloidin (1:2000) and secondary Alexa-633 (1:500) for 1h at room temperature. Invadopodia plates were then mounted in anti-fade mounting reagent before imaging. Functional invadopodia, indicated by dark holes in the fluorescent matrix (FITC-FN) colocalized with actin and coronin 1b puncta, were analyzed for absolute intensity of coronin 1b within a boxed area of 4X4 pixels.

Mass Spectrometry And LC-MS/MS Analysis

Shotgun proteomic analysis

Shotgun proteomic analysis of purified exosomes was performed by first resuspending the exosomes in LDS sample buffer (Life Technologies), resolving the proteins approximately 1 cm using a 10% Novex precast gel, and then

performing in-gel tryptic digestion to recover peptides. The peptides were analyzed via MudPIT (Multidimensional Protein Identification Technology) essentially as described earlier [119, 120]. Briefly, digested peptides were loaded onto a biphasic pre-column consisting of 4 cm of reversed phase (RP) material followed by 4 cm of strong cation exchange (RP) material. Once loaded, the column was placed in line with a 20 cm RP analytical column packed into a nanospray emitter tip directly coupled to a linear ion trap mass spectrometer (LTQ). A subset of peptides was eluted from the strong cation-exchange (SCX) material onto the RP analytical via a pulse of volatile salt, separated by an RP gradient, and then ionized directly into the mass spectrometry where both the intact masses (MS) and fragmentation patters (MS/MS) of the peptides were collected. The peptide spectral data was used to query a protein database using Sequest [121] and the resulting identifications were collated and filtered using IDPicker [122] and Scaffold (http://www.proteomesoftware.com). Relative protein abundances were evaluated via spectral counting techniques using the Quasitel [123] program for P-value calculations. Protein groups were classified using Uniprot database and a Venn diagram was made using Microsoft Excel for Mac 2011, version 14.4.8.

Rescue Of Cortactin Knockdown (KD) Phenotypes By Exosomes

Serum-independent growth assay

On day 1, 25,000 cells (SCC61 control, cortactin-KD, shLacZ, and Rab27a-KD) were seeded in 6-well dishes in medium containing serum. The next day, cells were washed 3 times with PBS. Serum-free media containing no

exosomes or exosomes from either control or KD cell lines was then added to control and KD cells. After 4 days, cells cultured with or without exosomes were trypsinized and counted using a hemocytometer. N=3 independent experiments with duplicate technical replicates per condition.

Transwell Invasion assay

An equal number of SCC61 control, cortactin-KD, shLacZ, and Rab27a-KD cells were seeded on the top of BD Biocoat Matrigel-coated invasion chambers (8.0 μm pore size) in the presence of 2.5% exosome-depleted serum in DMEM on both sides of the filter. When added, exosomes derived from control or KD cells were added together with the cells on the topside of the filter. 48h later, cells were removed from the top of the filter using cotton swabs before staining for cells that had migrated to the bottom of the filter (Hematology staining kit, Richard Allen Scientific, Thermo Fisher Scientific, Waltham, MA). 5 bright field images per insert were taken using a Nikon Eclipse TE2000-E microscope equipped with a 20X Plan Fluor 0.3 NA objective. Cells per image were counted and averaged per replicate.

Semi- orthotopic rat trachea model for head and neck cancer (HNSCC)

The HNSCC tumor model was performed as described previously [124] and carried out under an IACUC approved animal protocol. SCC61 control, cortactin KD, shLacZ, and Rab27aKD cells ($1x10^6$) were suspended in 20 - 30 μl of DMEM containing 20% FBS with 0.4 μg/ml hydrocortisone in the presence or absence of 100 μg/ml of exosomes purified from control cells and inserted into the lumen of a denuded rat trachea through a small incision that was subsequently sutured

shut. Rat tracheas containing tumor cells were then inserted subcutaneously into the flanks of nude mice (1 trachea per flank). After one week, KD mice received biweekly subcutaneous injection at the site of tracheal implants of either 50 μg/ml of control exosomes in PBS or PBS. 5 weeks later, mice were sacrificed and tracheas were harvested and processed. Two independent experiments were carried out for each condition. Sample size for each experiment was 3 mice (6 tracheas per condition). A total of 12 tracheas from 6 mice per condition were processed. The Leica SCN400 slide scanner was used to scan tumors within tracheal cross section slides. Online digital image hub was used to measure the area of tumor.

Data Analysis And Statistics

Fixed Imaging conditions

Confocal Imaging: For confocal live cell imaging, SCC61 control, and cortactin-KD cells were cultured and transiently transfected with EGFP-CD63. After 24h, images were captured every 2s for 2 min. Imaris image processing software (Bitplane) was used to track CD63 positive MVEs from the confocal images to determine squared displacement of each MVE. A defined area located away from the nuclear region of each cell was selected for analysis (see representative tracks within the areas in Figure 9). Vesicles greater than 2 □m in size were excluded from the analysis. The autoregressive model algorithm was used and the tracks were generated. Diffusion coefficients (D) as $\mu m^2/s$ were calculated from the tracks.

Live Imaging conditions

TIRF imaging: For TIRF live cell imaging, SCC61 control, cortactin-KD, cortactin-OE and Rab27a-KD cells were plated on 25 μg/ml fibronectin-coated dishes. After 24h, images were captured every 100ms for 30s. For the shallow TIRF movies, imaging was performed with a standard laser angle to observe only fluorescence present at the cell-substrate interface whereas for the deeper TIRF movies the depth of penetration was calculated to be up to 1 μm from the plasma membrane using fluorescent 5 μm bead standards (FS05F, Bangs Laboratories, Inc., Fishers, IN). For Fixed TIRF imaging for visualizing endogenous CD63 and cortactin, cells were processed for immunofluorescence as described above. Images were captured with a standard laser angle to observe CD63 puncta present at the cell-substrate interface. For visualizing actin turnover at invadopodia, control, Rab27a-KD, cortactin OE and cortactin OE/Rab27a-KD cells were treated with 10 μM Latrunculin A (L5163, Sigma, St. Louis, MO). TIRF images were captured at 3 frames per second for 2 minutes.

TIRF image analysis: For shallow TIRF movies, the levels for all the cell lines were all reduced to the same level to lower nonspecific background. Then automated thresholding in Speckle Tracker plugin was used to identify MVEs. Mobile MVEs were defined as MVE that had a change in X, Y coordinates. Immobile MVEs defined in the graph were those that were immobile for ≥ 5 sec. In deeper TIRF movies, MVEs were manually selected using Speckle Tracker plugin feature. The data generated was further processed using Count Speckle Displacement plugin in Fiji to determine the number of MVE as well as calculate

diffusion coefficients. For quantification of TIRF fixed cell experiments, the cell area was outlined and images were thresholded in MetaMorph. The middle of the cell was excluded from analysis. MVE intensity and number data along with corresponding cell area data were exported to Excel for calculation of MVE number/area. For analysis of actin turnover in invadopodia from TIRF movies, Image J plugin Intensity versus time monitor was used to determine actin fluorescence intensity at invadopodia for 4X4 pixel areas. A separate 4X4 pixel area outside of each invadopodia was selected to determine the background fluorescence intensity. The specific invadopodia actin fluorescence intensity was determined by subtracting the neighboring cytoplasmic background intensity from the total invadopodia actin fluorescence intensity. The data were then normalized to the frame at which Latrunculin A was added. GraphPad Prism version 6 was used to plot the data and non-regression analysis was used to determine the half-life of actin fluorescence intensity decay.

Statistics

For both quantitated data and representative images from experiments, the n value and independent experiment numbers are listed in the figure legends. For non-quantitated western blots (e.g. checking knockdown or overexpression), they were generally performed a single time. All statistical analysis was carried out using SPSS version 22 and graphs were generated in Prism Graphpad version 5 or 6. All data were first tested for normality using a Kolmogorov-Smirnov normality test. Parametric data were analyzed by a two-tailed t-test and plotted with bar graphs showing mean+/-standard error. Data that were non-

parametric were analyzed by Mann-Whitney U test and plotted using box and whiskers plots, where the median is shown as a line, the box indicates 25th-75th percentile and the whiskers indicate 5th-95th percentile.

CHAPTER III

CORTACTIN PROMOTES EXOSOME SECRETION BY REGULATING BRANCHED ACTIN DYNAMICS

Introduction

Exosomes are small extracellular vesicles that are secreted upon fusion of multivesicular late endosomes (MVE) with the plasma membrane. Exosomes carry a variety of bioactive protein and RNA cargoes, including growth factors, transmembrane receptors, angiogenic factors, proteinases, and microRNAs [1, 125]. Exosomes have been shown to affect various cellular and organismal functions, including immune cell communication, coagulation, and Drosophila mating behavior [126-130]. In cancer, exosome secretion has been shown to promote tumor growth, angiogenesis, and metastasis, and to modify the cellular composition of the tumor microenvironment [5, 37, 48, 49, 131, 132].

For many years, exosome secretion was thought to occur only under specialized circumstances, such as during reticulocyte maturation and by dendritic cells [133]. However, recent studies have demonstrated secretion of exosomes by diverse cell types [125, 134] and identified key regulators of MVE docking and fusion with the plasma membrane, including Ral1, Rab35, Rab27, and Synaptotagmin-7 [5, 35, 36, 38, 135]. Both Rab27 and Rab35 are deregulated in cancer, suggesting that cancer cells may develop mechanisms to control exosome secretion [136-139]. Exosomes can also be regulated earlier in the

endocytic trafficking pathway. Thus, receptor ubiquitination, ceramide synthesis, or recruitment of the adaptor molecule syntenin or the GTPase Ral1 are mechanisms that can regulate cargo content and intraluminal vesiculation [28, 135, 140, 141]. However, the molecular mechanisms that control and promote exosome secretion are still poorly understood.

Along the endocytic pathway, there may be key decision points that control whether MVE will be degraded in lysosomes or secreted. Thus, fusion of autophagosomes with MVE has been shown to promote MVE degradation and inhibit exosome secretion [142]. In addition, transport of MVE to the plasma membrane or subsequent membrane docking could also control the likelihood of MVE secretion. Indeed, I recently reported that cancer cell invadopodia are docking sites for MVE [35]. Furthermore, I found that the number of invadopodial docking sites greatly affected the rate of exosome secretion [35].

Cortactin is an actin binding protein that is overexpressed in many tumors and controls both formation and activity of cancer cell invadopodia [58]. In HNSCC, cortactin overexpression is associated with poor patient prognosis, including decreased survival [105, 114, 143-145]. At the cellular level, cortactin is a key regulator of branched actin dynamics through its interactions with the Arp2/3 complex and actin filaments [63, 92, 93]. Thus, cortactin controls numerous branched actin-dependent processes, including cell motility and invasion, and membrane trafficking [58]. Recently, we identified cortactin as a regulator of late endosomal trafficking [63, 77, 100]. Since MVE are late endosomes, those data suggested that cortactin might control exosome secretion.

Here, in my dissertation, I report that cortactin expression levels control the number of exosomes secreted from cancer cells. Consistent with our previous studies, I confirmed a role for cortactin in late endosomal trafficking [63, 77] via electron microscopy and live imaging analyses. I further show that cortactin expression levels control the number of MVE docking sites at the plasma membrane. Investigation of the mechanism by which cortactin controls MVE docking revealed that cortactin, coronin1b, and Rab27a coordinately control actin turnover at invadopodia, which are cortical MVE docking sites [35], as well as exosome secretion. Structure-function rescue studies with cortactin binding mutants demonstrate that the interaction of cortactin with the Arp2/3 complex and actin filaments is essential for exosome secretion. Functionally, cortactin-KD cell defects in serum-independent growth and invasion were rescued by addition of purified exosomes. Altogether my data indicates that control of branched actin dynamics by cortactin and other accessory proteins is a critical regulatory point for exosome secretion.

Results

Cortactin regulates exosome secretion

We previously found that cortactin regulates late endosomal secretion [100] and trafficking [77]. To test whether cortactin controls exosome secretion, I downregulated or overexpressed cortactin protein levels in SCC61 HNSCC cells by expression of specific targeting shRNAs or by overexpression of mouse cortactin (Figure 4A, B). To collect exosomes, cells expressing cortactin-specific shRNA (KD1, KD2) or scrambled control shRNA were cultured in OptiMEM media without serum for 48 h before performing sequential differential centrifugation of the conditioned media [146]. OptiMEM contains growth factors, so it sustains cell growth while avoiding contamination with exosomes from serum. Consistent with our previous finding that cortactin does not affect proliferation of cells in a growth factor-replete environment [115], there was no effect of cortactin-KD on either cell number or the percent of cells that were viable after 48 h in OptiMEM (Figure 4C,D).

To distinguish between microvesicles (MV, up to 1 μm in size) and exosomes (40-100 nm), the respective 10,000 x g and 100,000 x g fractions were analyzed by NanoSight Nanoparticle Tracking Analysis (NTA) (Figures 4E-I and 5A-C). Based upon NTA, we did not see any significant difference in the average number or size of vesicles in the MV fractions from control and cortactin KD cells (Figure 4E-I). By contrast, NTA of the exosome fractions revealed a decrease in

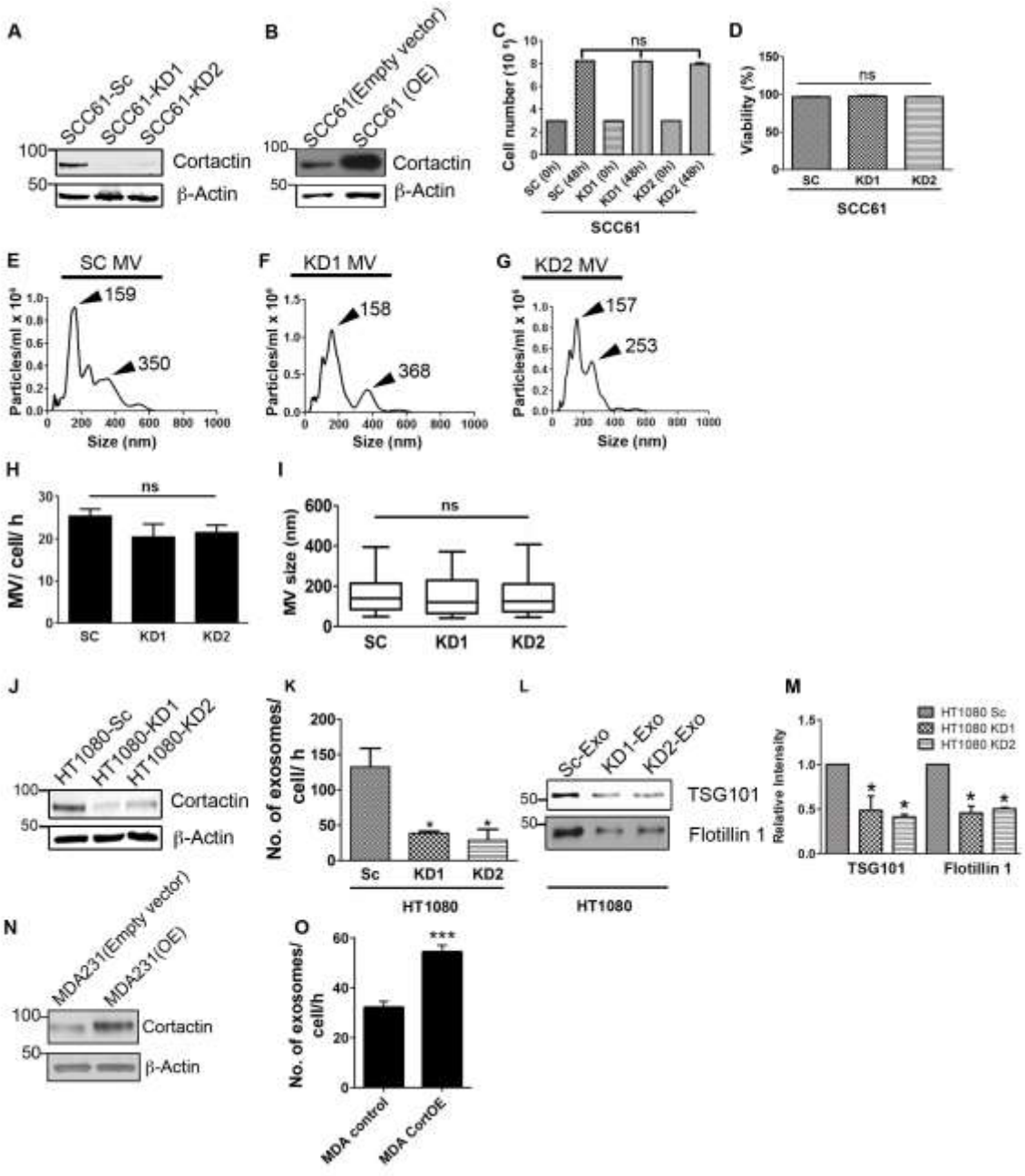

Figure legend next page.

Figure 4. Characterization of cell lines for exosome secretion. (A, B) Western blot analyses of cortactin expression levels, as indicated. (A) SCC61 cell lines stably expressing either scrambled oligo control shRNA (SCC61-Sc) or two different shRNAs targeting cortactin (KD1 and KD2). (B) SCC61 cells stably expressing empty vector (Control) or wild-type full-length mouse cortactin for overexpression (OE). (C) Cell counts of SCC61 control (Sc) and cortactin KD cells at the time of plating (0 h) and after 48 h in OptiMeM medium. N=3 independent experiments. (D) Percent of cells excluding trypan blue staining after 48 h in OptiMeM (Viability %). N=3 independent experiments. (E-I) NanoSight analysis of microvesicles (MVs) (E-G) NanoSight size distribution of representative MV preparations obtained from conditioned media of scrambled control and cortactin-KD cell lines. (H, I) Quantitation of number and size of the same vesicles by NanoSight NTA from N≥3 independent samples. (J) Representative Western blot of cell lysates from HT1080 cells stably expressing scrambled oligo control or two different shRNAs targeting cortactin. (K) NanoSight NTA quantitation of exosomes secreted from HT1080 Sc and cortactin-KD cell lines. N=3 independent experiments. (L) Representative Western blots of HT1080 control and cortactin-KD exosome (Exo) fractions isolated from equal numbers of cells for TSG101 and Flotillin-1. (M) Quantitation of Western blots as in (L), N=3. (N) MDA231 cell lines stably expressing either empty vector (Control) or wild-type full-length mouse cortactin for overexpression (OE). (O) NanoSight NTA quantitation of exosomes secreted from MDA-MB-231 empty vector (Control) and MDA-MB-231 (OE) cells. N=3 independent experiments. Parametric data are plotted as bar graphs, which plot mean ± SE, and analyzed for statistical significance using a Student's t-Test. Nonparametric data are graphed with box and whiskers plots, where the line indicates the median, the box indicates the 25th-75th percentile and the whiskers indicate the 5th-95th percentile . Mann-Whitney U test was used for determining statistical significance of nonparametric data. *$p<0.05$, ***$p<0.001$, ns= not significant.

the number of exosomes secreted by cortactin-KD SCC61 cells compared to control cells (Figure 5A,B). Re-expression of mouse full-length wild-type cortactin in the human-specific cortactin shRNA-expressing cells (Western blot of expression in Figure 5) fully rescued exosome secretion, indicating the specificity of the exosome secretion phenotype to cortactin (Figure 5B, KD1/ WT cells). Finally, we found that cortactin overexpression significantly increased exosome secretion (Figure 5B, OE) compared to control cells. There was no difference in the NTA-calculated average exosome vesicle size (Figure 5C). Quantitation of the number and size of exosomes from transmission electron microscopy (EM) images of negatively stained preparations (Figure 5D-F) confirmed the significant decrease in the number of exosomes secreted from cortactin-knockdown (KD) cells without any effect on vesicle size (Figure 5D-F).

To characterize further the secreted vesicles in the exosome fraction, we performed Western blot analyses. Consistent with the isolated vesicles being exosomes, they were positive for the exosome markers TSG101, CD63, and Flotillin1, and negative for the Golgi marker GM130 (Figure 5G). In addition, the exosomes were positive for several cargo proteins whose trafficking is known to be regulated by cortactin: the matrix metalloproteinases MMP9 and MT1-MMP [98, 115, 118], and for EGFR (Figure 5H) [147]. Since the exosome fractions were loaded on Western blots based on equal cell number, KD fractions showed decreased intensity of exosome cargo bands (Figure 5G-I). Cortactin-KD or OE likewise decreased or increased exosome secretion by HT1080 fibrosarcoma cells or MDA-MB-231 cells (Figure 4J-O). These data indicate that the level of cortactin

expression significantly regulates exosome secretion in cancer cells, both in the positive and negative direction.

Cortactin does not control exosome cargo composition

To determine whether cortactin controls exosome protein cargo composition, shotgun proteomics analysis was performed on an equal number of exosomes purified from SCC61-control and cortactin-KD cells. The results were filtered and collated using IDPicker with a target peptide false discovery rate (FDR) of 5% and requiring a minimum of 2 distinct peptides and 6 spectra per protein identification. This yielded a 4% protein false discovery rate (FDR) for the nine MudPIT samples (three biological replicates each for control, cortactin-KD1 and KD2 exosomes). Gene Ontology in Uniprot database was used to classify the common exosome proteins (Figure 6A). Of the 2102 identified proteins, 2065 were found to be common between all of the three conditions (Figure 6B).

Comparison of protein abundance in each sample was evaluated by spectral counting using QuasiTel software [123]. The software predicted statistically significant differences in the spectral count numbers for detected proteins between control and KD exosomes for only 22 out of the 2102 proteins (excel sheet separately attached). Because QuasiTel bases part of its significance estimate on spectral count variability across biological replicates, only proteins demonstrating sufficient consistency in detection enable confident quantitative comparisons. Thus, if a substantial number of differentially packaged proteins exist, they are below our ability to reliably quantitate them using this technology platform. As a measure of variability, the coefficient of variation (CV) within a

group of biological replicates was examined for control and KD-derived exosomes (Table 2). As expected, proteins with lower spectral counts have higher CV values. We also performed WB analyses for candidate proteins, comparing equal numbers of control and cortactin-KD exosomes (Figure 6C and D). As expected from the spectral count analysis, there were no significant differences in EGFR levels in the exosome preparations. In addition, although our Quasitel analysis identified collagen I and MMP2 as potentially significantly different cargoes between control and KD exosomes (excel sheet separately attached), they were present at equivalent levels by WB analysis. Notably, MMP2 is a bona fide exosome component as it is not present in the supernatant of conditioned media after 100,000xg centrifugation to pellet exosomes (Figure 6E). These data suggest that cortactin controls exosome number but not cargo content.

Quartile (Based on total spectral counts)	CV1 (Sc)	CV2 (KD)
1st (top 25%)	0.329807193	0.425287548
2nd (25% - 50%)	0.462004456	0.563452177
3rd (50%- 75%)	0.643604994	0.748210453
4th (bottom 25%)	0.833073943	0.988859553

Table 2. Coefficient of variation for proteomics data set. Also see excel sheet, separately attached.

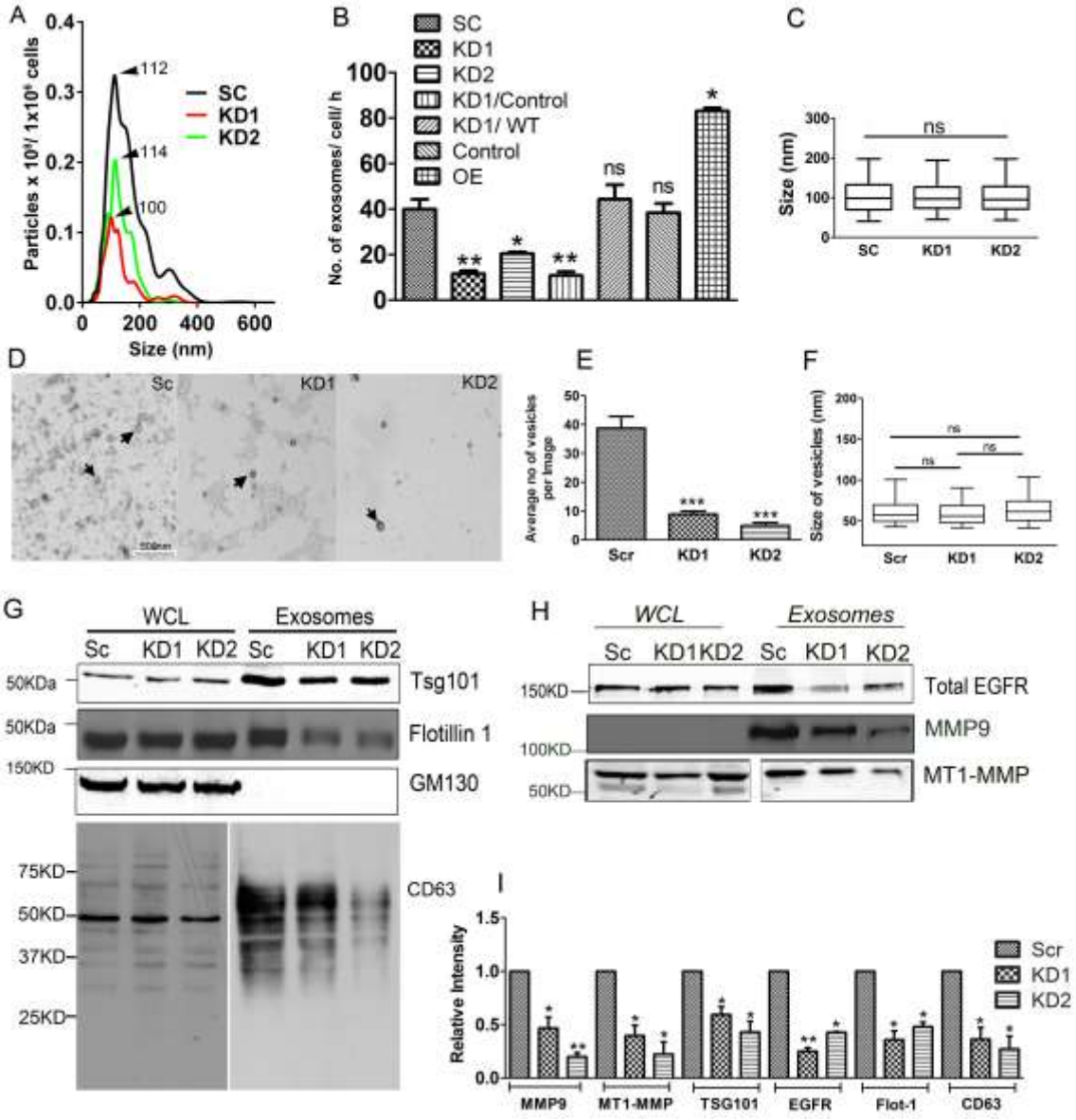

Figure legend next page

Figure 5: Cortactin levels control exosome secretion. Exosome preparations purified from equal numbers of cells were analyzed. (A) Representative nanoparticle tracking analysis (NTA) traces of exosomes derived from SCC61 control (SC) and cortactin knockdown (KD1, KD2) cells, normalized to cell number (B) Quantification from n=3 independent experiments. Rescue constructs indicated after the slash (/): empty vector (Control) or WT for wild type cortactin. OE: cortactin overexpression in parental cells. Western blots (WB) of cortactin levels in KD and OE cells shown in Fig. S1 and of KD/Rescue cells in Fig. 5. (C) Quantitation of vesicle size by NTA. (D) Representative TEM images of exosome preparations from scrambled control (Sc) and cortactin knockdown (KD1, KD2) cells. (E) Quantification of average exosome number per EM image. (F) Size of vesicles ≥ 40 nm quantitated from EM images. Quantitations in E and F from 28-30 images per condition, n=3 independent experiments (total number of vesicles across all images = 1146 for control, 277 for KD1, and 129 for KD2). (G-H) Representative WB of control and cortactin-KD whole cell lysates (WCL) and exosomes (Exo). WCL are loaded according to equal protein whereas exosomes are loaded according to cell number. (I) Quantitation of WB. N=3 independent experiments. Parametric data plotted as bar graphs, mean ± SE, and analyzed for statistical significance using a Student's t-Test. Nonparametric data graphed with box and whiskers plots, where the line indicates median, the box indicates 25th-75th percentile and the whiskers indicate 5th-95th percentile, and analyzed by Mann-Whitney U test. ns=not significant. *p<0.05, **p<0.01, ***p<0.001.

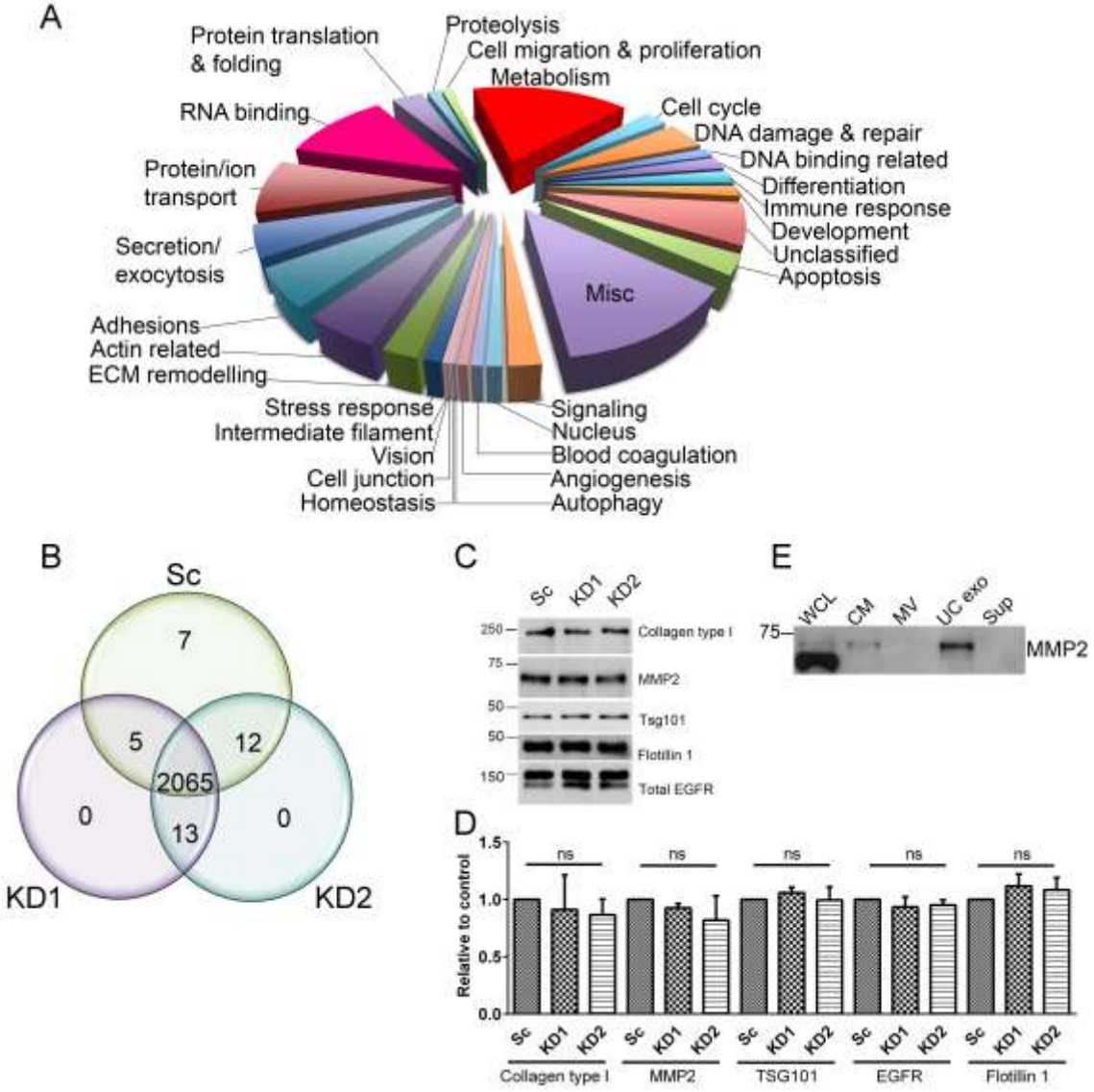

Figure 6: Cortactin does not control exosome cargo selection. (A) Classification of proteins identified in equal numbers of exosomes that are common between SCC61-control (Sc), cortactin-KD1 (KD1) and cortactin-KD2 (KD2) cells based on their Uniprot identified function. (B) Venn diagram representing the presence, absence, or overlap of proteins identified through LC-MS/MS in exosomes purified from the indicated cell lines. Proteomics data n=3 independent experiments. (C) WB analysis of proteins present in an equal number of exosomes purified from control and cortactin-KD cells. (D) Quantitation of WB. N=3. Bar graphs = mean +/- SE. Significance analyzed by Student's t-Test. ns = not significant. (E) WB analysis of MMP2 in whole cell lysate (WCL), conditioned media (CM), microvesicle (MV), exosomes (UC exo), and supernatant (Sup) from the UC exo centrifugation step. Representative of n=3 experiments

Cortactin regulates MVE trafficking

Secretion of exosomes could be regulated at several points in the endocytic pathway, including exosome biogenesis within early endosomes, and trafficking and secretion of MVE. Previously, we showed that cortactin-KD cells have a defect in late endosomal trafficking and accumulate enlarged late endosomal/lysosomal compartments [63, 77, 100]. Similar to these findings, we confirmed that SCC61 cortactin-KD cells contain enlarged late endosomal/lysosomal hybrid organelles by transmission EM of 50 nm cell sections (Figure 7A) [77]. In addition, we observed intact MVE in both control and cortactin-KD cells (Figure 7A). We also observed a few vacuole-like structures (Figures 7A and 8D, marked with "V" in KD cell images), which in KD cells could represent endosomes that were unable to form intraluminal vesicles [31, 140]. To test this possibility, MVE were labeled by allowing control and KD cells to bind and endocytose anti-CD63 antibody conjugated to horse radish peroxidase. They were then fixed, developed with diaminobenzidine (DAB) cytochemistry, and processed for transmission EM. In both control and cortactin-KD cells, DAB staining was concentrated in MVE structures, while the empty vacuoles were negative for the stain (Figure 8A-D). These data suggest that the empty vacuoles are not pre-MVE structures and that cortactin is unlikely to affect exosome biogenesis.

To further examine the role of cortactin in exosome biogenesis, we used a previously reported light microscopy assay that utilizes the constitutively active Q79L mutant of Rab5a to promote enlargement of early-to-late transitioning endosomes [140, 148]. Within those enlarged endosomes, intraluminal vesicle accumulation is easily visualized and quantitated by immunostaining for the exosome/MVE marker CD63 [31, 140]. GFP-Rab5a Q79L was transiently expressed in control and cortactin-KD SCC61 cells, followed by immunostaining for CD63 (Figure 7B). Analysis of confocal images revealed that there was no difference between control and cortactin-KD cells in the percent of GFP-Rab5a Q79L-positive endosomes that were filled with luminal CD63 (Figure 7C). Together with our finding that cortactin affects the number but not cargo content of exosomes (Figures 5 and 6) and that MVE are present in cortactin-KD cells (Figures 7A and 8A-D), these data indicate that cortactin does not affect exosome biogenesis.

In both the GFP-RabQ79L experiments (Figure 7B) and in separate immunostaining experiments of cells not overexpressing any fluorescent constructs (Figure 7D-F), we observed that cortactin-KD leads to an enlargement of individual CD63-positive endosomal structures (Figure 7B, D, and F) while not changing the total cell area occupied by CD63-positive compartments (Figure 7E). In addition, confocal imaging of both control and cortactin-KD cells expressing GFP-CD63 and the exosome cargo mCherry-MMP9 revealed that MMP9 localized within CD63-positive endosomes in both control and cortactin-KD cells (Figure 9A). These data suggest that cortactin affects MVE trafficking

downstream of exosome biogenesis, such as transport to the plasma membrane or docking at the plasma membrane.

To determine whether cortactin controls the transport of MVE within the cell, we analyzed the dynamics of GFP-CD63 positive endosomes in control and cortactin-KD cells by live confocal imaging. We found that many GFP-CD63-positive endosomes were transported back and forth to the cell periphery in fast, directional movements consistent with microtubule-based transport (Figure 9B and Video 1). For the purpose of analysis, we excluded CD63 positive endosomes larger than 2 μm (refer methods section). Dynamic tracking analysis revealed that cortactin-KD cells contained fewer moving GFP-CD63-positive endosomes compared to control cells (Figure 9B, C). By contrast, a similar number of moving GFP-CD63-positive endosomes were observed in cortactin-OE and control cells. Since overexpression of cortactin increases exosome secretion, altered numbers of moving MVE cannot fully account for the role of cortactin in exosome secretion. To analyze motility of CD63-positive endosomes in cells with various levels of cortactin expression, diffusion coefficients (mean square displacement/time, D) were calculated for individual endosomes. For both fast and slow moving endosomes (> or < 3 μm^2/sec), there was no significant difference in D between control, KD or OE cells (Figure 9D, E). These data indicate that, although KD cells have a decrease in the number of moving endosomes, MVE transport cannot account for the positive effects of cortactin overexpression on exosome secretion.

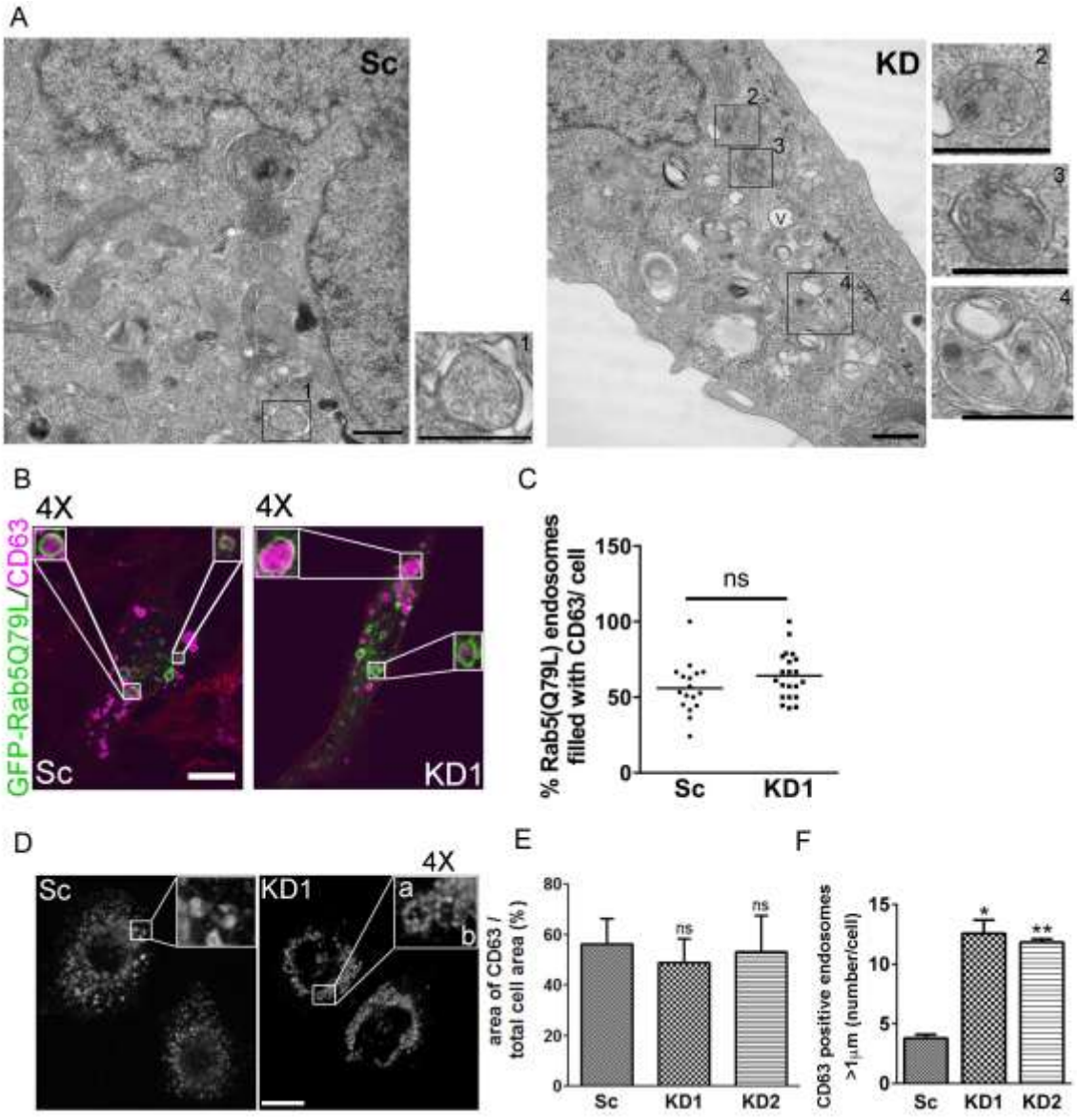

Figure legend next page

Figure 7: Cortactin affects MVE trafficking downstream of biogenesis. (A) Representative TEM images of 50 nm cell sections. SCC61-Control (Sc, left), cortactin-KD (KD, right). MVE (seen in zooms) from control (1) and cortactin-KD cells (2-3). "V" (empty vacuole like structure). Example LE/Lys hybrid organelle shown in zoom 4. Scale bars = 500 nm. (B) Representative confocal micrographs of SCC61 control (Sc) and cortactin-KD1 (KD1) cells transiently transfected with GFP-Rab5Q79L (green) and stained for endogenous CD63 (purple) along with actin filaments (rhodamine phalloidin, red). Insets show 4X zooms. Scale bar = 15 μm. (C) Quantitation of percent GFP-Rab5Q79L positive endosomes filled with CD63. N≥ 17 cells per condition n≥3 independent experiments. Lines show mean values. (D) Representative confocal images of immunostained CD63. Scale bar = 10 μm. Insets (4X zooms). a and b, two example endosomes in a KD cell. (E) Quantitation of CD63-positive area/cell area. (F) Quantitation of the number of large (>1 μm) CD63-positive endosomes per cell. N≥ 31 cells per condition n≥ 3 independent experiments. Bar graphs = mean +/- SE. ns = not significant; *p<0.05; **p<0.01. Student's t-Test used to determine statistical significance.

In addition to transport of MVE, exosome secretion could be affected by control of MVE docking or fusion with the plasma membrane. Cortactin localizes strongly to and regulates actin-rich invadopodial structures [58], which we recently identified as key MVE docking sites [35]. Thus, cortactin is a likely regulator of MVE docking. To test this possibility, TIRF microscopy was performed to visualize MVE docking at the basal surface of cells. TIRF microscopy of cells immunostained with an antibody against CD63 revealed that both cortactin-KD and Rab27a-KD cells exhibited a reduced number of endogenous CD63 positive endosomes at the cell-substrate interface compared to control cells (Figure 10A, B, Figure 11A). Conversely, cortactin-OE cells exhibited an increased number of CD63-positive puncta at the cell-substrate interface.

To further examine MVE docking at the basal plasma membrane-substrate interface, live TIRF microscopy was performed on cells expressing GFP-CD63 (Figure 10C-E, Figure 11B, Videos 2-5). Since docked vesicles are immobile, live TIRF imaging is ideal for assessing alterations in vesicle docking [36]. Rab27a-KD cells were used as a positive control, since the role of Rab27a in MVE docking was recently defined using a similar approach [36]. In cells expressing GFP-CD63, the profile of CD63-positive endosomes present at the basal surface was similar to that of immunostained cells, with a decrease in cortactin- and Rab27a-KD cells and an increase in cortactin-OE cells compared with control (Figure 10C). From the time-lapse images, the percent and number

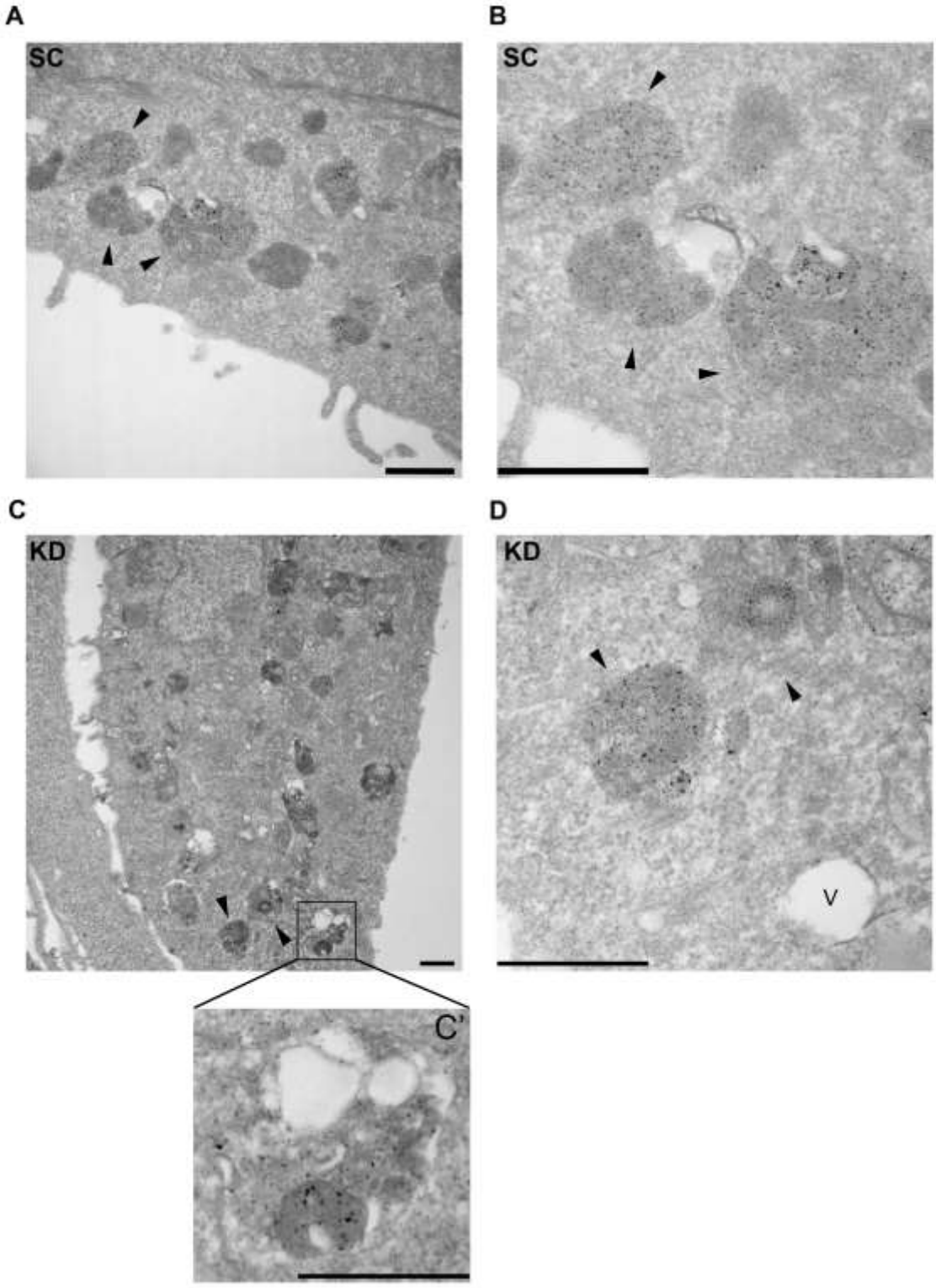

Figure legend next page

Figure 8. Cortactin expression does not affect morphology of CD63-positive structures. Anti-CD63-HRP uptake assay was carried out followed by DAB staining and preparation for transmission EM. (A-D) Representative TEM images of 50 nm cell sections. Black precipitate shows the presence of CD63-HRP. (A-B) Representative images from a SCC61-Control (SC) cell. Arrowheads point to the same example CD63-positive multivesicular endosomes (MVE) present in images taken at 30,000X (A) and 67,000X magnification (B). (C-D) Representative images from a SCC61-cortactin KD1 (KD) cell. Arrowheads point to the same example CD63-positive multivesicular endosomes (MVE) present in images taken at 15,000X (C) or 67,000X magnification (D). Boxed area (C' zoom) shows a late endosomal/lysosomal structure containing MVE. A vacuole-like structure (V) negative for CD63 staining is indicated in D. Scale bars = 500 nm for all.

of MVE per cell that were immobile for ≥ 5 sec were quantitated (Figure 10, D and E, Videos 2-5). Rab27a- and Cortactin-KD cells exhibited a decrease in both the percent and number of immobile MVE compared to controls. Conversely, cortactin-OE cells exhibited no increase in the percent of immobile MVE; however, due to the overall increase in the number of MVE at the plasma membrane, cortactin-OE cells exhibited a large increase in the number of immobile MVE per cell. In separate experiments using a deeper TIRF angle to allow tracking of MVE movement near the plane of the membrane [36], individual MVE movement was tracked and diffusion coefficients were calculated for each MVE as a measurement of motility (Videos 6-9, Supplementary Figure 10C,D). As previously published [36], MVE motility in the TIRF field was significantly increased in Rab27a-KD cells, indicating a docking defect (Figure 11D, Video 9). Similarly, the motility of CD63-positive MVE was significantly increased in cortactin-KD cells compared to control cells. While the MVE in cortactin-OE cells were slightly less mobile than control cell MVE (Figure 11D), the difference was not statistically significant, potentially due to the very low mobility of MVE in both cell types. Overall, these data indicate that cortactin controls MVE docking at the plasma membrane.

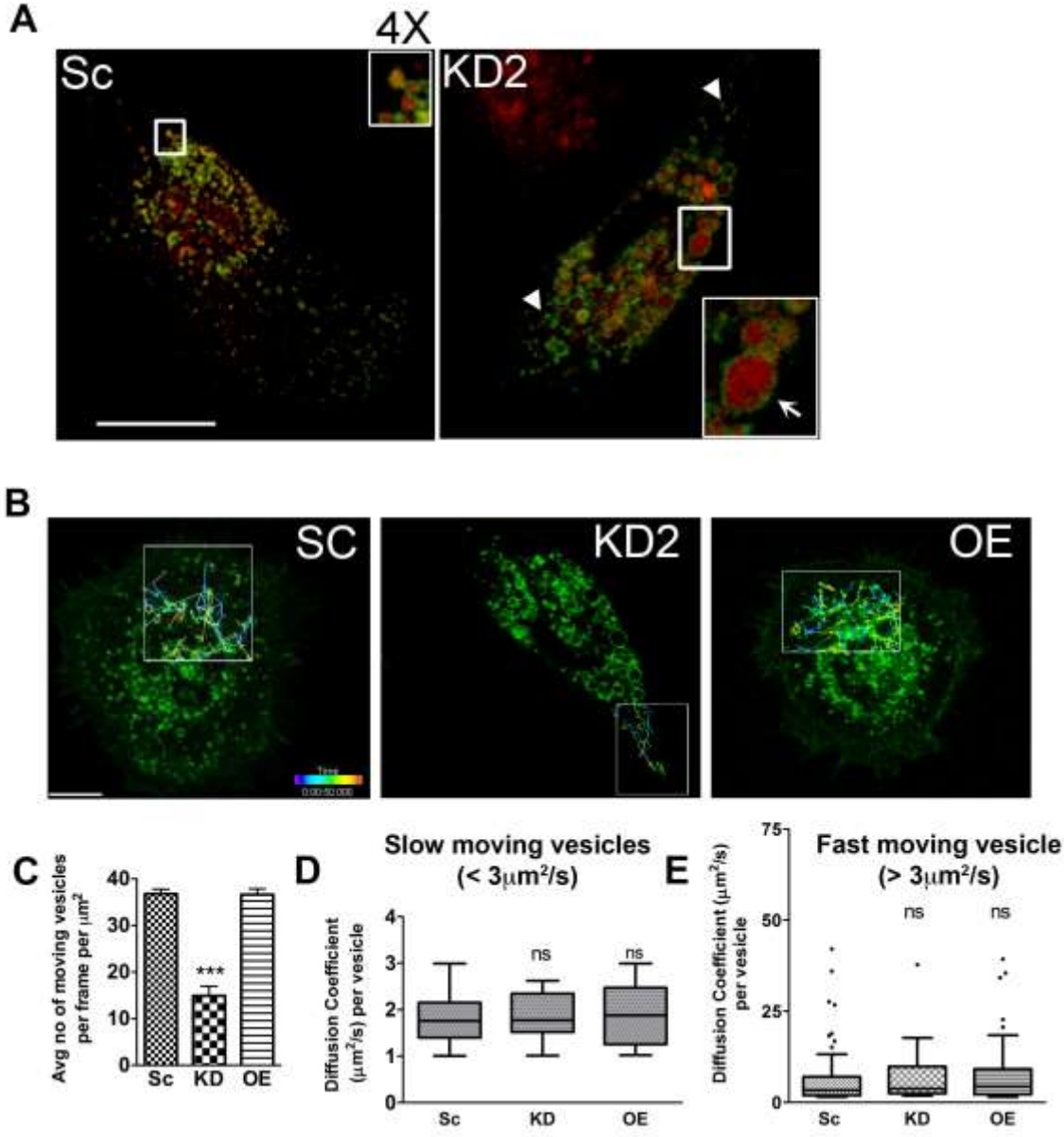

Figure legend next page

Figure 9. Cortactin affects number but not speed of MVE. (A) Representative confocal micrographs of SCC61 control and cortactin-KD cells transiently transfected with EGFP-CD63 and mCherry-MMP9. Scale bar = 20 μm. Zoom insets show MMP9 inside of CD63-positive endosomal compartments. Arrowheads point towards small sized CD63 in cortactin-KD cells, while arrow points towards enlarged CD63 compartment in cortactin-KD cell. Data from ≥ 9 cells per condition from 3 independent experiments. (B)-(D) Live confocal imaging of GFP-CD63 expressing cells was performed to visualize late endosomal movement within SCC61 control, cortactin-KD and cortactin-OE cells. See also Video 1. (B) Representative tracks of moving endosomes generated by Imaris are shown within the boxes. Scale bar = 10 μm. (C) Average number of moving endosomes per μm^2 was quantitated. Mean+/-SE plotted. Statistical significance determined by Student t-Test. (D) and (E) Diffusion coefficients (D) for endosomes with speeds > or < 3 μm^2/sec are equivalent in cortactin-manipulated cells. Data from ≥9 cells per condition from ≥3 independent experiments. Mann-Whitney U test was used to determine statistical significance for D and E. Box and whiskers plots show median as a line, 25th-75th percentile in the box and 5th-95th percentile with the whiskers. ***p<0.001. ns=not significant.

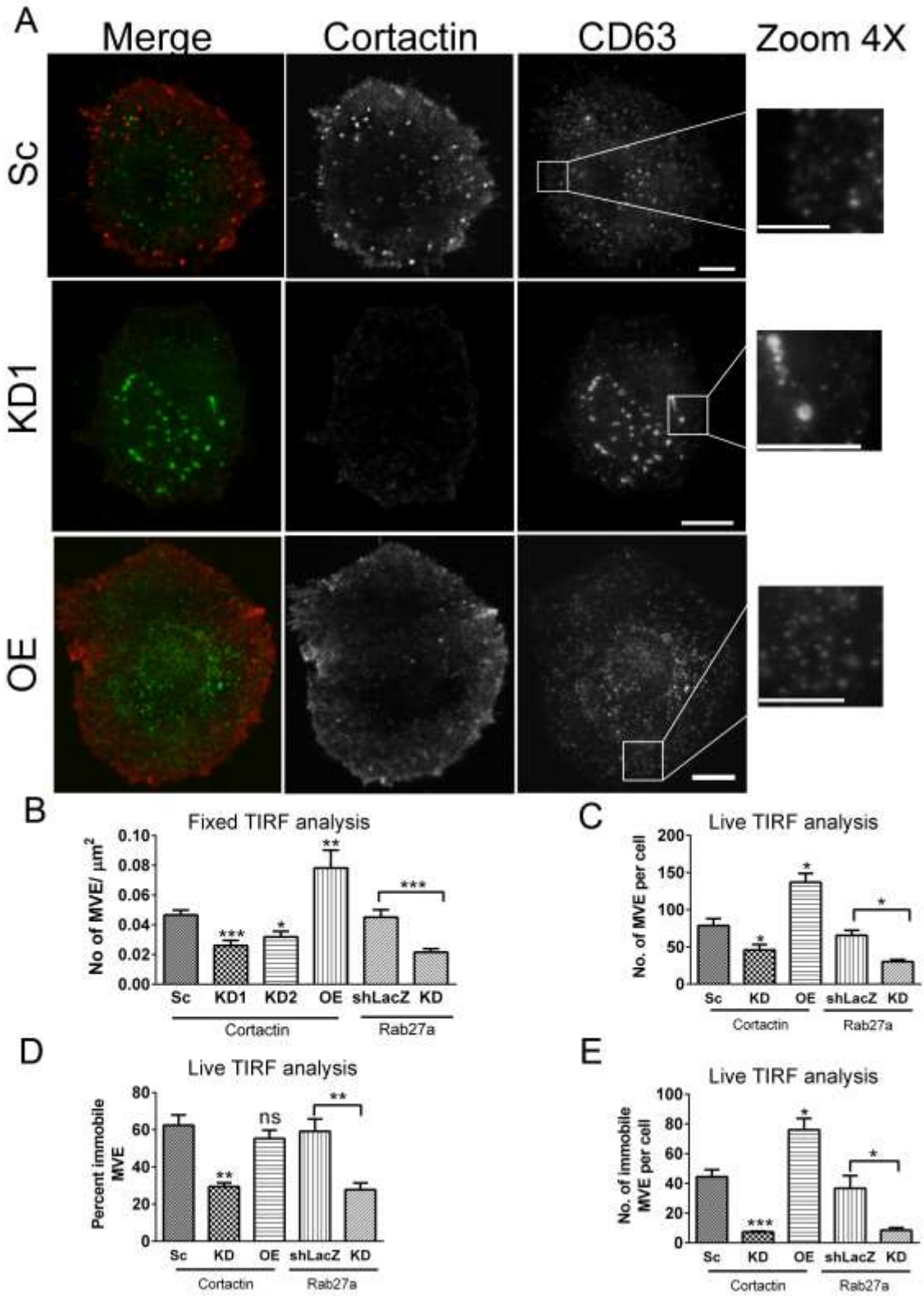

Figure legend next page

Figure 10: Cortactin controls MVE docking at the PM. (A)-(E) TIRFM of fixed and live cells. For analyses of TIRF images in (B)-(E), the center of the cell (demarcated by the yellow circle in A) was excluded. (A) and (B) Cells were immunostained for CD63 (green) and cortactin (red). (A) Representative images. Scale bars in main images = 10 μm, whereas zoom scale bars = 5 μm. Note increased vesicle number in Sc and OE cells compared to KD in zooms. (B) Number of CD63-positive vesicles per μm^2 cell area. N≥ 20 cells per condition from ≥3 independent experiments. (C-E) Cells were transiently transfected with GFP-CD63 and imaged live. Individual vesicles were tracked to yield quantitation of total number of MVE (C), percentage of immobile MVE (D) and number of immobile MVE (E) present at the PM. See Supplementary Fig. 4B for representative images. N≥8 cells for each condition, n≥ 3 independent experiments. Bar graphs = mean +/- SE. ns = not significant, *p<0.05, **p<0.01, ***p<0.001. Student's t-Test determined statistical significance.

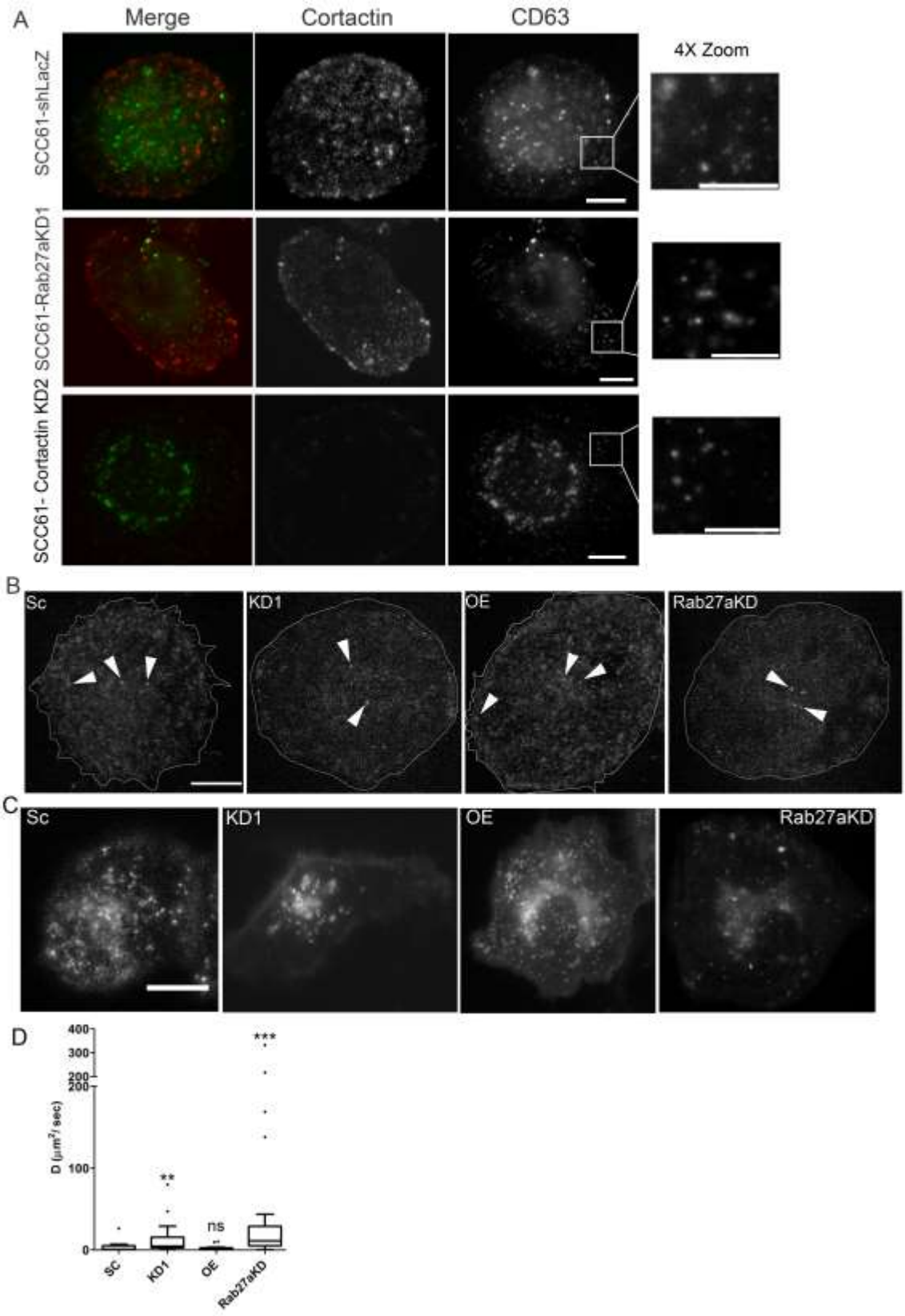

Figure legend next page

Figure 11. Cortactin and Rab27a affect MVE docking. (A) Endogenous distribution of CD63 at the subplasmalemmal level for control, Rab27a-KD1 and cortactin-KD2. These representative images correspond to the data quantitated in Figure 10B. Scale bars on main images = 10 μm, and on zooms = 5 μm. (B) Representative TIRF images of GFP-CD63-positive MVE at the basal surface of cells. Arrowheads point to example MVE that would be tracked. Scale bar = 10 μm. These correspond to the data quantitated in Figure 10C-E. Fluorescence levels of the shown images were enhanced for visualization only, not for quantitation. See also Videos 2-5. (C) Representative TIRF images from movies using a deeper TIRF angle (up to 1 μm into the cell) in order to obtain tracks of moving CD63 positive MVE and quantitate diffusion coefficients. See also Videos 6-9. (D) Mean diffusion coefficient values (D) of individual MVE is plotted to determine the effect of cortactin-KD1, cortactin-OE and Rab27a-KD on vesicle motion at the subplasmalemmal level. Data from n ≥ 4 MVE per cell was quantitated for ≥ 10 cells per condition from 3 independent experiments. Box and whiskers plot indicates median as a line, 25-75th percentile in the box and 5-95th percentile with the whiskers **p<0.01, ***p<0.001. ns = not significant. Mann-Whitney U test used to determine statistical significance

Interaction of cortactin with Arp2/3 complex and F-actin is critical for exosome secretion

Cortactin is a unique branched actin regulator that controls actin dynamics by linking the actin nucleating Arp2/3 complex to actin filaments via its N-terminus [58]. Cortactin also binds to a variety of cytoskeletal, membrane trafficking and signaling proteins at its C-terminus [58]. To understand the molecular mechanism by which cortactin controls exosome secretion, we performed a structure-function analysis of cortactin binding interactions that are required for exosome secretion. shRNA-insensitive wild type cortactin or cortactin proteins with mutations in the binding sites for Arp2/3 complex (W22A), actin filaments (Δ4RP), or SH3 domain binding partners (W525K) or in the Src phosphorylation sites (3Y) [88, 95, 149, 150] were re-expressed in cortactin-KD1 cells (Figure 12A, B). Exosomes were purified from the conditioned media of equal numbers of control, KD1, and KD1/rescue cells. The number of exosomes secreted by each cell type was quantitated by NanoSight NTA (Figure 12C). Reexpression of wild-type cortactin (WT) or cortactin molecules with mutations in the Src phosphorylation sites (3Y) or in the SH3 domain (W525K) fully rescued the exosome secretion defect of KD cells. However, there was no rescue by reexpression of cortactin molecules with mutations in the Arp2/3 complex (W22A) or actin filament (Δ4RP) binding sites, each of which are necessary for cortactin to control branched actin dynamics [92-95]. Consistent with this hypothesis, inhibition of Arp2/3 complex with the drug CK-666 reduced exosome secretion at concentrations that do not affect

cell viability (Figure 12D, E). These data suggest that cortactin-mediated control of branched actin dynamics is important for efficient exosome secretion.

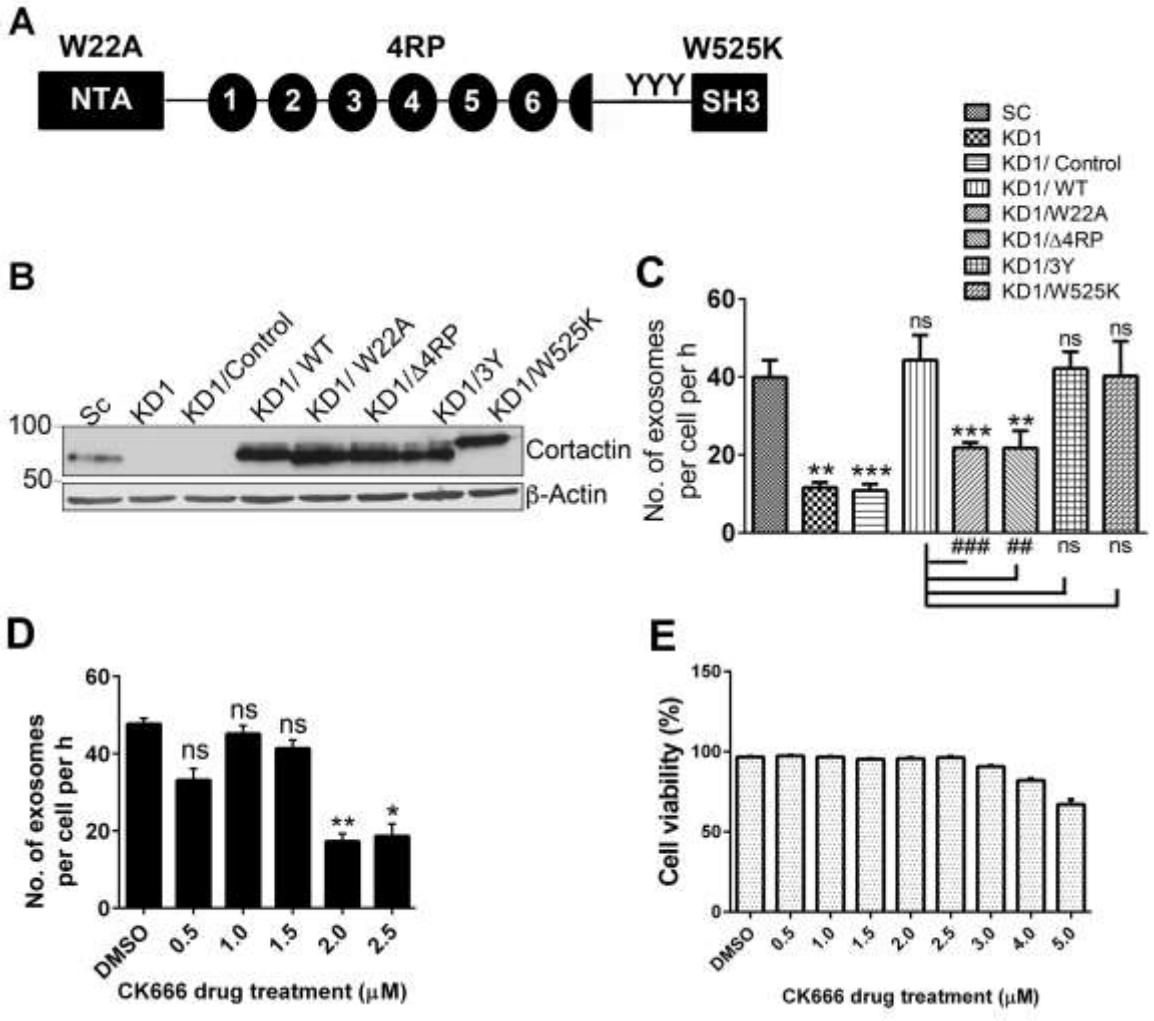

Figure 12: Binding of cortactin to Arp2/3 complex and F-actin is critical for exosome secretion. (A) Cortactin domain structure indicating mutation sites: W22A, prevents Arp2/3 binding; NTA, (N-terminal acidic Arp2/3-binding domain); ∆4RP, deletion of 4th repeat in tandem repeats region prevents F-actin binding; 3Y, Src kinase phosphorylation sites (tyrosines 421, 466, 482 mutated to phenylalanine); W525K, prevents binding to SH3 domain binding partners. (B) WB analysis of cortactin wild type (WT) and mutant (W22A, ∆4RP, 3Y, and W525K) re-expressed proteins in cortactin-KD1 cell lines. "Control" indicates empty vector for rescue constructs. (C) NTA quantitation of exosomes secretion rate of indicated cell lines. N≥3 independent experiments. (D) NTA quantitation of exosomes secreted from SCC61 cells in the presence of DMSO or various concentrations of CK666 (Arp2/3 inhibitor) for 24 h. N≥3 independent experiments. (E) Cell viability for SCC61 cells treated with DMSO or CK666 for 48 h. N≥3 independent experiments. Bar graphs represent mean +/- SE. **p<0.01, ***p<0.001 indicates comparison to Sc control; ##p<0.01, ###p<0.001 indicates comparison to KD1/WT rescue. ns = not significant. Analyzed by Student's t-Test.

Cortactin, Rab27a, and Coronin 1b coordinately control cortical branched actin dynamics and exosome secretion

Invadopodia are key plasma membrane sites of branched actin assembly that are regulated by cortactin and can serve as docking sites for MVE [35, 58]. Our TIRF microscopy experiments revealed that both Rab27a and cortactin control MVE docking, presumably by different mechanisms: respectively tethering MVE to docking sites at the membrane [36] and creating new docking sites via branched actin assembly [58]. To test this model, we knocked down Rab27a in cortactin-OE cells and quantitated the number of exosomes secreted from equal numbers of cells by NanoSight NTA (Figure 13A,B). Contrary to our expectation that loss of Rab27a should reverse the enhanced exosome secretion of cortactin-OE cells, we found no change in exosome secretion. These data suggest that overexpression of cortactin may compensate for the lower Rab27a levels and potentially work in the same process.

The best-validated role of cortactin in cells is to regulate branched actin assembly and stability [58, 92, 93]. Although control of actin assembly has not been highly studied for Rab27a, some reports have demonstrated that Rab27a can regulate both cortical and endosome-associated actin [151-154]. In addition, two reports have demonstrated that Rab27a can control the localization of the actin binding protein coronin to actin assemblies [152, 154]. Since coronin directly antagonizes cortactin at actin branch points [155], such a mechanism could explain compensatory interactions between cortactin and Rab27a. To test whether Rab27a controls localization of coronin to invadopodial branched actin

assemblies, control, Rab27a-KD, cortactin-OE and cortactin-OE/Rab27a-KD cells were cultured on FITC-FN/gelatin plates before fixation and immunostaining for the common epithelial isoform coronin 1b (Figure 13C, D). Invadopodia are evident in this assay as actin-filament-rich puncta that colocalize with dark spots of degraded matrix in the FITC-FN image [73]. Consistent with previous reports for endosomal and phagosome actin [152, 154], Rab27a-KD cells had increased intensity of coronin at invadopodial actin puncta (Figure 13D, E). This increase did not occur in cortactin OE Rab27a-KD cells, suggesting that cortactin may antagonize coronin binding to invadopodial branched actin, similar to their interactions in lamellipodia and in vitro [155]. To directly test whether cortactin affects coronin localization to invadopodia, cortactin-KD cells were also immunostained for coronin 1b and indeed exhibited an increase in coronin fluorescence intensity at invadopodia, despite no change in actin fluorescence intensity (Figure 13C; Figure 14B-D). Likewise, KD of coronin 1b in Rab27a-KD cells led to increased cortactin fluorescence intensity at invadopodia, without affecting actin intensity (Figure 14E-H). Coronin 1b-KD in Rab27a-KD cells also led to an increase in both invadopodia activity (Figure 14I) and exosome secretion (Figure 13B).

To test whether Rab27a and cortactin affect actin stability at invadopodia, control, Rab27a-KD, cortactin OE and cortactin OE Rab27a-KD cells were transiently transfected with the actin marker EGFP-F-Tractin. To specifically observe the turnover of actin at invadopodia, 10 µM Latrunculin (LatA), was added to cells and live TIRF imaging was performed (Video 10). Since LatA

prevents actin polymerization by sequestering monomeric actin [156], its addition to cells allows us to specifically monitor disassembly of dynamic actin structures [63]. Consistent with the dynamic nature of actin in invadopodia [157, 158], EGFP-F-Tractin fluorescence was rapidly lost over time in control cells, with a $t_{1/2}$ of actin intensity loss of 39 seconds (Figure 13H, Video 10). The invadopodial actin disassembled faster in Rab27a-KD cells than in control cells, with a disassembly $t_{1/2}$ of 14 seconds. In both cortactin OE and cortactin OE Rab27a-KD cells, the invadopodial actin was much more stable and did not fully disassemble by the end of the movie (Figure 13H, Video 10). Since Rab27a controls coronin localization to invadopodia (Figure 13C-E)), we also tested whether coronin KD could reverse the rapid actin disassembly that occurs in Rab27a-KD cells. Indeed, knockdown of Coronin 1b in Rab27a-KD cells led to more stable actin dynamics such that the actin disassembly rate was similar to that of control cells (Figure 13H). In addition, analysis of exosome secretion by NanoSight NTA revealed that coronin 1b-KD likewise rescues the inhibitory effect of Rab27a-KD on exosome secretion (Figure 13B). These data demonstrate that Rab27a and cortactin coordinately promote cortical actin stability and exosome secretion. Coronin antagonizes these activities.

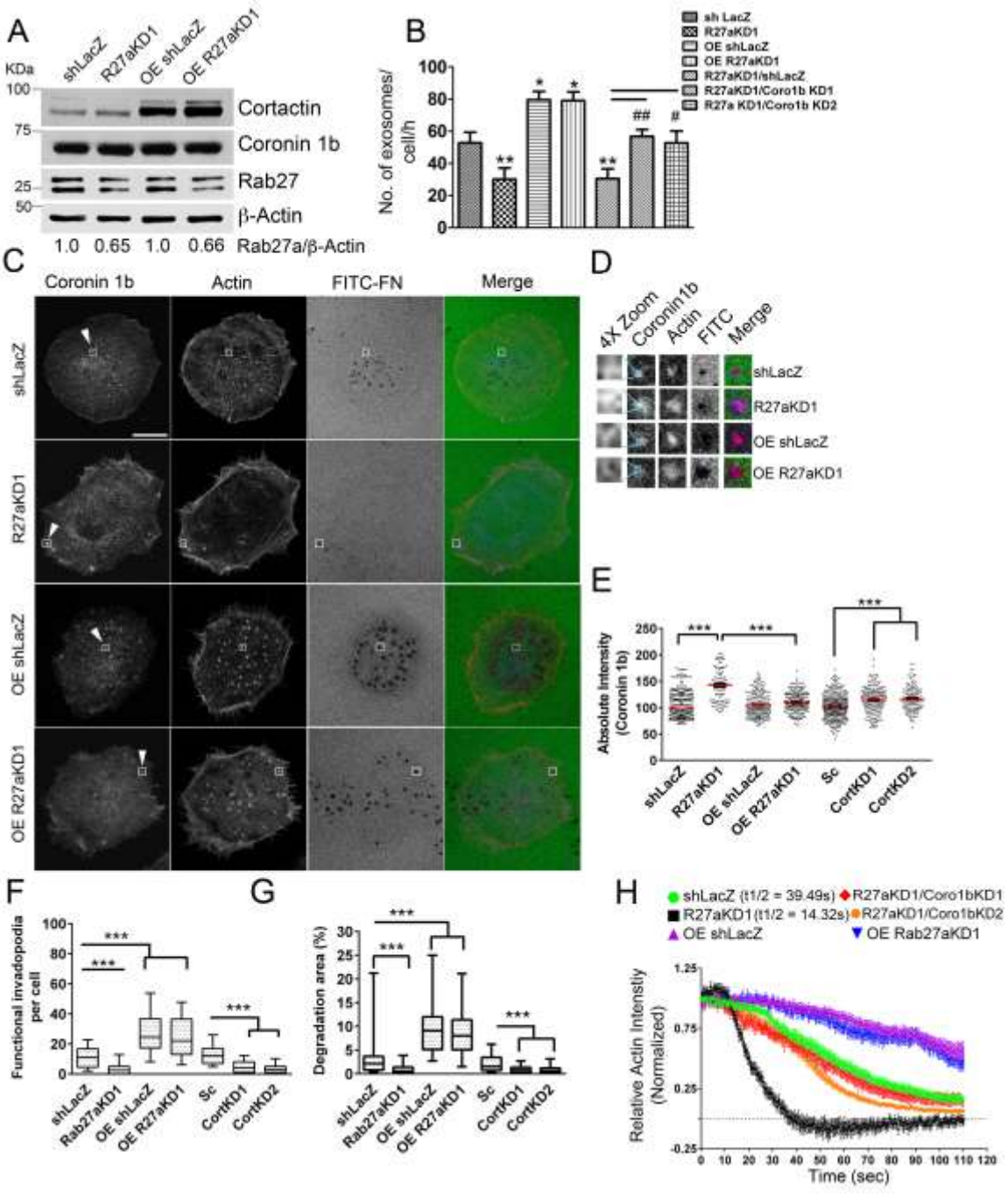

Figure legend next page

Figure 13. Cortactin, Rab27a, and Coronin 1b coordinately control invadopodia dynamics. (A) WB analysis of SCC61 control (shLacZ), Rab27a-KD1 (R27aKD1), cortactin-OE (OE shLacZ) and cortactin-OE cells knocked down for Rab27a (OE R27aKD1). Numbers indicate Rab27 levels normalized to β-actin levels, as a fraction of control. (B) NTA quantitation of exosomes secreted from the indicated cell lines. (C) Representative confocal immunofluorescence images showing localization of coronin 1b and actin to invadopodia. ECM degradation evident as dark spots in FITC-Fibronectin (FN) images. Fluorescence levels of the images were enhanced equally across all images for visualization only, not for quantitation. Scale bar = 15 μm. Boxes outline example invadopodia and are shown in (D). (C, D) Quantitation of the absolute intensity of coronin 1b at invadopodia was measured using 4X4 pixel boxes. Representative blue 4x4 pixel boxes are shown within the coronin 1b zooms and are further zoomed 4X and shown on the left (C). Quantitations shown in (E). N≥5 invadopodia per cell from ≥ 35 cells per condition, n≥3 independent experiments Scatter plot with median is plotted. Analyzed by Mann-Whitney U test. (F, G) Quantification of functional invadopodia per cell and ECM degradation area percentage. Box and whisker plots with median shown as a line, box indicates 25th-75th percentile and whiskers indicate 5th-95th percentile. N≥ 3 independent experiments. *$p<0.05$, **$p<0.01$, ***$p<0.001$, determined by Mann-Whitney U test. (H) Actin turnover in invadopodia after 10 μM Latrunculin A (LatA) treatment was assessed by live TIRF imaging. See also Video 10. Actin fluorescence intensity at invadopodia after LatA treatment is plotted. ≥ 5 invadopodia per cell were quantitated for ≥10 cells for each condition, n≥3 independent experiments.

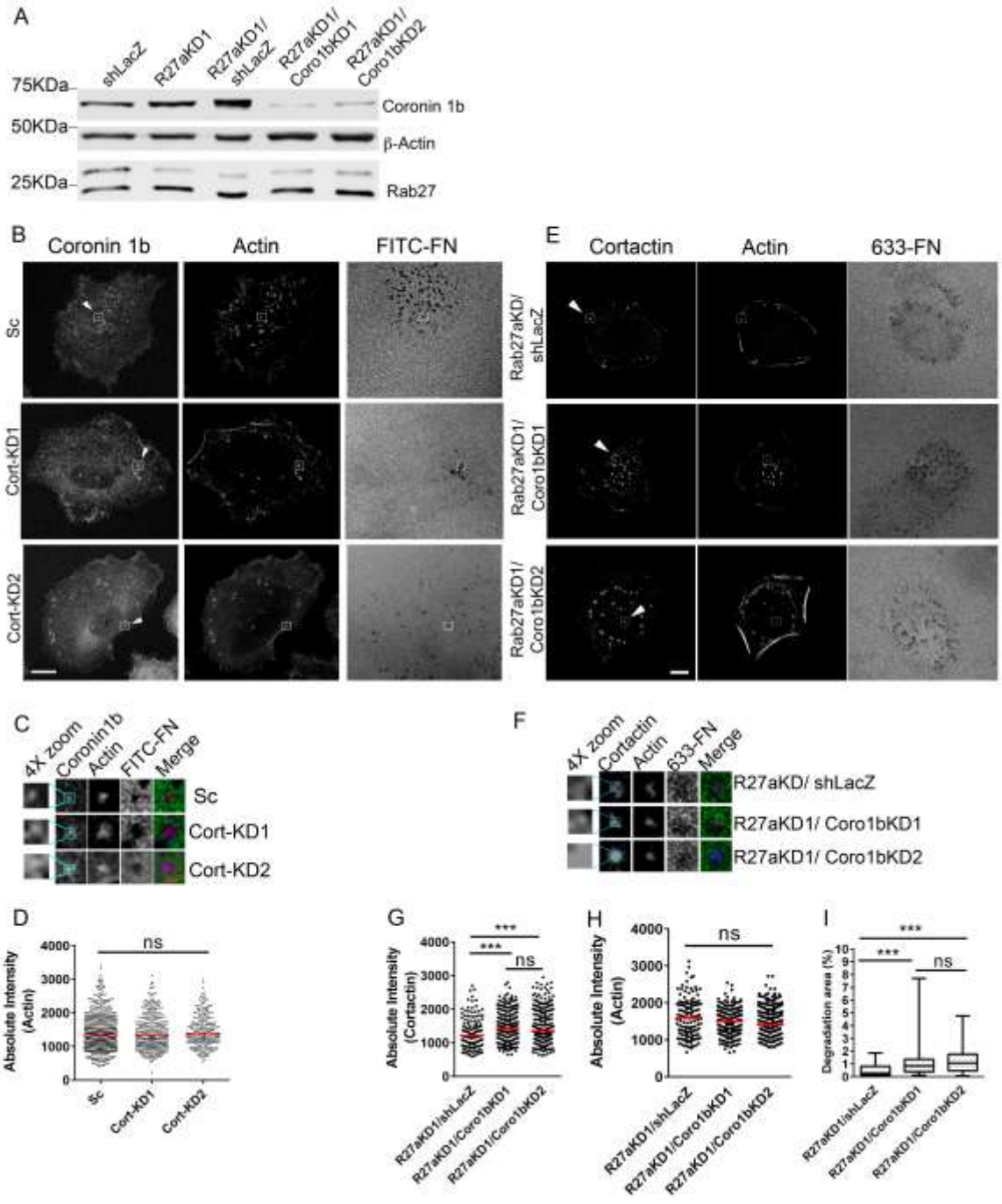

Figure legend next page

Figure 14. Cortactin affects coronin 1b localization to invadopodia (A) Western blot analysis of coronin 1b and Rab27a levels in SCC61 cells expressing control and gene-specific shRNAs as indicated, with β-actin as a loading control. (B) Representative confocal immunofluorescence images showing localization of coronin 1b and actin to invadopodia in SCC61 control and cortactin-KD cells. ECM degradation is evident from dark spots in FITC-Fibronectin (FN) images. Fluorescence levels of the shown images were enhanced for visualization only, not for quantitation, and equally across all images. Scale bar = 15 μm. Boxes outline single example invadopodia and are shown as zooms in (C). (C). Representative blue 4x4 pixel boxes are shown within the coronin 1b zooms (zoomed 8X from above images) and are further zoomed 4X and shown on the left. Coronin 1b quantitations from such images are shown in Fig. 6E. (D) Absolute actin intensity is quantitated (total number of actin puncta quantitated is 683 for Sc, 403 for Cort-KD1, 280 for Cort-KD2). Scatter plot with median is plotted. N≥35 cells for 3 independent experiments. (E) Representative confocal immunofluorescence images showing localization of cortactin and actin to invadopodia in SCC61 Rab27aKD1/shLacz (control), Rab27aKD1 and Coronin 1b double knockdown (KD1, KD2) cells. Fluorescence levels of the shown images were enhanced for visualization only, not for quantitation, and equally across all images. Scale bar = 10 μm. Boxes outline single example invadopodia and are shown in zooms in (F). (F) Representative blue 4x4 pixel boxes are shown within the cortactin zooms (zoomed 8X from above images) and are further zoomed 4X and shown on the left. (G,H) Absolute intensity of cortactin and actin within 4x4 pixel boxes is quantitated. Scatter plot with median is plotted. Total number of cortactin and actin puncta quantitated are 135 for Rab27aKD1, 248 for Rab27aKD1/Coro1bKD1, and 270 for Rab27aKD1/Coro1bKD2. Number of cells ≥30 cells for 3 independent experiments. (I) ECM degradation area for cells in (E) is plotted. Box and whiskers plots show median as a line, 25th-75th percentile in the box and 5th-95th percentile with the whiskers. Mann-Whitney U test used to determine statistical significance. **p<0.01, ***p<0.001. ns = not significant.

Discussion

Secreted exosomes have been implicated in multiple aspects of cellular function and communication [1, 125, 159]. Since few regulators of exosome secretion have been identified [5, 28, 35, 36, 38, 135, 140], the current understanding of cellular and molecular mechanisms that control exosome secretion is limited. Here, we show that the cytoskeletal protein cortactin controls secretion of exosomes but has little effect on their cargo content. Cortactin controls both late endosomal trafficking and MVE docking. Structure-function analyses revealed that binding of cortactin to Arp2/3 complex and actin filaments is critical for exosome secretion. Further investigation of the mechanism revealed that cortactin, Rab27a, and coronin 1b coordinately control branched actin dynamics at cortical invadopodial MVE docking sites and exosome secretion (see model in Figure 15). Overall, these data indicate that branched actin dynamics are critical for controlling exosome secretion.

Exosome secretion occurs when MVE fuse with the plasma membrane. An alternative fate for exosomes is degradation after MVE fusion with lysosomes. It is currently thought that the majority of MVE are degraded in lysosomes [1, 125, 160]; however how the balance between secretion and degradation is regulated is unclear. We previously found that invadopodia are key docking sites for MVE and that the number of invadopodia can control the number of exosomes secreted from cells [35]. In this study, I investigated the role of cortactin, which regulates branched actin assembly on both late endosomes [63] and at invadopodial MVE docking sites [35]. Our studies with KD cells indicate that cortactin controls both the

number of MVE that are trafficked (and presumably could be secreted) and the number of plasma membrane docking sites, while overexpression of cortactin only affected MVE docking. The trafficking data (Figure 9) together with our previous studies [63, 77, 100] suggest that cortactin plays an essential role in late endosomal maturation, such that cortactin loss leads to endosomal dysfunction and decreased numbers of MVE that can be trafficked to the plasma membrane. Since cortactin-overexpressing cells did not affect MVE trafficking and only exhibited a change in MVE docking, I focused on that phenotype for further in-depth studies. I found that control of branched actin assembly is critical to create MVE docking sites and subsequent secretion of exosomes.

Numerous membrane trafficking pathways are controlled by the Rab family of small GTPases [40]. Amongst them, Rab27a was recently shown to be a critical docking factor for MVE in cancer cells [36]. Rab27a also regulates peripheral capture and docking of other endolysosomal organelles, such as melanosomes and T-cell granules [161-165]. As Rab proteins function through multiple effectors, it is likely that the process of exosome secretion requires multiple events. For example, synaptotagmin-like proteins such as Slp4 and Slp2a have been shown to be important for exosome secretion from HeLa cells and for T cell granule exocytosis [36, 164] and likely link Rab27a-bound organelles to the plasma membrane. Likewise, binding of Rab27a to MyoVa allows off-loading of endolysosomal organelles from microtubules to peripheral actin assemblies [161-163, 165]. Our data suggest that Rab27a has an additional function in docking which is to regulate actin dynamics at cortical docking sites in coordination with

cortactin (Figure 8). Indeed, live TIRF imaging revealed that Rab27a and cortactin both control MVE docking and stability of cortical invadopodial actin assemblies. Furthermore, overexpression of cortactin reversed Rab27a-KD cell defects in exosome secretion and invadopodial actin stability. I also found that Rab27a levels control the localization of coronin 1b to invadopodial actin puncta and that KD of coronin 1b could likewise rescue Rab27a-KD cell defects in exosome secretion and invadopodial actin stability. As coronin 1b opposes the function of cortactin in stabilization of branched actin networks [155], these data suggest that a key role of Rab27a in the docking process is not only to bring and tether MVE [36] to the plasma membrane but also to stabilize the docking sites themselves (Figure 15).

The role of cortical actin in vesicle docking and fusion is not well-understood [166, 167]. On one hand, cortical actin must be disassembled in order for vesicles to access and bind the plasma membrane [168]. On the other hand, actin meshworks are known to promote vesicle docking [166]. Cortical actin docking sites may capture vesicles by connecting to other cytoskeletal elements, including unconventional myosins carrying vesicles or by linking to microtubules, which are

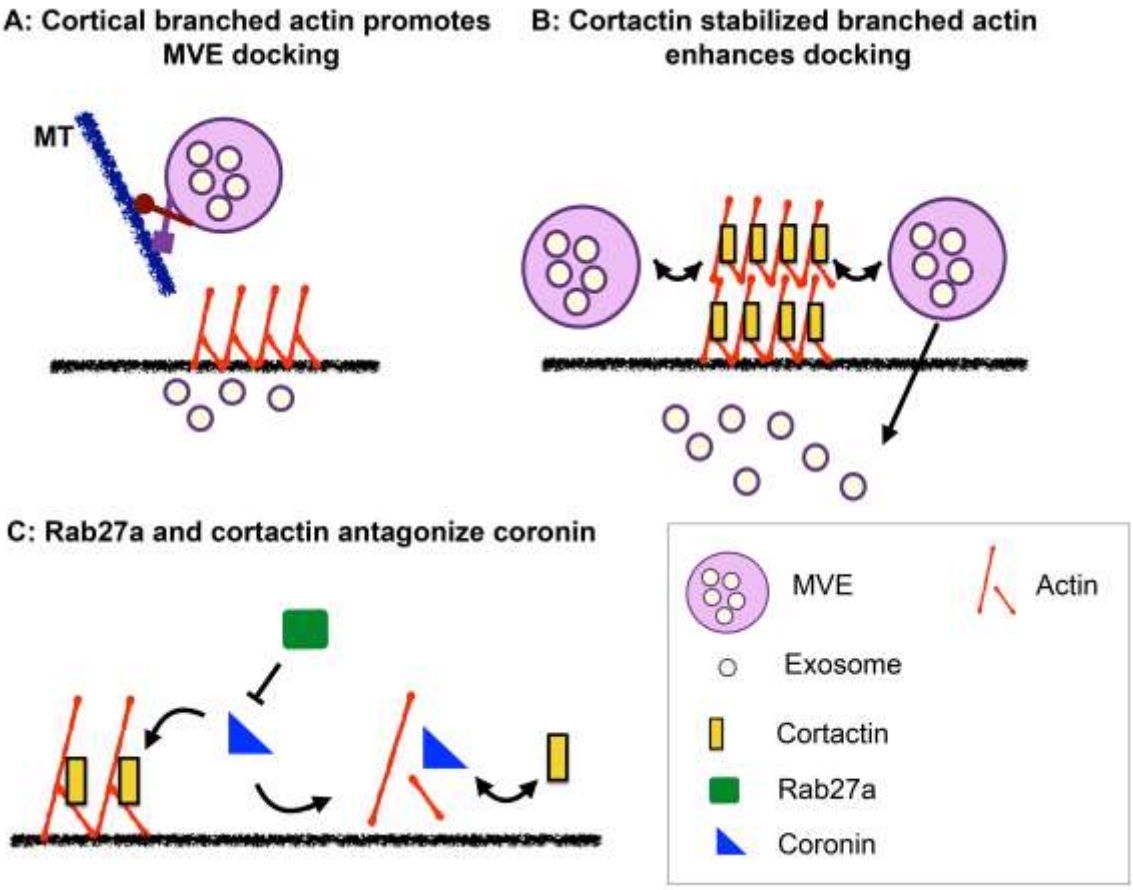

Figure 15. Model for regulation of exosome secretion by Cortactin, Rab27a, and Coronin. (A) Cortiacal branched actin helps create MVE docking sites, such as invadopodia at the plasma membrane [35]. (B) Cortactin stabilizes branched actin, which enhances MVE docking [35, 93]. (C) Coronin antagonizes cortactin at actin branches points [153], leading to destabilization of actin branches and fewer MVE docking sites. Rab27a opposes this antagonism by inhibiting coronin binding to invadopodia-associated actin [150, 152].

major vesicle transport highways. They may also act as signaling platforms that facilitate vesicle docking and fusion by creating suitable specialized lipid domains [169-171]. Invadopodia have all of these features: dynamic actin assembly, microtubule capture, and concentration of phosphorylated phosphatidylinositol lipids, lipid raft components, and other signaling molecules [172, 173]. At this point, the full mechanism of how dynamic actin functions to promote MVE docking at invadopodia is not clear; however, our data indicate that stabilization of actin is a key regulatory point for MVE secretion [35].

In summary, I found that cortactin promotes exosome secretion from cancer cells by regulating the stability of branched actin. My data suggests that modulation of branched actin dynamics is a critical control point that regulates MVE docking and exosome secretion.

CHAPTER IV

CORTACTIN MEDIATED EXOSOME SECRETION PROMOTES TUMOR PROGRESSION

Introduction

Cortactin was initially found to be overexpressed in head and neck squamous cell carcinoma and breast cancer [145]. Subsequently, several different cancer types have been shown to harbor cortactin overexpression such as gastric cancer, colorectal cancer, melanoma, hepatic, ovarian, and esophageal cancer [105-111]. Cortactin gene CTTN, which is found on 11q13.3 region of the genome, is often amplified in these cancers [104, 144]. Besides gene amplification that parallels protein expression, cortactin expression is found to be increased in several cancer types due to an alternative mechanism that remains poorly understood [105, 174]. Overall, cortactin overexpression due to these non-random events would suggest that cortactin provides tumors a selective advantage during the progression of the disease. Specifically, in head and neck squamous cell carcinoma (HNSCC), 11q13 amplification occurs in nearly 30% - 40% of the tumors and is predictive of survival and metastasis independent of tumor stage, lymph node status and distant metastasis [114, 175, 176]. In addition, the cancer genome atlas (TCGA) has identified 11q13 as an important alteration in a pan-cancer analysis. The analysis comprised of twelve human cancer types that were divided into distinct classes based on either mutations or copy number changes.

11q13 was defined as a distinct subclass within one of these classes [177]. Furthermore, 11q13 amplification is thought to be a late stage event that drives tumor progression instead of initiation [178, 179]. The 11q13 amplicon that comprises of cortactin is nearly 1.5Mb and contains twelve genes (Table 3)[112, 114, 144, 180-183]. Amongst the genes that are present, cyclin D1 (CCND1) and cortactin (CTTN) are studied in the context of driving cancer progression. Work done by Rodrigo et. al. clearly demonstrates that CTTN and CCND1 are present on the opposite ends of the amplicon, and CTTN amplification independent of CCND1 correlated with poor patient outcome [114].

Cortactin, a src kinase substrate has been shown to play an important role in promoting cell motility, invasion, functioning of invadopodia, along with regulation of protease secretion [75, 76, 98, 118]. Also, it has been shown that cortactin regulates additional aggressive cancer traits like tumor growth, serum-, and anchorage- independent growth [115]. Taking together these studies one underlying question is whether cortactin mediated exosome secretion can account for these tumor related phenotype? This is of great importance as it would suggest that cortactin functions in an autocrine manner to sustain tumor survival and proliferation. Indeed my dissertation work clearly shows that exosomes derived from head and neck squamous cell carcinoma cells could account for cortactin knockdown phenotype both in vitro and in vivo.

Table 3. Genes found in HNSCC 11q13 amplicon	
Gene	Function
Two pore segment channel 2 (TPCN2)	Ion channel
Cyclin D1 (CCND1)	Cell cyle
Myeloma overexpressed gene (MYEOV)	Proliferation and invasion
Oral cancer overexpressed 1 (ORAOV1/TAOS1)	Prevention of ROS damage
Fibroblast growth factor 19 (FGF19)	Growth factor in FGF signaling
Fibroblast growth factor 4 (FGF4)	Growth factor in FGF signaling
Fibroblast growth factor 3 (FGF3)	Growth factor in FGF signaling
Anoctamin 1 (ANO1)	Ca^{2+} activated Cl^- channel
Fas-associated via death domain (FADD)	Apoptosis
Protein tyrosine phosphatase, receptor type, f polypeptide (PTPRF) interacting protein (liprin) α1 (PPFIA1)	Tyrosine phosphatase
Cortactin (CTTN)	Activates and binds to Arp2/3, and F-actin
Shank 2 (SHANK2)	Scaffolding protein

Results

Cortactin expression correlates with patient survival in HNSCC cancer

Numerous small studies have associated cortactin overexpression with a worse patient prognosis, especially in HNSCC [58, 114, 184, 185]. To confirm this finding in a larger and standardized human tumor sample set, we utilized newly available genomic data from The Cancer Genome Atlas (TCGA). Consistent with previous findings, multivariate Cox regression analysis of RNA sequencing and patient follow up data revealed that patient tumors with high levels of cortactin mRNA expression were significantly associated with decreased patient survival (Figure 16A), independent of tumor stage and lymph node status (N). In separate statistical tests, cortactin RNA expression was significantly associated with higher lymph node status (e.g. N2 and N1, compared to N0) but not with tumor stage (Figure 17). Consistent with gene amplification driving cortactin RNA expression, cortactin mRNA expression correlated with cortactin copy number alterations (Figure 16B).

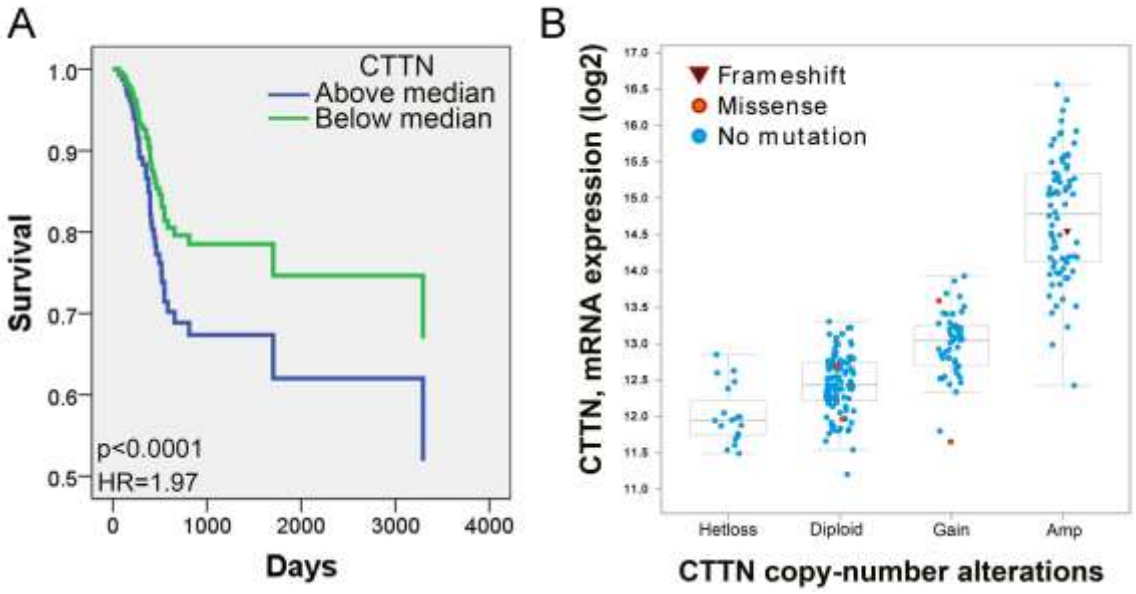

Figure 16. High cortactin mRNA expression levels in HNSCC tumors is associated with decreased patient survival. (A) Cox regression analysis of survival of HPV-negative HNSCC patients segregated by cortactin (CTTN) mRNA expression levels of their tumors, as indicated. Analysis was adjusted for both stage and lymph node status. N=245 patients H.R.=hazard ratio. (B) Graph of CTTN mRNA expression in patients with different types of copy number alterations and/or mutations, as indicated.

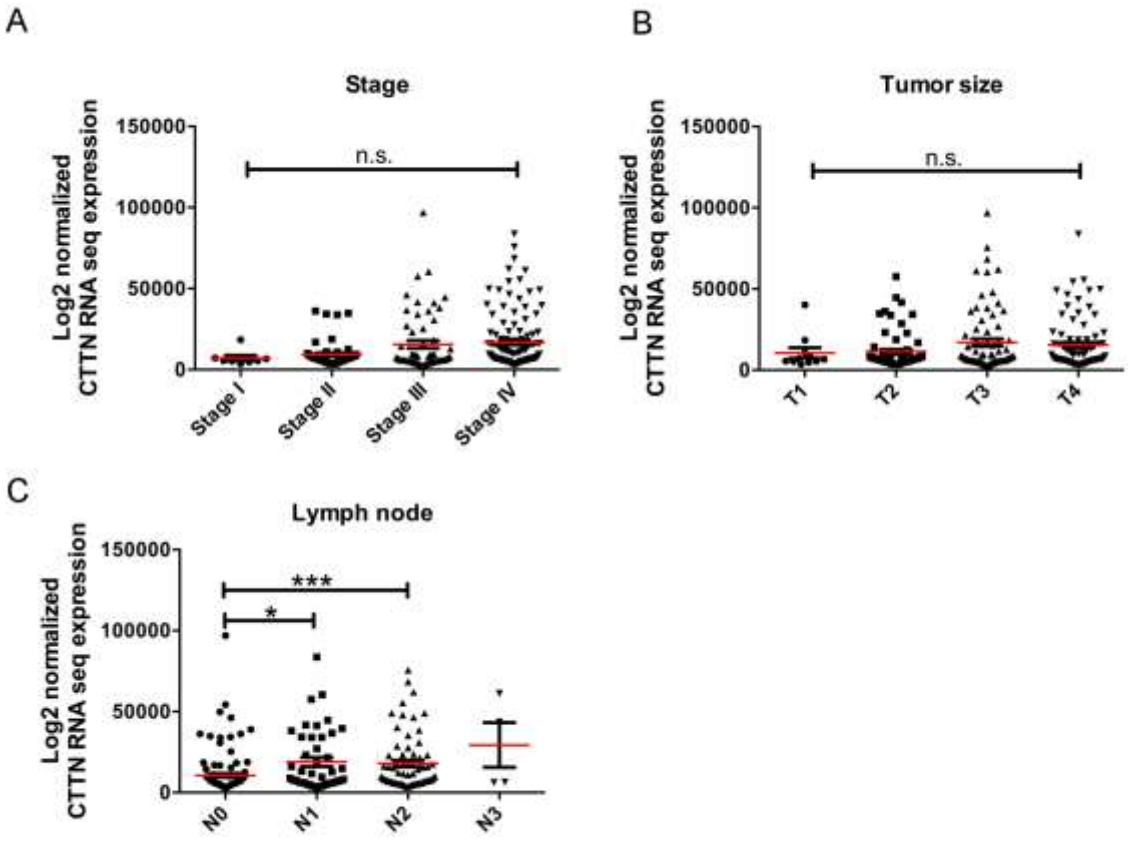

Figure 17. Cortactin mRNA expression in patients. Analysis of association of CTTN mRNA expression with patient stage (A), tumor stage (B), or lymph node stage (C). *p<0.05, ***p<0.001. For tumor stage n=236 patients. For tumor size n=236 patients. For lymph node status n=233 patients. Y-axis represents normalized log2 transformed mRNA expression (RNA-seq by Expectation Maximization (RSEM)).

Exosomes promote serum independent growth and transwell invasion

Cortactin is known to control a variety of oncogenic cellular traits, including serum- and anchorage-independent growth, and cellular invasiveness [58, 73, 115, 186]. To test whether control of exosome secretion is a component of cortactin function in cancer cell aggressiveness, we determined whether coincubation of cortactin-KD cells with purified exosomes could rescue defects of those cells in serum independent growth and invasion. To test serum-independent growth, an equal number of control and cortactin-KD1 cells were incubated for 4 days in serum-free, growth factor-free media in the presence or absence of 50 □g/ml exosomes purified from control or cortactin-KD1 cells, and then trypsinized and counted. This concentration was chosen based on a previous range of 25 µg-100 µg shown to be effective in modulating cell proliferation and migration [187] and represent 35 X 10^8 exosomes per well. As a positive control, Rab27a-KD cells were also tested [5, 36]. As previously reported [115], cortactin-KD cells proliferated less under serum-independent conditions than control cells (Figure 18A, left panel). Consistent with an important role for exosomes in serum-independent growth, Rab27a-KD cells also proliferated less than control cells in the absence of serum (Figure 17A, right panel). However, in the presence of 50 µg/ml of ultracentrifuge-purified exosomes (UC-exosomes), the defects in serum-independent growth of either cortactin- or Rab27a-KD cells were fully rescued (Figure 18A). Consistent with our finding that cortactin controls primarily the number of secreted exosomes and not their cargo content (Figures 4-6), exosomes purified from cortactin-KD cells rescued cortactin-KD cell defects to

the same extent as an equivalent concentration of exosomes purified from control cells. Likewise, consistent with the reported role of Rab27a in controlling docking of MVE with the plasma membrane [36] rather than upstream exosome biogenesis, 50 μg/ml of UC-exosomes purified from control or Rab27a-KD cells also had equivalent bioactivity in rescuing serum–independent growth of Rab27a-KD cells.

To determine whether purified exosomes can rescue cortactin-KD cell defects in cellular invasion, 50 μg/ml of UC-exosomes derived from either control or cortactin-KD cells were mixed with control or cortactin-KD cells and added to the top of Matrigel-coated Transwell invasion chambers. The matrix metalloproteinase inhibitor GM6001 was used as a positive control to prevent invasion of control cells (Figure 18B, left panel). After 48 h, the number of cells that had invaded to the bottom of the filter were counted. Similar to the serum-independence assay results, defects in Transwell invasion of cortactin-KD and Rab27a-KD cells were equivalently rescued by exosomes derived from either control or the appropriate KD cells (Figure 18B).

Since ultracentrifuge preparations of exosomes can contain protein aggregates [146], we further purified ultracentrifuged exosomes (UC) by density gradient sedimentation into a 5%-40% gradient of iodixanol. Western blot analysis of the fractions revealed that exosomes were primarily present in fraction 7 (Figure 18C, DG-exosomes), consistent with their expected density of ~1.11 [188]. NTA analysis revealed a similar peak size of DG exosomes to that of UC exosomes, although with a slightly more narrow size distribution (Figure

17D). TEM images of negatively stained DG exosomes confirmed typical exosome morphology of the vesicles and revealed less background staining when compared to UC-exosomes (compare Figure 18E to Figure 5D, note some background is typical in all samples due to drying of the negative stain on the grid).

To determine whether DG exosomes could rescue serum-independent growth defects of cortactin-KD cells similarly to UC-exosomes, cortactin-KD cells were cultured in serum free media in the presence or absence of various concentrations of microvesicles (MV, 10,000 x g fraction), UC-exosomes, or DG-exosomes for 96 h. Based on the numbers of exosomes that we purify from control cells over a period of 48 h, we estimate that control cells secrete approximately 40-50 exosomes per cell per hour (Figure 5B). This estimate does not take into account exosome uptake by cells or loss during the purification process. Based on that estimate and the number of cells in each well, we estimated that control cells would secrete approximately 120 X 10^6 exosomes over a period of 96h (see Figure 17F for details). Hence, we treated cortactin-KD cells with doses ranging from 12 X 10^6 to 120 X 10^6 exosomes for the 96 h period of the assay (Figure 18G). MV were used as a negative control and tested at the highest dose of 120 X 10^6 vesicles per well. Serum-independent proliferation growth defects of KD cells were fully rescued by coincubation of cells with

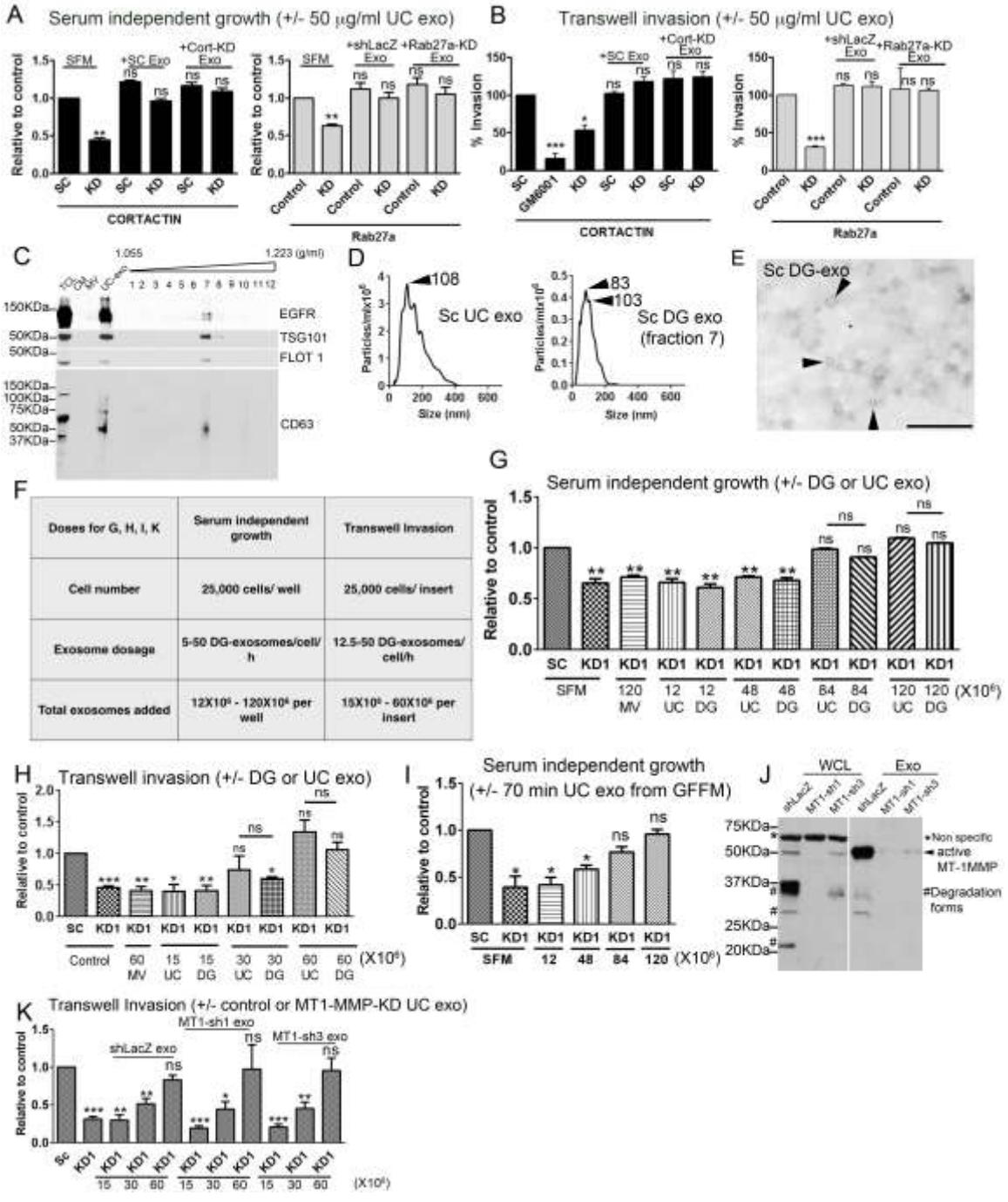

Figure legend next page

Figure 18: Cortactin-dependent oncogenic phenotypes are controlled by exosomes *in vitro*. (A) Cells were cultured in serum-free medium (SFM) or SFM supplemented with equal concentrations (50 µg/ml, calculated to be 35 X 10^8 exosomes per well) of control (+SC Exo or +shLacZ Exo) or cortactin-KD or Rab27a-KD UC exosomes, as indicated, for 4 days. Relative number of cells compared to control cells (SFM condition) shown as mean +/- SE, N=3 independent experiments with triplicate wells. (B) 48 h invasion across Matrigel-coated invasion chambers in the presence or absence of equal concentrations (50 µg/ml) control or KD UC exosomes. Cells per image were averaged for each replicate. N=3 independent experiments with duplicate wells. (C) WB of exosome markers in control and cortactin-KD total cell lysates (TCL), conditioned medium (CM), microvesicles (MV), UC exosomes, or density gradient (DG) fractions 1-12. Note the presence of exosome markers in fraction 7. (D) Representative (from N=3) NTA size distribution traces of UC exosomes and DG exosome fraction #7. (E) Representative TEM images of DG exosome fraction #7 preparation from scrambled control (Sc) cells. (F) Table outlining exosome doses used in experiments G-I, K. (G) Serum-independent growth of control (Sc) and cortactin-KD1 cells cultured in the presence of various concentrations (12-120x10^6, indicated below) of UC or DG exosomes, or MV derived from control cells. N=3 independent experiments with triplicate wells. (H) 48 h invasion across Matrigel-coated invasion chambers in the presence of various concentrations of control cell UC or DG exosomes, or MV. N=3 independent experiments with duplicate wells. (I) Serum-independent growth of control (Sc) and cortactin-KD1 cells cultured in the presence or absence of exosomes purified by 70 min ultracentrifugation from Sc cells cultured in growth factor-free medium (GFFM). N=3 independent experiments with triplicate wells. (J) WB of whole cell lysate and UC exosomes derived from SCC61 cells shLacZ (control), and MT1-MMP knockdown (MT1-sh1 and sh3). Note active MT1-MMP ~ 55KDa, * = non specific bands, #. = degradation forms (K). Bar graphs = mean+/-SE. *$p<0.05$, **$p<0.01$, ***$p<0.001$, determined by Student's t-Test.

UC-exosomes and DG-exosomes at both the 84 X 10^6 and 120 X 10^6 vesicle concentrations. By contrast, there was no effect of MV purified from the same CM on serum-independent proliferation of KD cells (Figure 18G). Similarly, both UC and DG exosomes rescued Transwell invasion of cortactin-KD cells whereas the highest concentration of MVs had no effect (Figure 18G, H). Although there was a trend towards increased efficacy of UC exosomes in these assays, the differences were small and not statistically significant. Since the OptiMEM media that we use to prepare conditioned medium and thus exosomes contains growth factors, we also tested whether exosomes purified from growth factor-free media with a 70 min UC step can rescue serum-independent growth of cortactin-KD cells. Indeed, exosomes purified this way did rescue serum-independent growth, at similar concentrations to UC or DG exosomes purified from OptiMEM (compare Figure 18I and Figure 18G). We also tested whether the key invadopodial proteinase MT1-MMP is an essential exosome cargo for promoting Transwell invasion. Cortactin-KD cells were incubated with UC exosomes purified from either control or MT1-MMP-KD cells in Transwell invasion chambers. Surprisingly, we found equivalent activity of control and MT1-MMP-KD exosomes in rescuing cortactin-KD cell Transwell invasion (Figure 18J and K). These data reveal that exosomes are key drivers of tumor progression in HNSCC and also these data provide further evidence that promotion of exosome secretion by cortactin is a major mechanism by which cortactin promotes aggressive cancer behavior. Furthermore, these data suggest that other

exosome cargoes are either more important or compensate for MT1-MMP function in this assay.

Autocrine exosome secretion is critical for HNSCC tumor progression in vivo

Tumor cells are known to rely on autocrine secretion in order to sustain their survival and proliferation [45]. Previously, we showed that cortactin expression directly controls tumor growth in a semi-orthotopic model of HNSCC growth [115]. To determine whether control of exosome secretion is the mechanism by which cortactin controls HNSCC tumor growth, I tested whether adding back purified exosomes to implanted tumors could rescue the growth defects of cortactin-KD cells. SCC61 control and cortactin-KD cells were placed inside denuded rat tracheas and implanted in the flanks of nude mice. This model provides a physiologic environment that permits growth and appropriate histology of tumors grown from both primary and culture-adapted HNSCC cells [58, 124]. Cortactin-KD cells were coincubated with either PBS or 100 µg of exosomes at the time of implantation. The tumors that received exosomes at the time of implantation also received bi-weekly injections of 50 µg/ml purified exosomes for the subsequent 4 weeks, whereas those that received PBS at the time of implantation, received only PBS injections. Rab27a-KD cells again served as a positive control for the system.

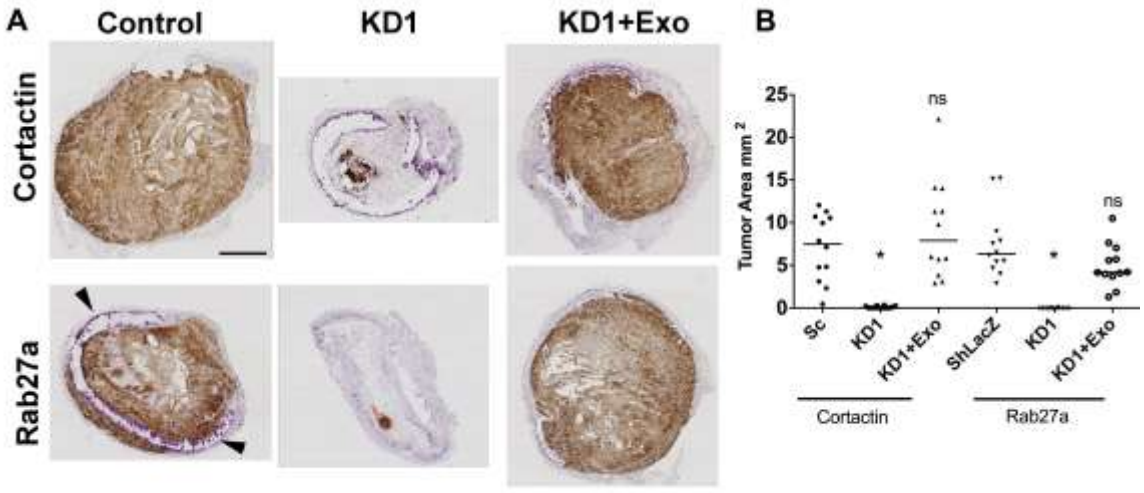

Figure 19. Cortactin-dependent oncogenic phenotypes are controlled by exosomes *in vivo*. (A) Exosomes derived from control cells rescue tumor size defects of cortactin-KD and Rab27a-KD cells. Images show immunohistochemistry staining of cytokeratin-positive tumors (brown stain). Arrowheads indicate a rat trachea that is surrounding the cytokeratin-positive tumor. Scale bar = 1 mm. Representative of 12 images per condition. (B) The cytokeratin-positive tumor section area was measured using online Digital Image Hub software. Line in scatter plot indicates median. N=12 tumors from two independent experiments for each condition. *p<0.05, **p<0.01, ***p<0.001.

As previously described [115], KD of cortactin led to greatly decreased tumor growth (Figure 19A, B). Consistent with an important role for exosomes in sustaining tumor growth, Rab27a-KD cells also exhibited greatly decreased tumor growth. However, tumor growth was fully rescued in the cortactin-KD and Rab27a-KD tumors that received purified exosomes. Immunostaining of tracheal sections with a pan-cytokeratin antibody to identify epithelial tumor cells revealed very few cancer cells within the tracheal tumors and full rescue by exosome coincubation (Figure 19A, B). In control tumors and in KD tumors that had received exosome injections, the tumor also frequently degraded or invaded past the tracheal ring indicating an invasive phenotype [115]. However, since the KD tumors exhibited such large growth defects, we were not able to assess whether there was also an *in vivo* invasion defect. These data suggest that exosome secretion is a major mechanism by which cortactin controls tumor growth in this model.

Discussion

Cortactin is known to regulate aggressive cancer cell traits, including tumor growth, cancer cell invasion and motility, and serum- and anchorage-independent growth [189]. The mechanisms by which cortactin controls many of these functions has been unclear and could be due to *in situ* control of cytoskeletal motility structures, secretion, or signaling [58]. Our finding that cortactin-KD cell defects in many of these traits can be rescued by incubation with purified exosomes suggest that a major way that cortactin promotes tumor aggressiveness is by enhancing exosome secretion. Exosomes could contribute growth and angiogenic factors to promote tumor cell survival and *in vivo* growth. Indeed, we previously showed that cortactin-KD led to reduced density of blood vessels in HNSCC tumors [115]. Also, proteinases associated with exosomes such as MT1-MMP and MMP9 (Figure 5F) could promote invasive behavior and counteract the secretion defects of cortactin-KD cells [98, 115].

In HNSCC, the cortactin gene (CTTN, also known as EMS1) is located on one end of a core 11q13 amplicon that contains 13 genes [112]. Cyclin D1 is usually located on the other end. Additional candidate oncogenes are also overexpressed. Enhanced exosome secretion due to cortactin overexpression could synergize with cyclin D1 and other cell cycle drivers such as the 11q13-amplified gene FADD [190] by providing growth factor support via exosomes. Since 11q13 amplification is often a late-stage event [191], enhancement of exosome secretion via cortactin overexpression is also likely to synergize with oncogenic drivers outside of the amplicon to promote tumor angiogenesis, growth and

invasiveness. Our previous finding that cortactin expression levels tune the intrinsic aggressiveness of diverse HNSCC cell lines is consistent with a role for exosomes in amplifying already present aggressive cancer phenotypes [115].

In summary, we find that cortactin promotes exosome secretion from cancer cells. These findings may explain the strong association of cortactin gene amplification with poor patient prognosis.

CHAPTER V

DISCUSSION AND FUTURE DIRECTIONS

Actin cytoskeleton dynamics plays a crucial role in membrane trafficking that is essential during cell migration and cell invasion. This dissertation addresses a novel role of an actin binding protein, cortactin, in regulating membrane trafficking and docking of the MVE at the plasma membrane. Furthermore, the work presented here represents a novel interface between actin dynamics at the plasma membrane along with key contributors regulating exosome secretion. We recently demonstrated invadopodia as key docking sites for MVE carrying the matrix metalloproteinases [35]. Indeed, in my dissertation I show that cortactin, Rab27a, and coronin coordinately control actin turnover at invadopodia along with the exosome secretion.

In a pathological disease like cancer, secretion of LE/Lys derived secretory vesicles called exosomes is upregulated and is also linked with the tumor aggressiveness and metastasis [192]. Infact, a positive correlation between increased exosome secretion and tumor stage and progression has been reported [193]. Exosomes can not only bring about modulation of local environment but they can also travel to distant organ sites where they help in preparing pre-metastatic niche, immune modulation, and cell to cell communication of pro-oncogenic signals (e.g. EGFRVIII, miRNAs) [1, 10, 37, 49]. However, the key effectors in the exosome secretion pathway are still poorly understood. Cortactin has

emerged as a key player intersecting actin cytoskeletal machinery as well as signaling pathways. Previous work in our lab has demonstrated that cortactin is essential for secretion of key invadopodia associated metalloproteinases like MMP2, MMP9, and MT1-MMP [98, 118]. Also, we have shown that these matrix metalloproteinases along with ECM proteins like FN in LE/Lys compartments are being regulated by cortactin [35, 46, 63, 77, 100]. Hence, in my dissertation, I hypothesized that cortactin promotes exosome secretion along with tumor progression. Indeed, I found that cortactin regulates exosome number secretion without affecting the cargo content of exosomes. Also, this exosome secretion regulated by cortactin expression can sustain HNSCC tumor growth *in vivo*.

Going forward, a critical future direction is to understand in the context of cortactin overexpression and Rab27a knockdown, whether cortactin directly or indirectly interacts with myosin Va for bringing about exosome secretion or whether cortactin bypasses myosin Va and interacts with alternative machinery like the SNARE machinery at the plasma membrane or both. Work done by Ostrowski et.al. elegantly shows Rab27a and Rab27b both as important players in the exosome secretion pathway [36]. Specifically, Rab27a was shown to play a key role in docking of the MVEs at the plasma membrane [36]. Research done in melanosome trafficking demonstrated that Rab27a binds to melanosome first followed by recruitment of melanophilin, a Rab27a effector followed by myosin Va recruitment [165]. Fixed and live imaging using labeled myosin Va and CD63 would help in determining in cortactin overexpressing cells lacking Rab27a the dynamics of interaction between MVEs and actin-based motor protein in the

exocytosis process. Additionally, knockdown of Rab27a and myosin Va in cortactin overexpressing cells will help demonstrate the importance of myosin Va and cortactin in exosome secretion. Alternatively, the exocyst complex at the plasma membrane can also serves as an important contender in this exocytic process. Work done by Monteiro et.al. described interaction between the exocyst complex and endosomal Arp2/3 activator WASH on MT1-MMP containing late endosomes [194]. Interestingly, depletion of WASH, led to a significant decrease in the endosomal cortactin [194] as both WASH and cortactin is associated with the LE/Lys structures [63, 77]. This also resulted in a decrease in MT1-MMP delivery to invadopodia and hence affecting matrix degradation [194]. Additionally, cortactin is thought of as a scaffolding protein, and is known to interact with an exocyst complex player Sec8/EXOC4 via SHANK2 and PSD-95. While my dissertation work shows that SH3 domain mutant of cortactin does not affect exosome secretion, it would be interesting to determine whether under cortactin overexpression conditions the SH3 domain of the overexpressed protein leads to the interaction of cortactin with its SH3 binding partners that further promotes exosome secretion with or without Rab27a knockdown. Does cortactin overexpression utilize SH3 domain binding partner SHANK2 and its association with the exocyst machinery that further leads to compensation for Rab27a loss?

Another interesting area that can be pursued is to understand the role of phosphoinositied (PI), PI (3,5) bisphosphate ($PI(3,5)P_2$) and cortactin in exosome secretion. $PI(3,5)P_2$ is enriched on the MVE membrane and recently we have shown that the $PI(3,5)P_2$ regulates cortactin and endosomal actin [63]. Also,

$PI(3,5)P_2$ has been shown to regulate endo-lysosomal acidification in yeast, *C.elegans, Drosophila*, and *Arabidopsis* via unknown mechanisms [195-198]. One likely candidate is V-ATPase. V-ATPase binds to the F-actin along with the WASH-mediated actin assembly on endosomes leading to the sorting of the V-ATPase that further regulates membrane fusion and exocytosis [67, 199, 200]. Also, F-actin and V-ATPase directly interact with the SNARE proteins affecting exocytosis [201]. Since our lab has shown the regulation of endosomal actin by $PI(3,5)P_2$, it is likely that it interacts with the V-ATPase and affects endosomal acidification. Also, upon bafilomycin A treatment, exosome secretion is affected (data not shown) as bafilomycin A affects endosomal acidification. It would be important to determine if cortactin, $PI(3,5)P_2$ and V-ATPase coordinately promote exosome secretion by affecting the endo-lysosomal acidification.

Furthermore, in my dissertation, cortactin that is located on the 11q13 amplicon has been shown to regulate exosome secretion. However, the amplicon comprises of an additional set of genes (Table 3). It is still unclear if 11q13 overall is associated with the exosome secretion in HNSCC patients. One important candidate gene within this amplicon is SHANK2. Future studies correlating the 11q13 amplification status of the primary tumors with the patient plasma will help determine the contribution of the entire amplicon. SHANK2 is both present on the amplicon and associates with cortactin and the exocyst complex including Sec8 [202]. It would be critical to determine whether both SHANK2 and cortactin cooperatively promote exosome secretion by binding to the exocyst complex.

Overall, these studies will help identify molecular and cellular mechanisms involved in the exosome secretion pathway. This is of great importance specifically in terms of potential anti-exosome therapy to limit tumor progression. Ultimately, this work will open new avenues of research in the cancer secretory pathways and in the study of cancer progression.

REFERENCES

1. Raposo, G. & Stoorvogel, W. Extracellular vesicles: exosomes, microvesicles, and friends. *J Cell Biol* **200**, 373-383 (2013).
2. Trams, E.G., Lauter, C.J., Salem, N., Jr. & Heine, U. Exfoliation of membrane ecto-enzymes in the form of micro-vesicles. *Biochimica et biophysica acta* **645**, 63-70 (1981).
3. Pan, B.T. & Johnstone, R.M. Fate of the transferrin receptor during maturation of sheep reticulocytes in vitro: selective externalization of the receptor. *Cell* **33**, 967-978 (1983).
4. Pan, B.T., Teng, K., Wu, C., Adam, M. & Johnstone, R.M. Electron microscopic evidence for externalization of the transferrin receptor in vesicular form in sheep reticulocytes. *J Cell Biol* **101**, 942-948 (1985).
5. Bobrie, A. *et al.* Rab27a supports exosome-dependent and -independent mechanisms that modify the tumor microenvironment and can promote tumor progression. *Cancer Res* **72**, 4920-4930 (2012).
6. Demory Beckler, M. *et al.* Proteomic analysis of exosomes from mutant KRAS colon cancer cells identifies intercellular transfer of mutant KRAS. *Mol Cell Proteomics* **12**, 343-355 (2013).
7. Hendrix, A. & Hume, A.N. Exosome signaling in mammary gland development and cancer. *Int J Dev Biol* **55**, 879-887 (2011).
8. Higginbotham, J.N. *et al.* Amphiregulin exosomes increase cancer cell invasion. *Curr Biol* **21**, 779-786 (2011).
9. Thery, C., Zitvogel, L. & Amigorena, S. Exosomes: composition, biogenesis and function. *Nat Rev Immunol* **2**, 569-579 (2002).
10. Valadi, H. *et al.* Exosome-mediated transfer of mRNAs and microRNAs is a novel mechanism of genetic exchange between cells. *Nat Cell Biol* **9**, 654-659 (2007).
11. Futter, C.E., Pearse, A., Hewlett, L.J. & Hopkins, C.R. Multivesicular endosomes containing internalized EGF-EGF receptor complexes mature and then fuse directly with lysosomes. *J Cell Biol* **132**, 1011-1023 (1996).
12. Hanson, P.I. & Cashikar, A. Multivesicular body morphogenesis. *Annu Rev Cell Dev Biol* **28**, 337-362 (2012).
13. Schmidt, O. & Teis, D. The ESCRT machinery. *Curr Biol* **22**, R116-120 (2012).
14. Raymond, C.K., Howald-Stevenson, I., Vater, C.A. & Stevens, T.H. Morphological classification of the yeast vacuolar protein sorting mutants: evidence for a prevacuolar compartment in class E vps mutants. *Mol Biol Cell* **3**, 1389-1402 (1992).
15. Rieder, S.E., Banta, L.M., Kohrer, K., McCaffery, J.M. & Emr, S.D. Multilamellar endosome-like compartment accumulates in the yeast vps28 vacuolar protein sorting mutant. *Mol Biol Cell* **7**, 985-999 (1996).
16. Katzmann, D.J., Stefan, C.J., Babst, M. & Emr, S.D. Vps27 recruits ESCRT machinery to endosomes during MVB sorting. *J Cell Biol* **162**, 413-423 (2003).

17. Bache, K.G., Brech, A., Mehlum, A. & Stenmark, H. Hrs regulates multivesicular body formation via ESCRT recruitment to endosomes. *J Cell Biol* **162**, 435-442 (2003).
18. Tamai, K. *et al.* Exosome secretion of dendritic cells is regulated by Hrs, an ESCRT-0 protein. *Biochem Biophys Res Commun* **399**, 384-390 (2010).
19. Razi, M. & Futter, C.E. Distinct roles for Tsg101 and Hrs in multivesicular body formation and inward vesiculation. *Mol Biol Cell* **17**, 3469-3483 (2006).
20. Pornillos, O. *et al.* HIV Gag mimics the Tsg101-recruiting activity of the human Hrs protein. *J Cell Biol* **162**, 425-434 (2003).
21. Piper, R.C., Cooper, A.A., Yang, H. & Stevens, T.H. VPS27 controls vacuolar and endocytic traffic through a prevacuolar compartment in Saccharomyces cerevisiae. *J Cell Biol* **131**, 603-617 (1995).
22. Colombo, M. *et al.* Analysis of ESCRT functions in exosome biogenesis, composition and secretion highlights the heterogeneity of extracellular vesicles. *J Cell Sci* **126**, 5553-5565 (2013).
23. Katzmann, D.J., Odorizzi, G. & Emr, S.D. Receptor downregulation and multivesicular-body sorting. *Nat Rev Mol Cell Biol* **3**, 893-905 (2002).
24. Babst, M., Wendland, B., Estepa, E.J. & Emr, S.D. The Vps4p AAA ATPase regulates membrane association of a Vps protein complex required for normal endosome function. *EMBO J* **17**, 2982-2993 (1998).
25. Wagner, K.U. *et al.* Tsg101 is essential for cell growth, proliferation, and cell survival of embryonic and adult tissues. *Mol Cell Biol* **23**, 150-162 (2003).
26. Komada, M. & Soriano, P. Hrs, a FYVE finger protein localized to early endosomes, is implicated in vesicular traffic and required for ventral folding morphogenesis. *Genes Dev* **13**, 1475-1485 (1999).
27. Stuffers, S., Sem Wegner, C., Stenmark, H. & Brech, A. Multivesicular endosome biogenesis in the absence of ESCRTs. *Traffic* **10**, 925-937 (2009).
28. Trajkovic, K. *et al.* Ceramide triggers budding of exosome vesicles into multivesicular endosomes. *Science* **319**, 1244-1247 (2008).
29. Strauss, K. *et al.* Exosome secretion ameliorates lysosomal storage of cholesterol in Niemann-Pick type C disease. *J Biol Chem* **285**, 26279-26288 (2010).
30. Laulagnier, K. *et al.* PLD2 is enriched on exosomes and its activity is correlated to the release of exosomes. *FEBS Lett* **572**, 11-14 (2004).
31. Ghossoub, R. *et al.* Syntenin-ALIX exosome biogenesis and budding into multivesicular bodies are controlled by ARF6 and PLD2. *Nature communications* **5**, 3477 (2014).
32. Escola, J.M. *et al.* Selective enrichment of tetraspan proteins on the internal vesicles of multivesicular endosomes and on exosomes secreted by human B-lymphocytes. *J Biol Chem* **273**, 20121-20127 (1998).
33. Perez-Hernandez, D. *et al.* The intracellular interactome of tetraspanin-enriched microdomains reveals their function as sorting machineries toward exosomes. *J Biol Chem* **288**, 11649-11661 (2013).
34. van Niel, G. *et al.* The tetraspanin CD63 regulates ESCRT-independent and -dependent endosomal sorting during melanogenesis. *Dev Cell* **21**, 708-721 (2011).

35. Hoshino, D. *et al.* Exosome secretion is enhanced by invadopodia and drives invasive behavior. *Cell Rep* **5**, 1159-1168 (2013).
36. Ostrowski, M. *et al.* Rab27a and Rab27b control different steps of the exosome secretion pathway. *Nat Cell Biol* **12**, 19-30; sup pp 11-13 (2010).
37. Peinado, H. *et al.* Melanoma exosomes educate bone marrow progenitor cells toward a pro-metastatic phenotype through MET. *Nat Med* **18**, 883-891 (2012).
38. Hsu, C. *et al.* Regulation of exosome secretion by Rab35 and its GTPase-activating proteins TBC1D10A-C. *J Cell Biol* **189**, 223-232 (2010).
39. Savina, A., Fader, C.M., Damiani, M.T. & Colombo, M.I. Rab11 promotes docking and fusion of multivesicular bodies in a calcium-dependent manner. *Traffic* **6**, 131-143 (2005).
40. Stenmark, H. Rab GTPases as coordinators of vesicle traffic. *Nat Rev Mol Cell Biol* **10**, 513-525 (2009).
41. Rao, S.K., Huynh, C., Proux-Gillardeaux, V., Galli, T. & Andrews, N.W. Identification of SNAREs involved in synaptotagmin VII-regulated lysosomal exocytosis. *J Biol Chem* **279**, 20471-20479 (2004).
42. Tiwari, N. *et al.* VAMP-8 segregates mast cell-preformed mediator exocytosis from cytokine trafficking pathways. *Blood* **111**, 3665-3674 (2008).
43. Puri, N. & Roche, P.A. Mast cells possess distinct secretory granule subsets whose exocytosis is regulated by different SNARE isoforms. *Proc Natl Acad Sci U S A* **105**, 2580-2585 (2008).
44. Proux-Gillardeaux, V., Raposo, G., Irinopoulou, T. & Galli, T. Expression of the Longin domain of TI-VAMP impairs lysosomal secretion and epithelial cell migration. *Biol Cell* **99**, 261-271 (2007).
45. Hanahan, D. & Weinberg, R.A. Hallmarks of cancer: the next generation. *Cell* **144**, 646-674 (2011).
46. Sung, B.H., Ketova, T., Hoshino, D., Zijlstra, A. & Weaver, A.M. Directional cell movement through tissues is controlled by exosome secretion. *Nature communications* **6**, 7164 (2015).
47. Zhou, W. *et al.* Cancer-secreted miR-105 destroys vascular endothelial barriers to promote metastasis. *Cancer cell* **25**, 501-515 (2014).
48. Costa-Silva, B. *et al.* Pancreatic cancer exosomes initiate pre-metastatic niche formation in the liver. *Nat Cell Biol* **17**, 816-826 (2015).
49. Hoshino, A. *et al.* Tumour exosome integrins determine organotropic metastasis. *Nature* **527**, 329-335 (2015).
50. Pollard, T.D. & Cooper, J.A. Actin, a central player in cell shape and movement. *Science* **326**, 1208-1212 (2009).
51. Egea, G., Lazaro-Dieguez, F. & Vilella, M. Actin dynamics at the Golgi complex in mammalian cells. *Curr Opin Cell Biol* **18**, 168-178 (2006).
52. Kaksonen, M. Taking apart the endocytic machinery. *J Cell Biol* **180**, 1059-1060 (2008).
53. Merrifield, C.J., Perrais, D. & Zenisek, D. Coupling between clathrin-coated-pit invagination, cortactin recruitment, and membrane scission observed in live cells. *Cell* **121**, 593-606 (2005).

54. Chesarone, M.A. & Goode, B.L. Actin nucleation and elongation factors: mechanisms and interplay. *Curr Opin Cell Biol* **21**, 28-37 (2009).
55. Cooper, J.A. & Sept, D. New insights into mechanism and regulation of actin capping protein. *Int Rev Cell Mol Biol* **267**, 183-206 (2008).
56. Ono, S. Mechanism of depolymerization and severing of actin filaments and its significance in cytoskeletal dynamics. *Int Rev Cytol* **258**, 1-82 (2007).
57. Paavilainen, V.O., Bertling, E., Falck, S. & Lappalainen, P. Regulation of cytoskeletal dynamics by actin-monomer-binding proteins. *Trends Cell Biol* **14**, 386-394 (2004).
58. Kirkbride, K.C., Sung, B.H., Sinha, S. & Weaver, A.M. Cortactin: a multifunctional regulator of cellular invasiveness. *Cell Adh Migr* **5**, 187-198 (2011).
59. Oikawa, T. *et al.* PtdIns(3,4,5)P3 binding is necessary for WAVE2-induced formation of lamellipodia. *Nat Cell Biol* **6**, 420-426 (2004).
60. Campellone, K.G., Webb, N.J., Znameroski, E.A. & Welch, M.D. WHAMM is an Arp2/3 complex activator that binds microtubules and functions in ER to Golgi transport. *Cell* **134**, 148-161 (2008).
61. Derivery, E. *et al.* The Arp2/3 activator WASH controls the fission of endosomes through a large multiprotein complex. *Dev Cell* **17**, 712-723 (2009).
62. Gomez, T.S. & Billadeau, D.D. A FAM21-containing WASH complex regulates retromer-dependent sorting. *Dev Cell* **17**, 699-711 (2009).
63. Hong, N.H., Qi, A. & Weaver, A.M. PI(3,5)P2 controls endosomal branched actin dynamics by regulating cortactin-actin interactions. *J Cell Biol* **210**, 753-769 (2015).
64. Derivery, E., Helfer, E., Henriot, V. & Gautreau, A. Actin polymerization controls the organization of WASH domains at the surface of endosomes. *PLoS One* **7**, e39774 (2012).
65. Puthenveedu, M.A. *et al.* Sequence-dependent sorting of recycling proteins by actin-stabilized endosomal microdomains. *Cell* **143**, 761-773.
66. Duleh, S.N. & Welch, M.D. WASH and the Arp2/3 complex regulate endosome shape and trafficking. *Cytoskeleton (Hoboken)* **67**, 193-206 (2010).
67. Carnell, M. *et al.* Actin polymerization driven by WASH causes V-ATPase retrieval and vesicle neutralization before exocytosis. *J Cell Biol* **193**, 831-839 (2011).
68. Zech, T. *et al.* The Arp2/3 activator WASH regulates alpha5beta1-integrin-mediated invasive migration. *J Cell Sci* **124**, 3753-3759 (2011).
69. Sokac, A.M., Co, C., Taunton, J. & Bement, W. Cdc42-dependent actin polymerization during compensatory endocytosis in Xenopus eggs. *Nat Cell Biol* **5**, 727-732 (2003).
70. Yu, H.Y. & Bement, W.M. Control of local actin assembly by membrane fusion-dependent compartment mixing. *Nat Cell Biol* **9**, 149-159 (2007).
71. Malacombe, M. *et al.* Intersectin-1L nucleotide exchange factor regulates secretory granule exocytosis by activating Cdc42. *EMBO J* **25**, 3494-3503 (2006).

72. Zuo, X. *et al.* Exo70 interacts with the Arp2/3 complex and regulates cell migration. *Nat Cell Biol* **8**, 1383-1388 (2006).
73. Weaver, A.M. Invadopodia. *Curr Biol* **18**, R362-364 (2008).
74. Buday, L. & Downward, J. Roles of cortactin in tumor pathogenesis. *Biochimica et biophysica acta* **1775**, 263-273 (2007).
75. Weaver, A.M. Cortactin in tumor invasiveness. *Cancer Lett* **265**, 157-166 (2008).
76. Wu, H., Reynolds, A.B., Kanner, S.B., Vines, R.R. & Parsons, J.T. Identification and characterization of a novel cytoskeleton-associated pp60src substrate. *Mol Cell Biol* **11**, 5113-5124 (1991).
77. Kirkbride, K.C. *et al.* Regulation of late endosomal/lysosomal maturation and trafficking by cortactin affects Golgi morphology. *Cytoskeleton (Hoboken)* **69**, 625-643 (2012).
78. Ohoka, Y. & Takai, Y. Isolation and characterization of cortactin isoforms and a novel cortactin-binding protein, CBP90. *Genes Cells* **3**, 603-612 (1998).
79. van Rossum, A.G. *et al.* Alternative splicing of the actin binding domain of human cortactin affects cell migration. *J Biol Chem* **278**, 45672-45679 (2003).
80. Katsube, T., Togashi, S., Hashimoto, N., Ogiu, T. & Tsuji, H. Filamentous actin binding ability of cortactin isoforms is responsible for their cell-cell junctional localization in epithelial cells. *Archives of biochemistry and biophysics* **427**, 79-90 (2004).
81. Zhan, X. *et al.* Murine cortactin is phosphorylated in response to fibroblast growth factor-1 on tyrosine residues late in the G1 phase of the BALB/c 3T3 cell cycle. *J Biol Chem* **268**, 24427-24431 (1993).
82. Zhan, X., Plourde, C., Hu, X., Friesel, R. & Maciag, T. Association of fibroblast growth factor receptor-1 with c-Src correlates with association between c-Src and cortactin. *J Biol Chem* **269**, 20221-20224 (1994).
83. Kelley, L.C., Hayes, K.E., Ammer, A.G., Martin, K.H. & Weed, S.A. Cortactin phosphorylated by ERK1/2 localizes to sites of dynamic actin regulation and is required for carcinoma lamellipodia persistence. *PLoS One* **5**, e13847 (2010).
84. Oser, M. *et al.* Specific tyrosine phosphorylation sites on cortactin regulate Nck1-dependent actin polymerization in invadopodia. *J Cell Sci* **123**, 3662-3673 (2010).
85. Boyle, S.N., Michaud, G.A., Schweitzer, B., Predki, P.F. & Koleske, A.J. A critical role for cortactin phosphorylation by Abl-family kinases in PDGF-induced dorsal-wave formation. *Curr Biol* **17**, 445-451 (2007).
86. Vuori, K. & Ruoslahti, E. Tyrosine phosphorylation of p130Cas and cortactin accompanies integrin-mediated cell adhesion to extracellular matrix. *J Biol Chem* **270**, 22259-22262 (1995).
87. Zhu, J., Yu, D., Zeng, X.C., Zhou, K. & Zhan, X. Receptor-mediated endocytosis involves tyrosine phosphorylation of cortactin. *J Biol Chem* **282**, 16086-16094 (2007).
88. Martinez-Quiles, N., Ho, H.Y., Kirschner, M.W., Ramesh, N. & Geha, R.S. Erk/Src phosphorylation of cortactin acts as a switch on-switch off

mechanism that controls its ability to activate N-WASP. *Mol Cell Biol* **24**, 5269-5280 (2004).
89. Zhang, X. *et al.* HDAC6 modulates cell motility by altering the acetylation level of cortactin. *Mol Cell* **27**, 197-213 (2007).
90. Zhang, Y. *et al.* Deacetylation of cortactin by SIRT1 promotes cell migration. *Oncogene* **28**, 445-460 (2009).
91. Rey, M., Irondelle, M., Waharte, F., Lizarraga, F. & Chavrier, P. HDAC6 is required for invadopodia activity and invasion by breast tumor cells. *Eur J Cell Biol* **90**, 128-135 (2011).
92. Uruno, T. *et al.* Activation of Arp2/3 complex-mediated actin polymerization by cortactin. *Nat Cell Biol* **3**, 259-266 (2001).
93. Weaver, A.M. *et al.* Cortactin promotes and stabilizes Arp2/3-induced actin filament network formation. *Curr Biol* **11**, 370-374 (2001).
94. Weaver, A.M. *et al.* Interaction of cortactin and N-WASp with Arp2/3 complex. *Curr Biol* **12**, 1270-1278 (2002).
95. Kinley, A.W. *et al.* Cortactin interacts with WIP in regulating Arp2/3 activation and membrane protrusion. *Curr Biol* **13**, 384-393 (2003).
96. Bryce, N.S. *et al.* Cortactin promotes cell motility by enhancing lamellipodial persistence. *Curr Biol* **15**, 1276-1285 (2005).
97. Lai, F.P. *et al.* Cortactin promotes migration and platelet-derived growth factor-induced actin reorganization by signaling to Rho-GTPases. *Mol Biol Cell* **20**, 3209-3223 (2009).
98. Clark, E.S., Whigham, A.S., Yarbrough, W.G. & Weaver, A.M. Cortactin is an essential regulator of matrix metalloproteinase secretion and extracellular matrix degradation in invadopodia. *Cancer Res* **67**, 4227-4235 (2007).
99. Cao, H. *et al.* Actin and Arf1-dependent recruitment of a cortactin-dynamin complex to the Golgi regulates post-Golgi transport. *Nat Cell Biol* **7**, 483-492 (2005).
100. Sung, B.H., Zhu, X., Kaverina, I. & Weaver, A.M. Cortactin controls cell motility and lamellipodial dynamics by regulating ECM secretion. *Curr Biol* **21**, 1460-1469 (2011).
101. Steffen, A. *et al.* MT1-MMP-dependent invasion is regulated by TI-VAMP/VAMP7. *Curr Biol* **18**, 926-931 (2008).
102. Sbai, O. *et al.* Differential vesicular distribution and trafficking of MMP-2, MMP-9, and their inhibitors in astrocytes. *Glia* **58**, 344-366 (2010).
103. Sinha, S. *et al.* Cortactin promotes exosome secretion by controlling branched actin dynamics. *J Cell Biol* **214** (2016).
104. Schuuring, E., Verhoeven, E., Litvinov, S. & Michalides, R.J. The product of the EMS1 gene, amplified and overexpressed in human carcinomas, is homologous to a v-src substrate and is located in cell-substratum contact sites. *Mol Cell Biol* **13**, 2891-2898 (1993).
105. Yuan, B.Z., Zhou, X., Zimonjic, D.B., Durkin, M.E. & Popescu, N.C. Amplification and overexpression of the EMS 1 oncogene, a possible prognostic marker, in human hepatocellular carcinoma. *J Mol Diagn* **5**, 48-53 (2003).

106. Cai, J.H. *et al.* Expression of cortactin correlates with a poor prognosis in patients with stages II-III colorectal adenocarcinoma. *J Gastrointest Surg* **14**, 1248-1257 (2010).
107. Lin, C.K., Su, H.Y., Tsai, W.C., Sheu, L.F. & Jin, J.S. Association of cortactin, fascin-1 and epidermal growth factor receptor (EGFR) expression in ovarian carcinomas: correlation with clinicopathological parameters. *Dis Markers* **25**, 17-26 (2008).
108. Luo, M.L. *et al.* Amplification and overexpression of CTTN (EMS1) contribute to the metastasis of esophageal squamous cell carcinoma by promoting cell migration and anoikis resistance. *Cancer Res* **66**, 11690-11699 (2006).
109. Wang, X. *et al.* VEGF and cortactin expression are independent predictors of tumor recurrence following curative resection of gastric cancer. *J Surg Oncol* **102**, 325-330 (2010).
110. Xie, H.L. *et al.* Differential gene and protein expression in primary gastric carcinomas and their lymph node metastases as revealed by combined cDNA microarray and tissue microarray analysis. *J Dig Dis* **11**, 167-175 (2010).
111. Xu, X.Z. *et al.* Cytoskeleton alterations in melanoma: aberrant expression of cortactin, an actin-binding adapter protein, correlates with melanocytic tumor progression. *Mod Pathol* **23**, 187-196 (2010).
112. Gibcus, J.H. *et al.* Amplicon mapping and expression profiling identify the Fas-associated death domain gene as a new driver in the 11q13.3 amplicon in laryngeal/pharyngeal cancer. *Clinical cancer research : an official journal of the American Association for Cancer Research* **13**, 6257-6266 (2007).
113. Roy, P.G. & Thompson, A.M. Cyclin D1 and breast cancer. *Breast* **15**, 718-727 (2006).
114. Rodrigo, J.P., Garcia, L.A., Ramos, S., Lazo, P.S. & Suarez, C. EMS1 gene amplification correlates with poor prognosis in squamous cell carcinomas of the head and neck. *Clinical cancer research : an official journal of the American Association for Cancer Research* **6**, 3177-3182 (2000).
115. Clark, E.S. *et al.* Aggressiveness of HNSCC tumors depends on expression levels of cortactin, a gene in the 11q13 amplicon. *Oncogene* **28**, 431-444 (2009).
116. Mori, H. *et al.* CD44 directs membrane-type 1 matrix metalloproteinase to lamellipodia by associating with its hemopexin-like domain. *EMBO J* **21**, 3949-3959 (2002).
117. Johnson, H.W. & Schell, M.J. Neuronal IP3 3-kinase is an F-actin-bundling protein: role in dendritic targeting and regulation of spine morphology. *Mol Biol Cell* **20**, 5166-5180 (2009).
118. Clark, E.S. & Weaver, A.M. A new role for cortactin in invadopodia: regulation of protease secretion. *Eur J Cell Biol* **87**, 581-590 (2008).
119. MacCoss, M.J. *et al.* Shotgun identification of protein modifications from protein complexes and lens tissue. *Proc Natl Acad Sci U S A* **99**, 7900-7905 (2002).
120. Martinez, M.N. *et al.* Obesity and altered glucose metabolism impact HDL composition in CETP transgenic mice: a role for ovarian hormones. *J Lipid Res* **53**, 379-389 (2012).

121. Yates, J.R., 3rd, Eng, J.K., McCormack, A.L. & Schieltz, D. Method to correlate tandem mass spectra of modified peptides to amino acid sequences in the protein database. *Analytical chemistry* **67**, 1426-1436 (1995).
122. Ma, Z.Q. *et al.* IDPicker 2.0: Improved protein assembly with high discrimination peptide identification filtering. *Journal of proteome research* **8**, 3872-3881 (2009).
123. Li, M. *et al.* Comparative shotgun proteomics using spectral count data and quasi-likelihood modeling. *Journal of proteome research* **9**, 4295-4305 (2010).
124. Shores, C.G. & Yarbrough, W.G. Three-dimensional xenograft model of dysplastic human laryngeal mucosa. *Laryngoscope* **108**, 1358-1362 (1998).
125. Thery, C. Exosomes: secreted vesicles and intercellular communications. *F1000 biology reports* **3**, 15 (2011).
126. Aatonen, M.T. *et al.* Isolation and characterization of platelet-derived extracellular vesicles. *Journal of extracellular vesicles* **3** (2014).
127. Aharon, A., Tamari, T. & Brenner, B. Monocyte-derived microparticles and exosomes induce procoagulant and apoptotic effects on endothelial cells. *Thrombosis and haemostasis* **100**, 878-885 (2008).
128. Choudhuri, K. *et al.* Polarized release of T-cell-receptor-enriched microvesicles at the immunological synapse. *Nature* **507**, 118-123 (2014).
129. Corrigan, L. *et al.* BMP-regulated exosomes from Drosophila male reproductive glands reprogram female behavior. *J Cell Biol* **206**, 671-688 (2014).
130. Mittelbrunn, M. *et al.* Unidirectional transfer of microRNA-loaded exosomes from T cells to antigen-presenting cells. *Nature communications* **2**, 282 (2011).
131. Kucharzewska, P. *et al.* Exosomes reflect the hypoxic status of glioma cells and mediate hypoxia-dependent activation of vascular cells during tumor development. *Proc Natl Acad Sci U S A* **110**, 7312-7317 (2013).
132. van Balkom, B.W. *et al.* Endothelial cells require miR-214 to secrete exosomes that suppress senescence and induce angiogenesis in human and mouse endothelial cells. *Blood* **121**, 3997-4006, S3991-3915 (2013).
133. Harding, C.V., Heuser, J.E. & Stahl, P.D. Exosomes: looking back three decades and into the future. *J Cell Biol* **200**, 367-371 (2013).
134. S, E.L.A., Mager, I., Breakefield, X.O. & Wood, M.J. Extracellular vesicles: biology and emerging therapeutic opportunities. *Nature reviews. Drug discovery* **12**, 347-357 (2013).
135. Hyenne, V. *et al.* RAL-1 controls multivesicular body biogenesis and exosome secretion. *J Cell Biol* **211**, 27-37 (2015).
136. Allaire, P.D. *et al.* Interplay between Rab35 and Arf6 controls cargo recycling to coordinate cell adhesion and migration. *J Cell Sci* **126**, 722-731 (2013).
137. Dong, W.W. *et al.* Differential expression of Rab27A/B correlates with clinical outcome in hepatocellular carcinoma. *World J Gastroenterol* **18**, 1806-1813 (2012).

138. Hendrix, A. *et al.* Effect of the secretory small GTPase Rab27B on breast cancer growth, invasion, and metastasis. *Journal of the National Cancer Institute* **102**, 866-880 (2010).
139. Ho, J.R. *et al.* Deregulation of Rab and Rab effector genes in bladder cancer. *PLoS One* **7**, e39469 (2012).
140. Baietti, M.F. *et al.* Syndecan-syntenin-ALIX regulates the biogenesis of exosomes. *Nat Cell Biol* **14**, 677-685 (2012).
141. Sorkin, A. & von Zastrow, M. Endocytosis and signalling: intertwining molecular networks. *Nat Rev Mol Cell Biol* **10**, 609-622 (2009).
142. Fader, C.M., Sanchez, D., Furlan, M. & Colombo, M.I. Induction of autophagy promotes fusion of multivesicular bodies with autophagic vacuoles in k562 cells. *Traffic* **9**, 230-250 (2008).
143. Rodrigo, J.P. *et al.* Distinctive clinicopathological associations of amplification of the cortactin gene at 11q13 in head and neck squamous cell carcinomas. *J Pathol* **217**, 516-523 (2009).
144. Schuuring, E. The involvement of the chromosome 11q13 region in human malignancies: cyclin D1 and EMS1 are two new candidate oncogenes--a review. *Gene* **159**, 83-96 (1995).
145. Schuuring, E., Verhoeven, E., Mooi, W.J. & Michalides, R.J. Identification and cloning of two overexpressed genes, U21B31/PRAD1 and EMS1, within the amplified chromosome 11q13 region in human carcinomas. *Oncogene* **7**, 355-361 (1992).
146. Thery, C., Amigorena, S., Raposo, G. & Clayton, A. Isolation and characterization of exosomes from cell culture supernatants and biological fluids. *Curr Protoc Cell Biol* **Chapter 3**, Unit 3 22 (2006).
147. Timpson, P., Lynch, D.K., Schramek, D., Walker, F. & Daly, R.J. Cortactin overexpression inhibits ligand-induced down-regulation of the epidermal growth factor receptor. *Cancer Res* **65**, 3273-3280 (2005).
148. Stenmark, H. *et al.* Inhibition of rab5 GTPase activity stimulates membrane fusion in endocytosis. *EMBO J* **13**, 1287-1296 (1994).
149. Huang, C., Liu, J., Haudenschild, C.C. & Zhan, X. The role of tyrosine phosphorylation of cortactin in the locomotion of endothelial cells. *J Biol Chem* **273**, 25770-25776 (1998).
150. Weed, S.A. *et al.* Cortactin localization to sites of actin assembly in lamellipodia requires interactions with F-actin and the Arp2/3 complex. *J Cell Biol* **151**, 29-40 (2000).
151. Desnos, C. *et al.* Rab27A and its effector MyRIP link secretory granules to F-actin and control their motion towards release sites. *J Cell Biol* **163**, 559-570 (2003).
152. Kimura, T., Taniguchi, S. & Niki, I. Actin assembly controlled by GDP-Rab27a is essential for endocytosis of the insulin secretory membrane. *Archives of biochemistry and biophysics* **496**, 33-37 (2010).
153. Singh, R.K. *et al.* Distinct and opposing roles for Rab27a/Mlph/MyoVa and Rab27b/Munc13-4 in mast cell secretion. *The FEBS journal* **280**, 892-903 (2013).

154. Yokoyama, K. *et al.* Rab27a negatively regulates phagocytosis by prolongation of the actin-coating stage around phagosomes. *J Biol Chem* **286**, 5375-5382 (2011).
155. Cai, L., Makhov, A.M., Schafer, D.A. & Bear, J.E. Coronin 1B antagonizes cortactin and remodels Arp2/3-containing actin branches in lamellipodia. *Cell* **134**, 828-842 (2008).
156. Morton, W.M., Ayscough, K.R. & McLaughlin, P.J. Latrunculin alters the actin-monomer subunit interface to prevent polymerization. *Nat Cell Biol* **2**, 376-378 (2000).
157. Baldassarre, M. *et al.* Actin dynamics at sites of extracellular matrix degradation. *Eur J Cell Biol* **85**, 1217-1231 (2006).
158. Li, A. *et al.* The actin-bundling protein fascin stabilizes actin in invadopodia and potentiates protrusive invasion. *Curr Biol* **20**, 339-345 (2010).
159. Yanez-Mo, M. *et al.* Biological properties of extracellular vesicles and their physiological functions. *Journal of extracellular vesicles* **4**, 27066 (2015).
160. Lakkaraju, A. & Rodriguez-Boulan, E. Itinerant exosomes: emerging roles in cell and tissue polarity. *Trends Cell Biol* **18**, 199-209 (2008).
161. Hume, A.N. *et al.* Rab27a regulates the peripheral distribution of melanosomes in melanocytes. *J Cell Biol* **152**, 795-808 (2001).
162. Jordens, I. *et al.* Rab7 and Rab27a control two motor protein activities involved in melanosomal transport. *Pigment cell research / sponsored by the European Society for Pigment Cell Research and the International Pigment Cell Society* **19**, 412-423 (2006).
163. Marks, M.S. & Seabra, M.C. The melanosome: membrane dynamics in black and white. *Nat Rev Mol Cell Biol* **2**, 738-748 (2001).
164. Menasche, G. *et al.* A newly identified isoform of Slp2a associates with Rab27a in cytotoxic T cells and participates to cytotoxic granule secretion. *Blood* **112**, 5052-5062 (2008).
165. Wu, X. *et al.* Rab27a enables myosin Va-dependent melanosome capture by recruiting the myosin to the organelle. *J Cell Sci* **114**, 1091-1100 (2001).
166. Eitzen, G. Actin remodeling to facilitate membrane fusion. *Biochimica et biophysica acta* **1641**, 175-181 (2003).
167. Cingolani, L.A. & Goda, Y. Actin in action: the interplay between the actin cytoskeleton and synaptic efficacy. *Nature reviews. Neuroscience* **9**, 344-356 (2008).
168. Porat-Shliom, N., Milberg, O., Masedunskas, A. & Weigert, R. Multiple roles for the actin cytoskeleton during regulated exocytosis. *Cellular and molecular life sciences : CMLS* **70**, 2099-2121 (2013).
169. Fratti, R.A., Jun, Y., Merz, A.J., Margolis, N. & Wickner, W. Interdependent assembly of specific regulatory lipids and membrane fusion proteins into the vertex ring domain of docked vacuoles. *J Cell Biol* **167**, 1087-1098 (2004).
170. Gabel, M. *et al.* Annexin A2-dependent actin bundling promotes secretory granule docking to the plasma membrane and exocytosis. *J Cell Biol* **210**, 785-800 (2015).
171. Regazzi, R. *Molecular mechanisms of exocytosis*. (Landes Bioscience/Eurekah.com ;

Springer Science+Business Media, Austin, Tex.

New York, N.Y.; 2007).
172. Hoshino, D., Branch, K.M. & Weaver, A.M. Signaling inputs to invadopodia and podosomes. *J Cell Sci* **126**, 2979-2989 (2013).
173. Murphy, D.A. & Courtneidge, S.A. The 'ins' and 'outs' of podosomes and invadopodia: characteristics, formation and function. *Nat Rev Mol Cell Biol* **12**, 413-426 (2011).
174. Greer, R.O., Jr., Said, S., Shroyer, K.R., Marileila, V.G. & Weed, S.A. Overexpression of cyclin D1 and cortactin is primarily independent of gene amplification in salivary gland adenoid cystic carcinoma. *Oral Oncol* **43**, 735-741 (2007).
175. Akervall, J.A. *et al.* Chromosomal abnormalities involving 11q13 are associated with poor prognosis in patients with squamous cell carcinoma of the head and neck. *Cancer* **76**, 853-859 (1995).
176. Meredith, S.D. *et al.* Chromosome 11q13 amplification in head and neck squamous cell carcinoma. Association with poor prognosis. *Arch Otolaryngol Head Neck Surg* **121**, 790-794 (1995).
177. Ciriello, G. *et al.* Emerging landscape of oncogenic signatures across human cancers. *Nat Genet* **45**, 1127-1133 (2013).
178. Forastiere, A., Koch, W., Trotti, A. & Sidransky, D. Head and neck cancer. *N Engl J Med* **345**, 1890-1900 (2001).
179. Leemans, C.R., Braakhuis, B.J. & Brakenhoff, R.H. The molecular biology of head and neck cancer. *Nat Rev Cancer* **11**, 9-22 (2011).
180. Huang, X., Godfrey, T.E., Gooding, W.E., McCarty, K.S., Jr. & Gollin, S.M. Comprehensive genome and transcriptome analysis of the 11q13 amplicon in human oral cancer and synteny to the 7F5 amplicon in murine oral carcinoma. *Genes Chromosomes Cancer* **45**, 1058-1069 (2006).
181. Belbin, T.J. *et al.* Molecular profiling of tumor progression in head and neck cancer. *Arch Otolaryngol Head Neck Surg* **131**, 10-18 (2005).
182. Ruiz, C. *et al.* Enhanced expression of ANO1 in head and neck squamous cell carcinoma causes cell migration and correlates with poor prognosis. *PLoS One* **7**, e43265 (2012).
183. Freier, K. *et al.* Recurrent coamplification of cytoskeleton-associated genes EMS1 and SHANK2 with CCND1 in oral squamous cell carcinoma. *Genes Chromosomes Cancer* **45**, 118-125 (2006).
184. Akervall, J.A. *et al.* Amplification of cyclin D1 in squamous cell carcinoma of the head and neck and the prognostic value of chromosomal abnormalities and cyclin D1 overexpression. *Cancer* **79**, 380-389 (1997).
185. Bockmuhl, U., Schluns, K., Kuchler, I., Petersen, S. & Petersen, I. Genetic imbalances with impact on survival in head and neck cancer patients. *The American journal of pathology* **157**, 369-375 (2000).
186. Timpson, P. *et al.* Aberrant expression of cortactin in head and neck squamous cell carcinoma cells is associated with enhanced cell proliferation and resistance to the epidermal growth factor receptor inhibitor gefitinib. *Cancer Res* **67**, 9304-9314 (2007).

187. Lee, J.K. *et al.* Exosomes derived from mesenchymal stem cells suppress angiogenesis by down-regulating VEGF expression in breast cancer cells. *PLoS One* **8**, e84256 (2013).
188. Greening, D.W., Xu, R., Ji, H., Tauro, B.J. & Simpson, R.J. A protocol for exosome isolation and characterization: evaluation of ultracentrifugation, density-gradient separation, and immunoaffinity capture methods. *Methods in molecular biology* **1295**, 179-209 (2015).
189. Kirkbride, K.C., Sung, B.H., Sinha, S. & Weaver, A.M. Cortactin: A multifunctional regulator of cellular invasiveness. *Cell Adh Migr* **5** (2011).
190. Hua, Z.C., Sohn, S.J., Kang, C., Cado, D. & Winoto, A. A function of Fas-associated death domain protein in cell cycle progression localized to a single amino acid at its C-terminal region. *Immunity* **18**, 513-521 (2003).
191. Myllykangas, S., Bohling, T. & Knuutila, S. Specificity, selection and significance of gene amplifications in cancer. *Semin Cancer Biol* **17**, 42-55 (2007).
192. Yang, C. & Robbins, P.D. The roles of tumor-derived exosomes in cancer pathogenesis. *Clin Dev Immunol* **2011**, 842849 (2011).
193. Taylor, D.D. & Gercel-Taylor, C. Tumour-derived exosomes and their role in cancer-associated T-cell signalling defects. *Br J Cancer* **92**, 305-311 (2005).
194. Monteiro, P. *et al.* Endosomal WASH and exocyst complexes control exocytosis of MT1-MMP at invadopodia. *J Cell Biol* **203**, 1063-1079 (2013).
195. Bak, G. *et al.* Rapid structural changes and acidification of guard cell vacuoles during stomatal closure require phosphatidylinositol 3,5-bisphosphate. *Plant Cell* **25**, 2202-2216 (2013).
196. Nicot, A.S. *et al.* The phosphoinositide kinase PIKfyve/Fab1p regulates terminal lysosome maturation in Caenorhabditis elegans. *Mol Biol Cell* **17**, 3062-3074 (2006).
197. Rusten, T.E. *et al.* Fab1 phosphatidylinositol 3-phosphate 5-kinase controls trafficking but not silencing of endocytosed receptors. *Mol Biol Cell* **17**, 3989-4001 (2006).
198. Gary, J.D., Wurmser, A.E., Bonangelino, C.J., Weisman, L.S. & Emr, S.D. Fab1p is essential for PtdIns(3)P 5-kinase activity and the maintenance of vacuolar size and membrane homeostasis. *J Cell Biol* **143**, 65-79 (1998).
199. Holliday, L.S. *et al.* The amino-terminal domain of the B subunit of vacuolar H+-ATPase contains a filamentous actin binding site. *J Biol Chem* **275**, 32331-32337 (2000).
200. Park, L. *et al.* Cyclical action of the WASH complex: FAM21 and capping protein drive WASH recycling, not initial recruitment. *Dev Cell* **24**, 169-181 (2013).
201. Vavassori, S. & Mayer, A. A new life for an old pump: V-ATPase and neurotransmitter release. *J Cell Biol* **205**, 7-9 (2014).
202. Riefler, G.M. *et al.* Exocyst complex subunit sec8 binds to postsynaptic density protein-95 (PSD-95): a novel interaction regulated by cypin (cytosolic PSD-95 interactor). *Biochem J* **373**, 49-55 (2003).